MULTISTAGE FIBRE LENGTH FRACTIONATION OF SOFTWOOD CHEMICAL PULP USING A PRESSURE SCREEN EQUIPPED WITH SMOOTH-HOLED SCREEN CYLINDER

by

Masita Mohamad

B. Eng., Vanderbilt University, 2009

A THESIS SUBMITTED IN PARTIAL FULFILLMENT OF

THE REQUIREMENTS FOR THE DEGREE OF

Master of Applied Science

in

The Faculty of Graduate Studies

(Chemical and Biological Engineering)

THE UNIVERSITY OF BRITISH COLUMBIA

(Vancouver)

August 2012

Abstract

Often, fibre fractionation produce a higher value long-fibred reject stream and a lower value short-fibred accept stream simultaneously. Fractionation is only practical when a mill can make use of all obtained fractions. This study sought to demonstrate the potential of upgrading the reject fraction through multiple stages of fractionation while creating a new market for the remaining low value pulp for an efficient use of the raw materials.

In this study, an NBSK pulp was fractionated on the basis of fibre length using a small industrial pressure screen Beloit MR-8 in multiple consecutive stages to isolate the low-value fines fraction from the feed pulp using the best combination of operating parameters. The best conditions to carry out fractionation were determined by conducting experiments to investigate the effect of varying volumetric reject ratio, R_v aperture velocity, V_s aperture diameter and rotor tip speed, V_t on reject thickening and passage ratio using several smooth-holed screen cylinders. This work shows that in general, increasing fines percentage in the accept and increasing fibre length in the reject were obtained by using the screen cylinder with 0.5 mm apertures, the highest R_v at 0.6 and the smallest V_s at 0.3 ms^{-1}.

The strength properties of the unfractionated pulp were compared to the reject pulp produced from the multistage fractionation. The tensile strength of the final reject pulp (which is 95 wt-% of the feed pulp) was increased up to 40% through the removal of only a small amount of fines. The TEA, burst and tear indexes also improved. The Gurley air resistance was decreased up to 50%.

The final accept fraction contains a significantly higher proportion of fines and it was analyzed by FPInnovations for its potential suitability as a raw material for a novel fibre based product, Nanocrystalline Cellulose (NCC).

Table of Contents

List of Tables

List of Figures

Nomenclature

A_o	Screen cylinder open area [m^2]
c	Pulp consistency [%]
c_a	Accept pulp consistency [%]
c_f	Feed pulp consistency [%]
c_r	Reject pulp consistency [%]
c_s	Pulp consistency in the flow through a screen aperture [%]
c_u	Pulp consistency immediately upstream of the aperture [%]
C_n	Average number concentration of fibres per unit volume [#/L]
l_i	Fibre length of length class *i* [mm]
L_n	Arithmetic average fibre length [mm]
L_w	Length-weighted average fibre length [mm]
$\dot{m}$	Mass flow [kg min^{-1}]
m_i	Mass of fibres of length class *i* [kg or g]
n_i	Number of fibres in length class *i*
$p(l_i)$	Length-weighted distribution of fibre length class *i*
p_w	Length-weighted distribution
P	Pulp passage ratio/ Bulk passage ratio
P(l)	Fibre passage ratio function
$P(l_i)$	Fibre passage ratio of length fraction *i*
Q_a	Accept volumetric flow rate [m^3s^{-1}]
Q_f	Feed volumetric flow rate [m^3s^{-1}]
Q_r	Reject volumetric flow rate [m^3s^{-1}]
R_m	Mass reject ratio [%]
R_v	Volumetric reject ratio [%]
T	Reject thickening factor
V_s	Aperture velocity [ms^{-1}]
V_t	Rotor tip speed/tangential velocity [ms^{-1}]
x_{ia}	Mass fraction or percentage of fibres in length class *i* to the total accept fibre mass
x_{if}	Mass fraction or percentage of fibres in length class *i* to the total feed fibre mass
x_{ir}	Mass fraction or percentage of fibres in length class *i* to the total reject fibre mass
z	Screen position [m]
β	Fibre length passage curve parameter or ‘shape constant’
λ	Fibre length passage coefficient or ‘size constant’
ω	Fibre coarseness [mgm^{-1}]
$\overline{\omega}_i$	Fibre coarseness of length l_i [mgm^{-1}]

Acknowledgments

I would like to express my gratitude to my thesis supervisors, Dr. James Olson and Dr. Mark Martinez for their guidance and also for the opportunity to work in their group. I also want to thank my thesis committee member, Dr. Richard Branion and Dr. Sheldon Duff for generously offering their time for the review of this manuscript.

To my colleagues at the Pulp and Paper Centre (PPC), thank you for providing a friendly and fun environment to learn and grow. I am especially thankful to Jaime Sossa, XinMei Shi and Francisco Fernandez for their friendship. Also, special thanks to Hayder Salem for his assistance with the experimental setup for this work, Dr. Junaid Qazi and George Soong for their help with everything else throughout my time at PPC.

Last but most definitely not least, I would like to acknowledge my parents and also my three sisters; Munira, Mahsuri and Maizun, whom are my best friends for their constant love and support.

This study was made possible through funding from NSERC.

To my mother, Rodziyah for her unconditional love

1 Introduction

Wood fibre structure and its properties are presented in this chapter. The approach to utilize the diverse fibre properties by means of fibre fractionation in a pressure screen is discussed. Pressure screen equipment is reviewed as well as the separation mechanism during screening which includes barrier screening and probability screening. A detailed explanation of the screening theory and parameters such as fibre passage ratio and reject thickening are also presented in this chapter. Pressure screen operating parameters and factors affecting the screening efficiency is discussed towards the end of the chapter. Last but not least, the objectives of this study are introduced and discussed.

1.1 Background

1.1.1 Wood and fibre structure

Softwoods and hardwoods are the two main divisions of tree species. Softwoods commonly originate from evergreen and coniferous trees. Examples of commonly used softwood papermaking species in North America include spruce, pine, fir and hemlock. Hardwoods come from deciduous, broadleaf species such as eucalyptus, maple, birch and poplar.

All trees are comprised of basic building cells which are known as fibres. Softwood fibres which are cylindrical with tapering ends are called tracheids and they are aligned longitudinally in a tree as shown in Figure 1. These tracheids are composed of cellulose and hemicellulose and they are bundled together in a tree matrix by a resin material called lignin. Lignin is contained in middle lamella which is labeled as ML in Figure 2.

Hardwood fibres are typically much shorter and thinner than softwood fibres. Besides the difference in the species type, hardwoods differ from softwoods in terms of their cell structures and components. The structure of hardwoods is much more complicated than softwood. The presence of pores called vessel elements as well as parenchyma cells in varying proportions is a feature of hardwoods that distinguish them from softwoods.

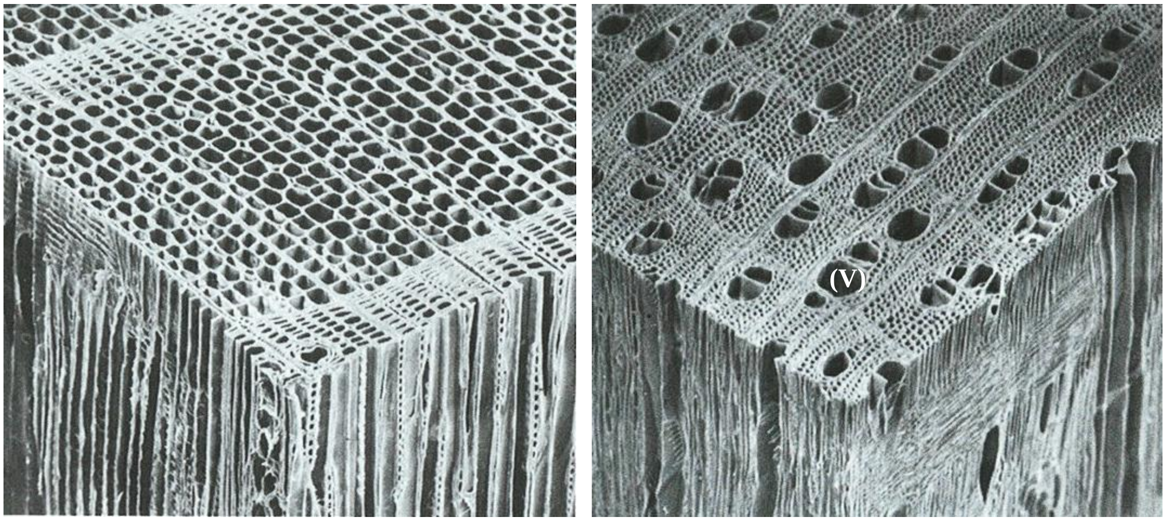

(a) **(b)**

Figure 1. Microscopic structures (transverse view) of (a) spruce (softwood) and (b) birch species (hardwood). (V) shows vessel elements. Handbook For Pulp & Paper Technologists, 2002, by permission.

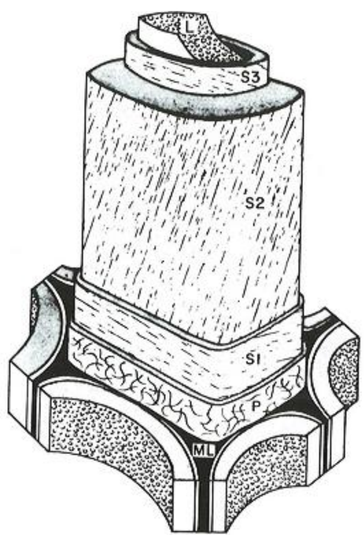

Figure 2. Illustration of a tracheid structure. ML is the middle lamella, P is the primary wall, S is the secondary wall and L is the lumen. Handbook For Pulp & Paper Technologists, 2002, by permission.

Despite the differences in the hardwoods and softwoods properties, the pulping and bleaching processes of both types of woods are quite similar. In a chemical pulping process, lignin and some hemicellulose are dissolved in an appropriate chemical mixture inside a pressurized digester to liberate the fibres. During mechanical pulping, wood chips are heated by a grinding action to soften and breakdown the lignin to separate the fibres. Therefore, most lignin remains with mechanical pulp fibres. Pulp also can be bleached or unbleached depending on its end use.

Fibre physical properties

Figure 3 illustrates typical length distributions of hardwood and softwood pulp fibres. Hardwood fibres have a narrower length distribution than softwood pulps indicating a more homogeneous length for hardwoods. Softwood fibres and hardwood fibres typically have a length-weighted average length of about 2.5 mm and 1 mm respectively.

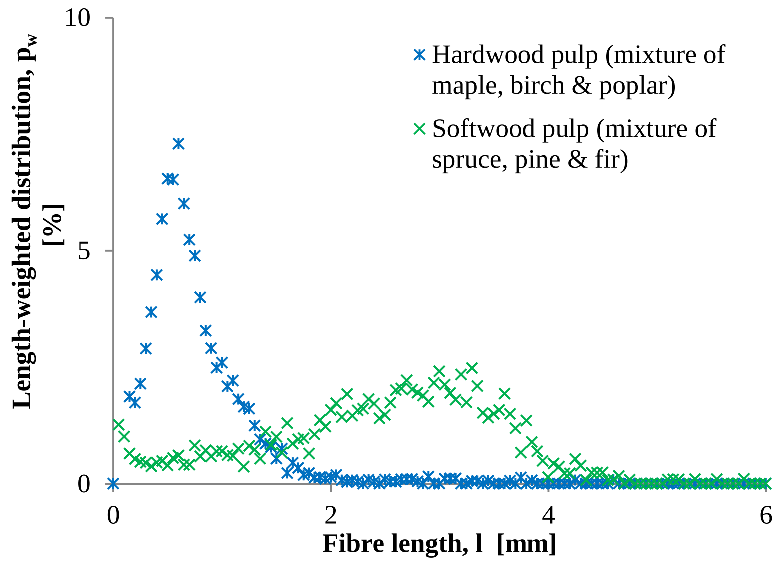

Figure 3. Length-weighted fibre length distributions of chemical softwood and chemical hardwood pulps

There is a considerable natural variation in fibre dimensions between species to species and even within the same tree. Variation also arises from the time of year during which the fibres are produced. This is especially true for softwoods as the tracheid growth is different during spring and winter. Earlywood softwood fibres are produced in the spring or rainy season. An earlywood fibre has a wide hollow core called lumen (shown as L in Figure 2) and a thin cell wall. The fibre cell wall comprises of secondary walls; S1, S2 and S3 as shown in Figure 2. Latewood fibres are formed during winter or at the end of a growing season and have much narrower lumen and very thick cell walls.

Apart from fibres, the lower end of the fibre length distribution consists of fibre particles called fines. There are two types of fines; primary and secondary fines. In chemical pulp, primary fines may come from very short fibres, vessel elements, ray cells or parenchyma cells, with the predominate portion of the primary fines being the ray cells [2]. Chemical pulp fines are also comprised of broken fibres generated as by-product of the wood chipping process, from cooking and bleaching processes or further refining stages. This type of fines or degraded pulp fibres is referred to as secondary fines [2]. From the literature, it is known that fines contain excessively high content of lignin as well as extractives [3].

Pulp quality and strategies for use

Hardwoods and softwoods are used for different purposes in papermaking due to the differences in their morphological properties. However, final paper products are usually made from the combination of softwood and hardwood pulps. Hardwood pulp provides bulkiness, smoothness and good optical properties such as better opacity and light scattering coefficient when added to paper products. This is because they can fill up the spaces between the fibre bonds better. Smoothness is particularly important for printing paper and tissue.

Long-fibred wood species such as softwood pulps are desirable in papermaking especially when strength properties are of importance. The strength of a paper is derived from the area of bonding or the number of inter fibre bonds in addition to the strength of individual fibres. Bonding happens when two or more fibres are in close contact with one another and form weak hydrogen bonds. Long fibres create paper with higher tensile, tearing resistance and a range of other strength-related properties due to their ability to be in contact and bond with more fibres compared to short fibres.

Figure 4 shows the light microscope image of the Northern bleached softwood kraft (NBSK) used in this study. NBSK pulp collapses more readily than hardwoods and can form ribbon-like structures. The ribbon-like structures provide higher surface area or contact area for bonding which consequently results in a superior paper strength properties. NBSK pulp is very sought after and is primarily used as reinforcement pulps in small proportions with hardwood pulps when additional strength is required.

Long fibres also contribute to paper machine runnability as they bond well. Paper machine runnability is a function of fibre bonding and pulp drainage. NBSK pulp provides high drainability due to its low fines content. This also means that NBSK pulp can contribute to better porosity when added to paper products. The fines content in a pulp is known to relate to the dewatering tendency of a pulp suspension as well as the porosity of the resulting paper [4].

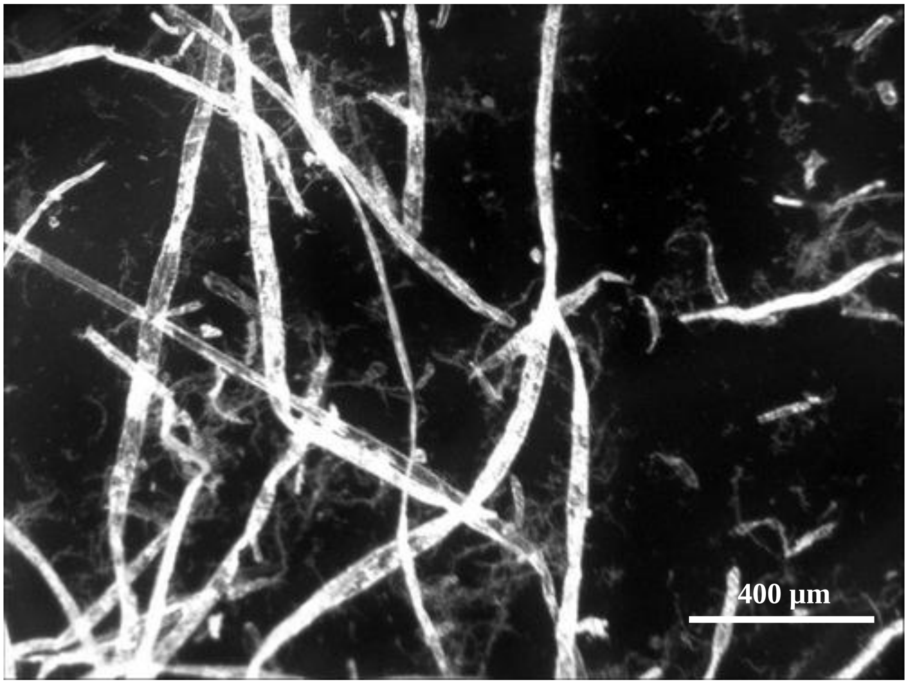

Figure 4. Light microscope image of NBSK pulp (mixture of spruce, pine and fir fibres). NBSK fibre collapses readily into a ribbon-like structure. Length-weighted average fibre length is about 2.5 mm.

Fines are typically considered to be of lower papermaking value because they do not contribute much to the sheet strength. Fines are also associated with diminished drainage. Removal of the undesired fines components has been commercially practiced in chemical pulps, for example, for the production of a high performance sack kraft paper to enable the pulp to be refined to a higher strength while preserving a high porosity [5]. Alternatively, fines may be used as a potential raw material for a novel product such as Nanocrystalline Cellulose (NCC).

Nanocrystalline Cellulose (NCC)

Nanocrystalline Cellulose (NCC) is a product derived from wood fibres. NCC has remarkable properties and has diverse applications for example as strengtheners in polymers or used as advanced coatings and in cosmetics. A natural source of NCC is the cellulose fibrils extracted from the fibre cell wall and therefore the morphology of the fibre itself might not have any effect on the NCC production. This is yet to be determined and will be examined in one part of this study. NCC is formed when a cellulose source is acid hydrolyzed under certain conditions with the assistance of mechanical shear, – e.g., sonication [6].

1.1.2 Fibre fractionation in a pressure screen

Pressure screens allow fibre fractionation by separating the fibres according to their physical properties, primarily by length [7] and secondarily by flexibility and wall thicknesses [8], although only fractionation by length is well established in the literature for industrial screens [9] [10] [11]. Fractionation is carried out through the use of mechanical barriers for separate processing of the resulting fractions. Fractionation in a pressure screen can also improve the homogeneity of the produced fractions. Fractionation of softwood pulp would likely be more successful than the hardwood pulp due to the wider length distribution of the softwood pulps.

Figure 5 shows a modern industrial pressure screen. Traditionally, pressure screens are used in both chemical and mechanical pulping processes to remove undesirable materials such as shives (unpulped fibre bundles), sand, plastic debris and other large contaminants from pulp before it reaches paper machines.

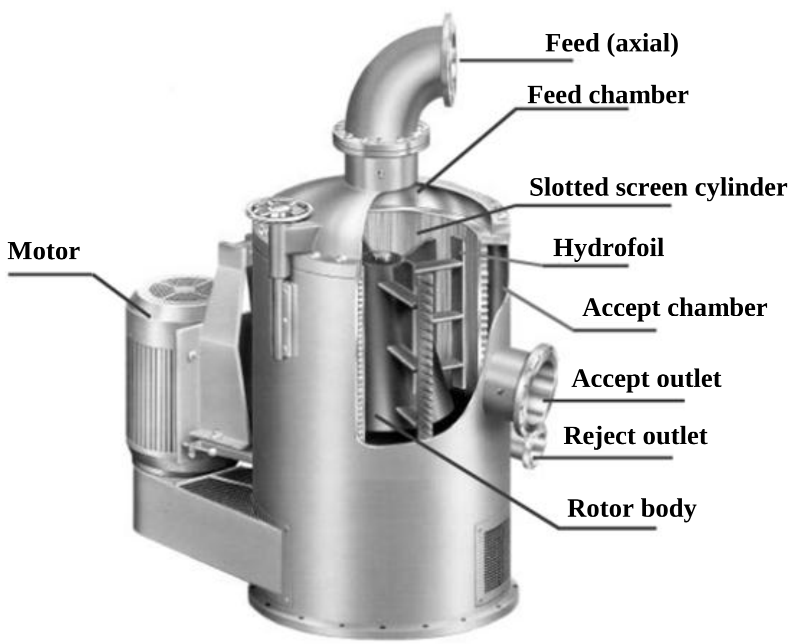

Figure 5. A modern industrial pressure screen. Handbook of Pulp, 2006, by permission.

Fractionation has been used for many years especially in mechanical pulping and in fibre recycling. In mechanical pulping, fractionation allows refining energy savings by selective refining of only the long, coarse fibres. In fibre recycling, fractionation is used as a mean to enhance the quality of secondary fibres by creating a more uniform pulp from the non-uniform waste pulp [12] [13]. Chemical pulp has also been increasingly studied for the purpose of refining energy savings [14] [15]. For chemical pulp producers, fractionation is a tool to optimize the properties of chemical softwood pulp fibres combined with refining [16] [15]. Fractionation also allows development of new pulp and paper grades. For example, the long fibre fraction could be directed to a separate stream for the production of a high-value reinforcing pulp to be used with a relatively weak pulp while the short fibre fraction could be directed to a multi-layer product that requires smooth surface and good optical properties with the core containing long fibres for strength [17]. Also, fractionation allows removal of fines from chemical pulp so that the remaining long fibre fraction can be refined to a higher tensile strength at a given freeness [5].

Figure 6 shows a schematic of a typical pressure screen. A pressure screen consists of two principal components; a rotor and a perforated cylinder located inside the pressure screen housing. Since the introduction of pressure screens, numerous screen cylinder and rotor designs have been made available. A screen cylinder may have a smooth or contoured/profiled surface and the apertures on the cylinder may either be in holed or slotted form. Holed screen cylinders are the first cylinder type that was introduced and they are shown in Figure 7. Three aperture sizes are used in this study; 1.0 mm, 0.8 mm and 0.5 mm. The screen cylinder with 0.5 mm apertures has a much bigger spacing between the apertures compared to the 1.0 mm. Large aperture spacing reduces the risk of screen blinding [18]. Smooth-holed screen cylinders typically give more capacity than the contour slotted cylinder due to their large open area. Smooth-holed screen cylinders have also been found to fractionate by length better than the contour-slotted ones [10].

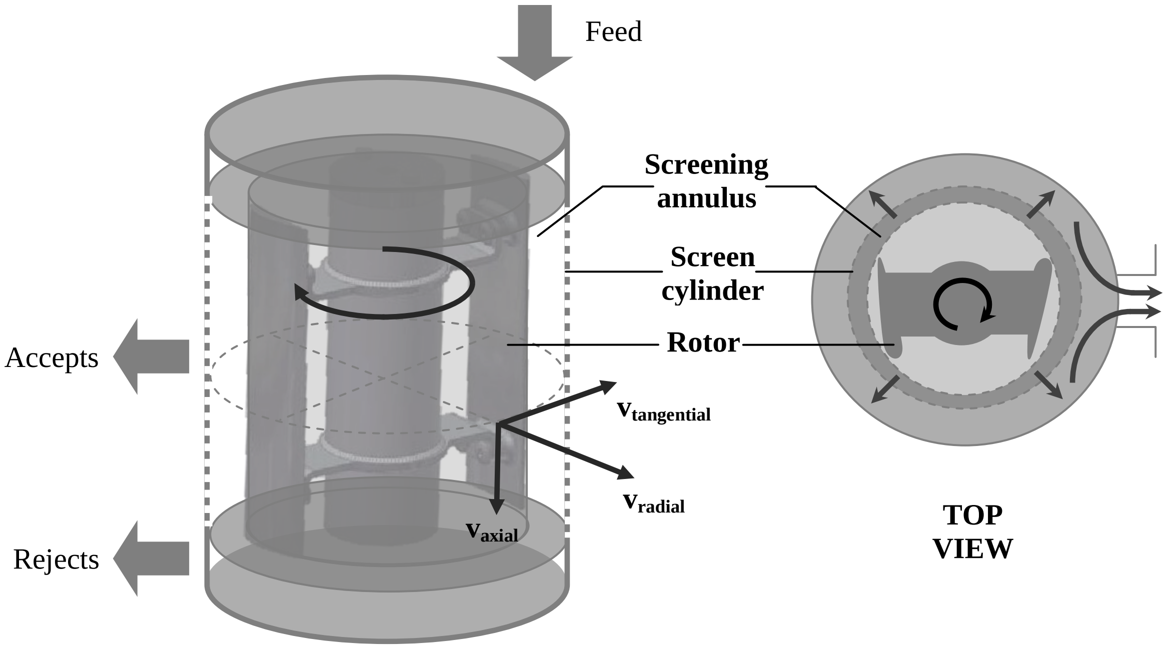

Figure 6. Schematic of an axially fed pressure screen with a two-foil rotor and the velocity components near the screen cylinder.

Figure 7. Smooth-holed screen cylinders with several aperture sizes (1.0 mm, 0.8 mm and 0.5 mm) used in this study.

During fractionation, pulp is directed to the inside of the perforated cylinder. Accepted materials (or accepts) are pushed outward radially through the screen apertures by a turbulence created by the rotor motion. Water, fines and short-fibred pulp that passed through the screen apertures are sent to the accept stream while the remaining long fibres or oversized materials (or rejects) are retained on the screen and continue along the screen cylinder towards the reject stream.

Gooding et al. [19] discussed the primary purposes of rotor. Basically, a rotor prevents pulp accumulation on the screen cylinder surface by continuously redispersing fibres near the screen apertures. The rotor motion creates pressure pulses that generate turbulence on the screen cylinder surface. This turbulence keeps the pulp suspension fluidized and therefore prevents the formation of a fibre mat on the screen cylinder surface which would hinder fibre passages through the screen aperture. If the rotor speed is not adequate however, a condition called reject thickening will occur. As thickening takes place, the screen cylinder starts to 'blind' and a fibre mat starts to form adjacent to the screen cylinder surface and blocks the passing of fibres to the accept side. Reject thickening can also lead to the plugging of the reject line.

As can be seen in Figure 6, there are three velocity components near the screen cylinder. The tangential velocity component is induced by the rotor rotating action. The axial feed introduces the axial velocity component from the feed to the reject side and it is parallel to the axis of rotor rotation. The radial velocity component which is also known as the aperture velocity, V_s is the average superficial passing velocity from the feed side through the apertures to the accept side and is an important operating parameter described in detail in the next chapters.

Aperture velocity is calculated from the accept flow rate divided by the open area of the screen cylinder as in Equation 1-1. The screen cylinder open area is the total area of the apertures.

$$v_s = \frac{Q_a}{A_o} \qquad \textbf{1-1}$$

where Q_a = accept flow rate (m^3s^{-1})
A_o = screen cylinder open area (m^2)

1.1.3 Screening mechanism

Oversized contaminants or fibres are separated by selective passage through the screen apertures. Generally, there are two types of solid-solid separation in a pressure screen; barrier screening and probability screening. Figure 8 illustrates the two types of screening. In barrier screening (Figure 8a), for the case of oversize contaminants removal, materials are rejected because they are physically larger than the screen aperture size in any dimension. This type of materials cannot physically fit through the apertures and can be removed with a 100% efficiency.

During fibre fractionation, fibre separation in a pressure screen is essentially governed by the probability screening. Fibres have a large aspect ratio – i.e., a large length to diameter (l/D) ratio. Also, fibre diameters are usually smaller than most screen aperture sizes available. Consequently, fibres can pass through the apertures in at least one dimension. As shown in Figure 8b, long fibres are able to go through the narrow screen apertures if the fibres approach the apertures at a correct orientation. In fractionation by length, the more desirable long fibre fraction can be found in the reject stream. Both types of separation; barrier and probability screening can occur simultaneously during contaminants screening. Therefore, during contaminants screening, fibre fractionation is an undesired effect as loss of fibres occurs with contaminants removal.

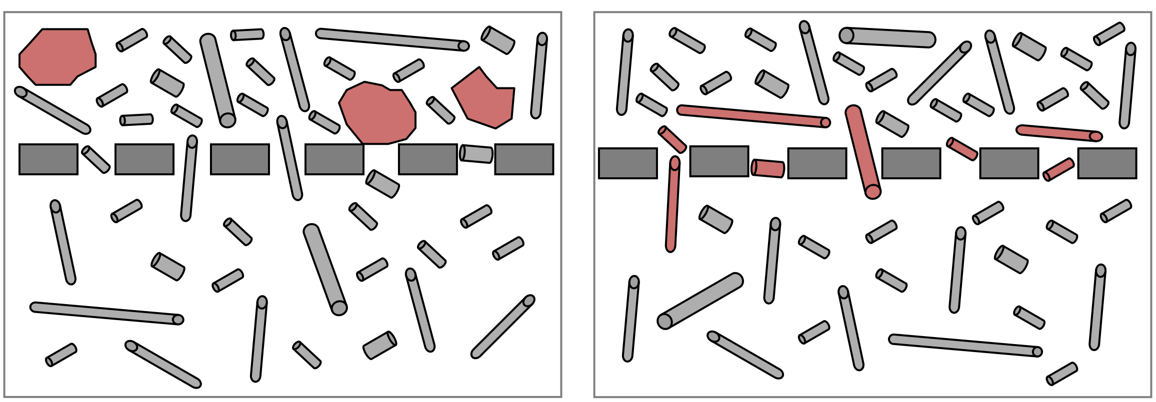

(a) **(b)**

Figure 8. Types of screening. (a) shows barrier screening and (b) shows probability screening.

Fibre fractionation is a statistical process with the pulp passing probability characterized by a parameter called pulp passage ratio, P which has a value between 0 to 1. A pulp passage ratio of 1 indicates no restrictions to fibre passage and therefore all fibres are accepted. The probability of fibre passage depends on many factors, with the most important one being the screen design and operating parameters as well as the pulp furnish. The effect of some of these parameters is investigated in this study.

1.1.4 Screening theory

Pressure screen performance can be evaluated quantitatively using various parameters such as reject thickening, T and pulp passage ratio, P. Additionally; qualitative analysis such as drainability (freeness), consistency or average length differential of the resulting fractions can be used to demonstrate screening efficiency.

Reject thickening or reject consistency changes, resulted from fibres having certain probabilities to pass through the screen apertures. Fines and water can flow freely through the apertures towards the accept side of the screen. As a result, under typical operating conditions the consistency of the reject pulp is always higher than accept or feed pulps. This condition is termed reject thickening. Reject thickening, T is simply defined as the ratio of the reject consistency to the feed consistency as shown in Equation 1-2. There is a maximum value for reject thickening, after which the plugging of the reject line would occur.

$$T = \frac{c_r}{c_f} \tag{1-2}$$

where c_r = reject pulp consistency
c_f = feed pulp consistency

The pulp passage ratio, P describes the probability of pulp passage through a single screen aperture and it is calculated using Equation 1-3.

$$P = \frac{c_s}{c_u} \tag{1-3}$$

where c_s = pulp consistency in the flow through a screen aperture
c_u = pulp consistency immediately upstream of the aperture

Both mixed-flow and plug-flow models have been developed by Gooding and Kerekes in the past to describe the consistency changes and to predict reject thickening in a pressure screen [20]. The plug-flow model assumes perfect radial mixing but no axial mixing. Only the plug flow model derivation is presented here. The plug flow analysis considers a series of an annular volume element such as in Figure 9 in the screening zone which is the area between the rotor and the screen cylinder.

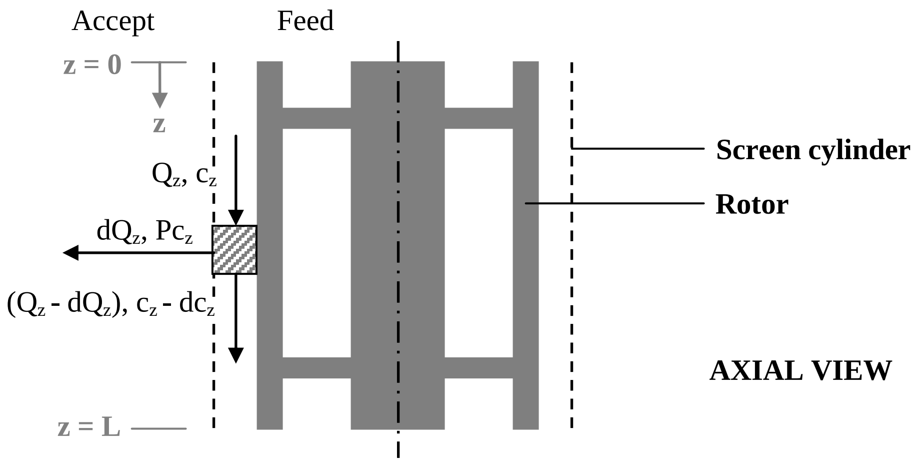

Figure 9. Flows and consistencies around an annular differential volume element. Adapted from [20].

From the conservation of mass, the mass flow entering the control volume (in kg min^{-1}) in Figure 9 is equivalent to the summation of the mass leaving in both radial and axial directions. The mass balance can also be written in terms of more practical measurements such as consistency, c and volumetric flow rates, Q. The subsequent steps for the derivation of the pressure screen performance equations presented here are taken from the aforementioned work by Gooding [20]. At low consistencies, the material balance can be written as follows:

$$Q_z c_z - dQ_z P c_z - (Q_z - dQ_z)(c_z - dc_z) = 0 \qquad \textbf{1-4}$$

where Q_z = total volumetric flow rate (m^3h^{-1}) entering the volume element
dQ_z = flow rate leaving the volume element in the radial direction

Rearranging Equation 1-4 gives:

$$\frac{dc_z}{c_z} = (P - 1)\frac{dQ_z}{Q_z} \qquad \textbf{1-5}$$

Under the assumption of plug flow conditions, where the pulp consistency does not change axially along the screening annulus, Equation 1-5 can be integrated along the length of the pressure screen using the following boundary conditions; $c_z = c_f$, $Q_z = Q_f$ at $z = 0$ and $c_z = c_r$, $Q_z = Q_r$ at $z = L$ (with subscripts f and r refer to feed and reject streams respectively). This yields:

$$\frac{c_r}{c_f} = \left(\frac{Q_r}{Q_f}\right)^{P-1} \qquad \textbf{1-6}$$

After substituting the reject thickening definition introduced earlier in Equation 1-2 to Equation 1-6, reject thickening is related to the total or bulk fibre passage ratio by the following equation:

$$T = {R_v}^{P-1} \qquad \textbf{1-7}$$

where R_v = volumetric reject ratio

The volumetric reject ratio, R_v is an important operating parameter of a pressure screen. It is defined as:

$$R_v = \frac{Q_r}{Q_f} \qquad \textbf{1-8}$$

where Q_r = reject volumetric flow rate
Q_f = feed volumetric flow rate

Figure 10 shows the predicted reject thickening behaviour modeled using Equation 1-7. Reject thickening is dependent on the volumetric reject ratio. As the reject ratio increases, the reject thickening increases. Also, reject thickening increases with decreasing probability of the overall pulp passage, P. The pressure screen acts as a flow splitter as P gets closer to 1 meaning there is no separation or concentration changes occurring. As P approaches 0, the screen acts as a filter, letting only the water to pass through the screen apertures [21]. Several researchers [19] [22] [23] confirmed that the plug flow model correlates the experimental data for reject thickening behaviour of industrial pressure screens better than the mixed-flow model.

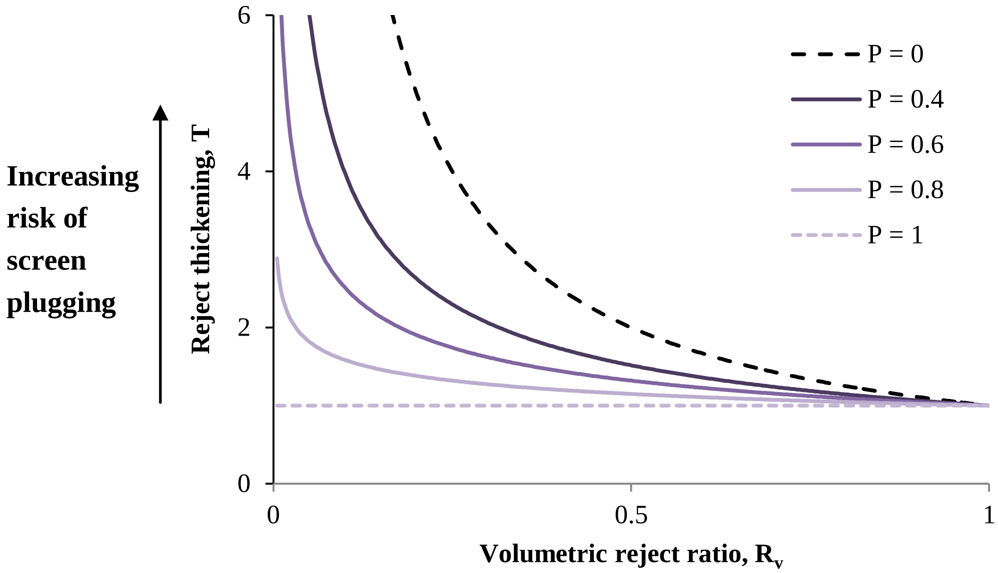

Figure 10. Reject thickening behaviour as predicted by the plug flow model. 0<P<1 represents probability screening.

The bulk passage ratio, P discussed earlier describes the probability of pulp passage which covers the entire range of fibre length. It is more useful to calculate the passage ratio separately for each fibre length – i.e., as a function of length especially in fractionation, since the aim of fractionation is to have selective length separation of the feed pulp. Based on the study by Gooding [20], Olson and Wherrett [24] extended Equation 1-3 to give Equation 1-9 to calculate the passage ratio of fibres in a length interval i (where subscripts f and a refer to feed and accept, respectively).

$$P(l_i) = \frac{C_{na} p_a(l_i)}{C_{nf} p_f(l_i)} \qquad \textbf{1-9}$$

where $P(l_i)$ = fibre passage ratio of length fraction i

C_n = average number concentration per unit volume of a sample

$p(l_i)$ = fibre length distribution of length fraction i

The length dependence on the probability of fibre passage through the screen apertures was extensively studied by Olson et al. [10] [11] [24]. They agreed that the fibre passage decreases as fibre length increases. A fibre with a passage ratio of one will pass through the screen apertures and fibres with a passage ratio of zero will be retained on screen. The difference in the fibre passage probability is the cause of fractionation. Fibre passage ratio has been shown to be approximated by the following empirical equation for both smooth-holed and slotted screen apertures [10] [11]:

$$P(l_i) = e^{-(\frac{l_i}{\lambda})^{\beta}}$$ **1-10**

λ is known as the 'size constant' because it is related to the screen cylinder aperture size. A higher λ value indicates an easier fibre passage which usually means a lower degree of fractionation. β is known as the 'shape constant'. Varying β modifies the shapes of the P(l) curves. β was found to be equal to 1 and 0.5 for smooth-holed and slotted screen cylinders respectively [10]. Figure 11 shows the effect of varying λ and β on fibre passage ratio. Smooth-holed screen cylinders can fractionate fibres more efficiently than the contour-slotted ones as can be seen from the differences in the shape of the P(l) curves [10]. The passage of long fibres decreases more slowly using smooth-holed screen cylinders than when using slotted cylinders. This model has been shown to fit real data reasonably well [9] [10].

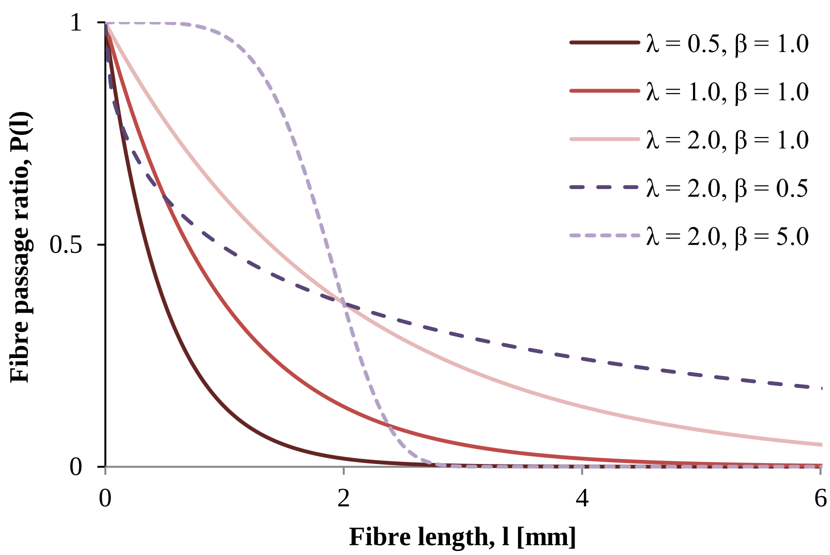

Figure 11. Examples of fibre passage behavior for smooth-holed screen cylinder as a function of fibre length (shown as smooth lines with β = 1). Dotted lines show the influence of β on the P(l) curves.

1.1.5 Pressure screen parameters

The performance of a pressure screen is dependent on the interaction among various design and operating parameters as well as fibre furnish. Some of the key parameters are shown below in Table 1.

Table 1. Classes of parameters.

Design parameter	Screen cylinder design (screen surface – smooth or profiled, aperture type – holes or slots, aperture size) Rotor design (bump, foil etc.)
Operating parameter	Aperture velocity, V_s Rotor tip/tangential speed, V_t Volumetric reject ratio, R_v Feed consistency
Furnish parameter	pH, temperature and fibre properties (length, wall thickness, flexibility), consistency

Numerous studies on the effect of these parameters can be found in the literature. Saint Amand and Perrin [8] found an improvement in the pulp passage ratio, P with an increase in aperture velocity, V_s, using contour-slotted screen cylinder. Sloane [14] found a decrease in pulp separation efficiency at increased V_s using smooth-holed screen cylinders. A high V_s is linked to a high pressure drop over the screen cylinder. This implies that a higher force is exerted on particles on the screen surface and therefore more large particles are accepted resulting in reduced fractionation efficiency.

The effects of pressure screen operating parameters have been studied extensively by Olson et al. on a pilot scale for the field of fractionation of mechanical pulp and removal of shives [10] [24] [11] [9]. In terms of the design parameter, for the smooth-holed screen cylinder, fractionation efficiency was found to be dependent entirely on the diameter of the holes for the fractionation of TMP pulp [11]. For the contoured-slotted screen cylinders, it was found that the aperture velocity, V_s and the aperture width greatly affects the fractionation results [10]. Increasing the slot width provides an easier passage for pulp. Another study by Braaten and Wakelin for TMP fibre length fractionation using smooth-holed screen cylinders and profiled-slotted screen cylinders showed improvement in fractionation was obtained by reducing the aperture size, rotor tip speed speed, V_t and V_s [22].

Foil type rotors are suitable for fractionation and is the one used in this study. There are ambiguous results on the effect of the rotor tip speed, V_t. For example, Gooding et al. [19], Ämmälä [25] and Sloane [14] found varied response to V_t with slotted and holed screen cyliders using both chemical and mechanical pulps; fractionation efficiency increases for some cylinder/pulp combinations but decreases in others. However, in general, fractionation efficiency decreases with an increase in V_t, V_s and aperture size.

A part of this thesis focuses on the effect of controllable operating parameters such as volumetric reject ratio, R_v aperture velocity, V_s rotor tip speed, V_t on fractionation.

Arrangements of pressure screen for multistage fractionation

It is common in the industry that fractionation is done in multiple stages to improve efficiency. The possible two-stage arrangements are shown in Figure 12. In a cascade system, the rejects from the first stage is passed to the feed of the second stage.

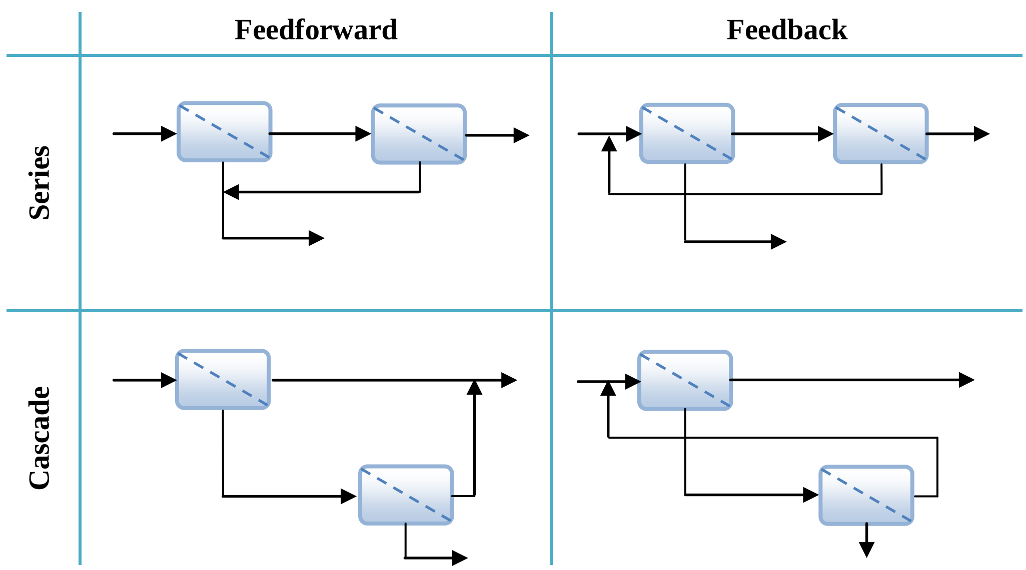

Figure 12. Possible arrangements of a two-stage screening system. Adapted from [26].

1.2 Summary of the literature

The following conclusions can be drawn from the literature:

- Wood is a complex structure and its fibre properties are widely distributed across species and within trees.
- The ability of a pressure screen to fractionate fibres according to the fibre length has been well established in the literature. Fractionation changes the length distribution of the resulting fractions. Many studies can be found in the literature that explore the utilization of pressure screens to fractionate mechanical, chemical or recycled pulp to produce value-added fractions as well as for energy savings purposes.
- Pressure screen performance can be evaluated numerically using parameters such as volumetric reject ratio, R_v and pulp passage ratio, P which were derived from the assumption of two ideal flow configurations; mixed flow model and plug flow model.
- Pressure screen operating parameters affecting fractionation include volumetric reject ratio, aperture velocity, rotor tip speed etc. There are opposing views on the effect of some of these parameters on fractionation. The design of the screen cylinders – e.g., the size and shape of the apertures also affects fractionation. Olson et al. showed that smooth-holed screen cylinders provide better size separation than the contour-slotted ones [9].

1.3 Objectives of the study

Often, fibre fractionation produces a higher-valued stream (long-fibred rejects) and a lower-value stream (short-fibred accepts) simultaneously. Fractionation is only practical when a mill can make use of all obtained fractions. This study sought to demonstrate the potential of upgrading the reject fraction through multiple stages of fractionation while creating a new market for the remaining low value pulp.

The objectives of this study are:

1) To carry out a multiple stages of fractionation to upgrade the strength properties and porosity of long-fibred reject fraction by removing the fines materials. The resulting long fibred fraction will have an increased average fibre length and has the potential to be developed as reinforcing pulp.

2) To extract the fines materials that comprised of the lower extreme of the length distribution such as shown in Figure 13 through multistage fractionation. This fines fraction will consist less than 5 wt-% of the main feed pulp and will be analyzed by FPInnovations for its suitability as a raw material for a novel fibre based product, Nanocrystalline Cellulose (NCC). Possible savings can be anticipated through replacing a high quality pulp for NCC production with the lower value fines fraction.

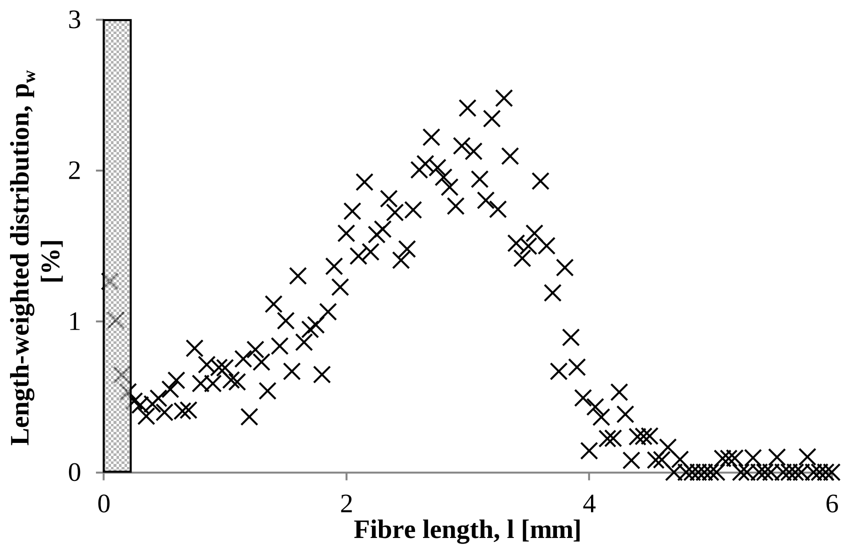

Figure 13. NBSK pulp fibre length distribution. Shaded area shows fines fraction to be extracted from the feed pulp for NCC analysis.

3) To experimentally investigate the effect of varying the pressure screen operating parameters; R_v, V_s and V_t on reject thickening and passage ratio. Single stage fractionation will be carried out using screen cylinders with 1.0 mm, 0.8 mm and 0.5 mm apertures with the goal of producing accepts with the highest fines content and rejects with the highest average fibre length. The best conditions for fractionation determined at this stage will be employed at the subsequent stages. The use of the smooth-holed screen cylinder with 0.5 mm apertures is novel to this study.

4) To conduct a Bauer-McNett fractionation to determine the relationship between coarseness and fibre length, $\omega(l)$ based on work by Madani et al. [27]. The length-weighted average values obtained from an optical analyzer such as the Fibre Quality Analyzer (FQA) assume constant coarseness, which is not the case for a highly distributed pulp. The information from the coarseness versus length relationship and an overall mass balance can then be used to calculate the actual mass percentage of the fibre length class of interest and determine the extent of fractionation by computing the enrichment of fines in the accept and long fibres in the rejects.

1.5 Structure of the thesis

This thesis is divided into seven chapters. The first chapter contains a short review of what is known about fractionation process, the mechanism and the screening theory. Chapter 2 describes the raw materials, the experimental setup as well as the procedures. The results of this study are presented in Chapter 3 through 6, starting from the influence of pressure screen operating parameters on fractionation in Chapter 3. The first fractionation stage and each subsequent stage as well as the fractionation results at each stage are described in Chapter 4 through 6. Additionally, Chapter 5 contains the results from handsheet analysis while Chapter 6 contains a summary of NCC analysis done by the FPInnovations. Concluding remarks can be found in Chapter 7.

2 Materials and methods

In this chapter, the raw materials and experimental setup for this study are discussed in details. The procedures as well as the operating parameters of the pressure screen are described. Appropriate pulp evaluations are presented at the end of this chapter.

2.1 Feed pulp

The pulp used in this fractionation study is Northern bleached softwood kraft (NBSK), a market pulp originated from Canfor's Prince George mill. NBSK pulp is a premium grade of bleached softwood kraft pulp, contains mainly long fibres but is very diverse in length as can be seen in Figure 14. This NBSK pulp is made from 100% SPF blend (spruce, pine and fir species) and the pulp suspension is not refined in this study. The freeness value was measured to be approximately 660 mL Canadian Standard Freeness (CSF). The fibre morphological properties of this feed pulp are summarized in Table 2. Dried pulp sheets were soaked in water at room temperature overnight in the feed tank and re-slurried prior to use. At the initial stage of fractionation, the pulp consistency was maintained at 1.1%±0.2% and kept at a temperature of 20^{o}C at the beginning of the experiment.

Table 2. NBSK pulp fibre morphological properties

Length-weighted average length, L_w [mm]	2.48
Length-weighted percent fines [wt-%]	2.90
Curl index	0.161
Kink index [mm^{-1}]	1.585
Coarseness, ω [mg m^{-1}]	0.126

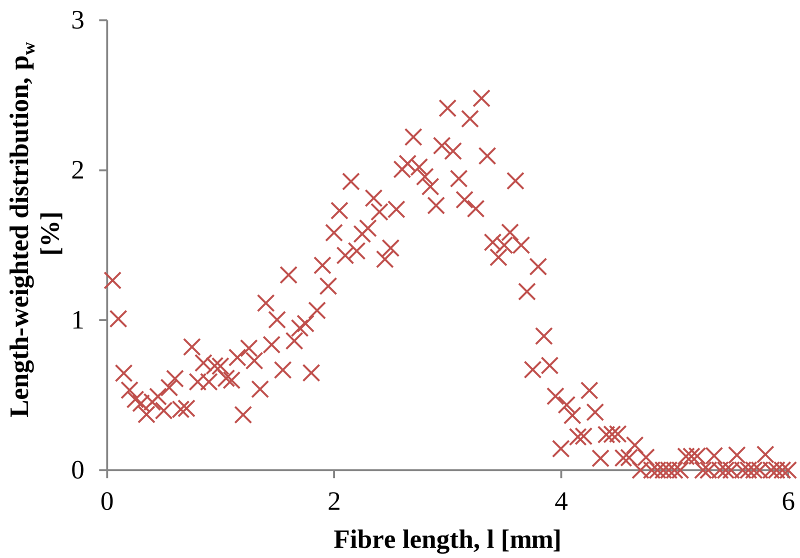

Figure 14. Typical fibre length distribution of NBSK pulp used in the study.

2.2 Pressure screen setup

All fractionation trials were carried out using a small industrial pressure screen Beloit MR8 and several 8-inch diameter smooth-hole screen cylinders. The MR8 is a centrifugal-type horizontal pressure screen. The schematic of the pressure screen setup is shown in Figure 15. Pulp is fed tangentially from a 1 m^3 feed tank to the screening annulus where it is accelerated to a high tangential velocity by a rotor. An AFT EP rotor with two foils was used in all trials and it is driven by a variable-frequency drive (VFD). The feed pressure is also adjusted using a VFD that is attached to a centrifugal pump. The pressure screen loop is fully automated and controlled by a computer program that was written using LabView. The accept and reject lines are equipped with pneumatic control valves and magnetic flow transmitters (FT) which are controlled by the computer program and allow a wide range of flow rates to be tested. The screen is also equipped with electronic pressure transducers to monitor and control pressures of the feed, accept and reject lines.

Accepts selectively pass through the screen apertures and then exit the screening area radially through an accept line located at the centre of the screening width. Rejects exits tangentially through a reject line located at the rear of the screen as shown in Figure 16. As shown in the schematic in Figure 15, accepts and rejects can be recirculated to the feed tank for continuous operation or be redirected to separate accept and reject tanks using manual three-way valves.

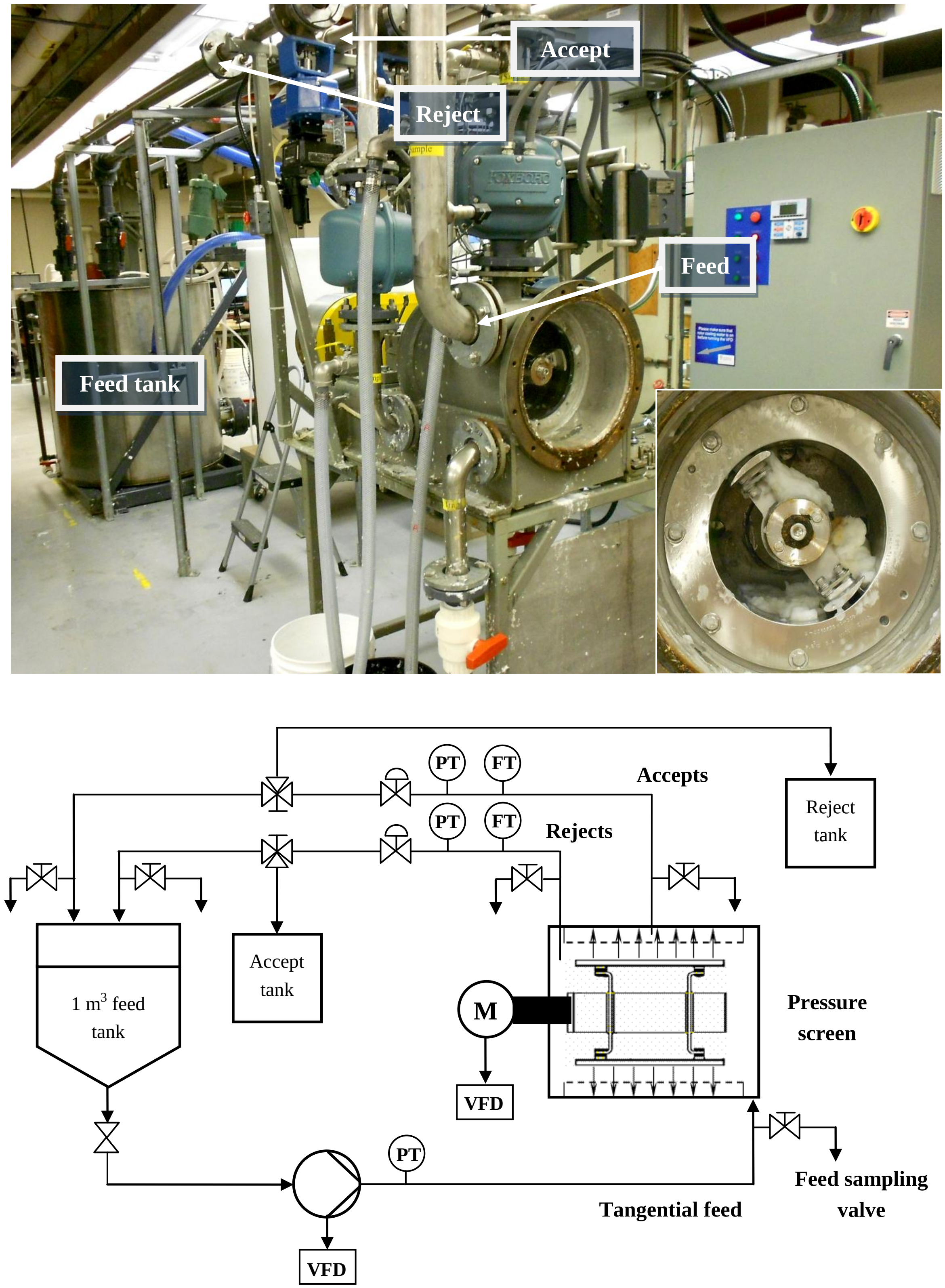

Figure 15. Photograph and schematic of the pressure screen fractionation loop. Inset photograph shows the front view of the screen cylinder and the EP foil rotor inside the pressure screen housing.

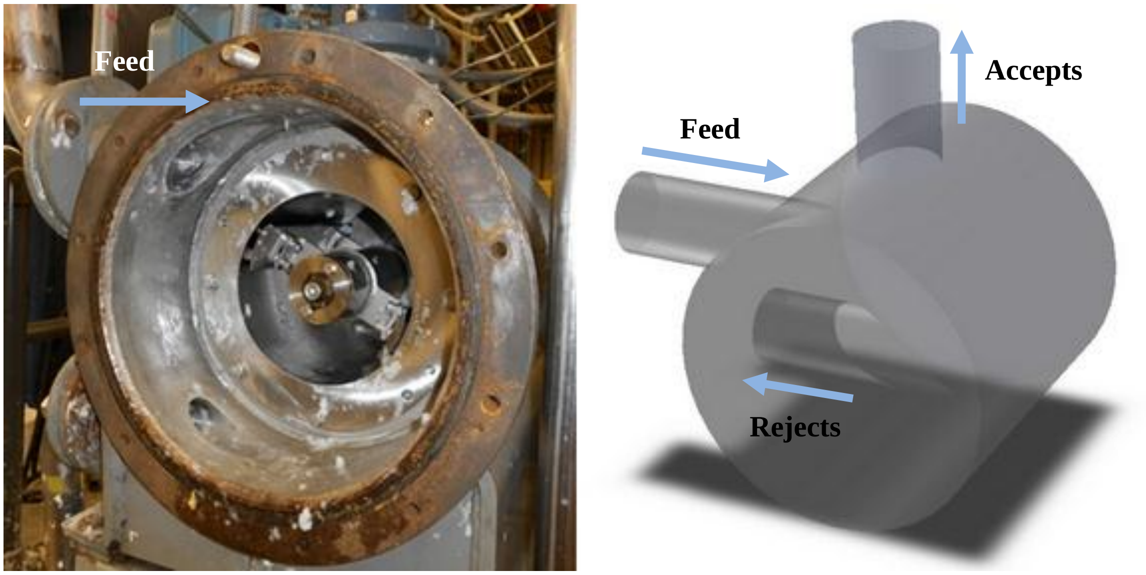

Figure 16. Feed, accept and reject lines location of the tangentially fed MR8.

2.3 Trial procedures

Figure 17 illustrates schematically the multi-stage fractionation. The fractionation trials consisted of the following:

(1) The first stage of fractionation was carried out to determine the best operating parameters for fractionation. During the first stage, accepts and rejects are recirculated to the feed tank. Several smooth surface screen cylinders with different aperture diameters; 0.5 mm, 0.8 mm and 1.0 mm were used in the trials. After installing the appropriate screen cylinder, accept and reject flow valves were manipulated to achieve a wide range of aperture velocities, V_s and volumetric reject ratios, R_v. During all trials at the first stage, the rotor speed was kept constant to facilitate the comparison of the effect other operating parameters on fractionation. The rotor speed was set at 1500 rpm which corresponds to a rotor tip speed of 16 ms^{-1}. The effects of operating parameters on the fractionation performance, including reject thickening and fibre passage ratio were examined using the three screen cylinders. The ranges of these operating parameters are summarized in Table 3. All experiments were conducted at room temperature.

Table 3. Summary of screen design and operating parameters used during the first stage of fractionation (total of 28 screening tests)

Screen cylinder design	Smooth-holed
Aperture diameter [mm]	0.5 , 0.8, 1.0
Operating parameter	
Rotor tip speed, V_t [ms^{-1}]	16
Aperture velocity, V_s [ms^{-1}]	0.3-1.0
Feed flow rate ($\times10^3$), Q_f [m^3s^{-1}]	1.416-13.833
Accept flow rate ($\times10^3$), Q_a [m^3s^{-1}]	0.850-6.417
Reject flow rate ($\times10^3$), Q_r [m^3s^{-1}]	0.425-8.299
Volumetric reject rate, R_v	0.3-0.7
Feed consistency, c_f [%]	1±0.2
Feed pressure [psi]	10-15
Temperature [^oC]	20

After the first set of fractionation trials was completed, the operating parameters that produced the highest fines content in the accept stream A1 and the highest average fibre length in the reject stream R1 were chosen for the subsequent accept and reject fractionation stages. Accept and reject fractions, A1 and R1 obtained at these optimal conditions were redirected to separate containers.

(2) During rejects fractionation stages (shown as (2) in Figure 17), reject R1 was re-diluted to reach a consistency of about 1.1±0.1% and it was then used as feed for the consecutive stage. Enough samples were collected for handsheet testing. Only the screen cylinder with 0.5 mm apertures was used at the second stage. Details on the rejects fractionation stages are discussed later on in Chapter 5.

(3) Accepts fractionation stages consist of a two-stage fractionation to concentrate fines in the final accept stream A2. After the first stage of fractionation, the A1 fraction was pumped back to the feed tank to be used as a feed to the second stage. Due to the low amount of A1 fraction produced at the first stage, several batches had to be run to acquire enough accept fraction for the subsequent A1 to A2 fractionation. It was not possible to increase the capacity of the pressure screen by increasing the feed consistency to more than 1.5% due to problems with reject pipeline plugging caused by reject thickening. The results from the accept fractionation stages are discussed in Chapter 6

The rejects fractionation stages comprised of about 97% of the mass of the feed pulp and the remaining 3% of the mass accounted for the accepts fractionation stages.

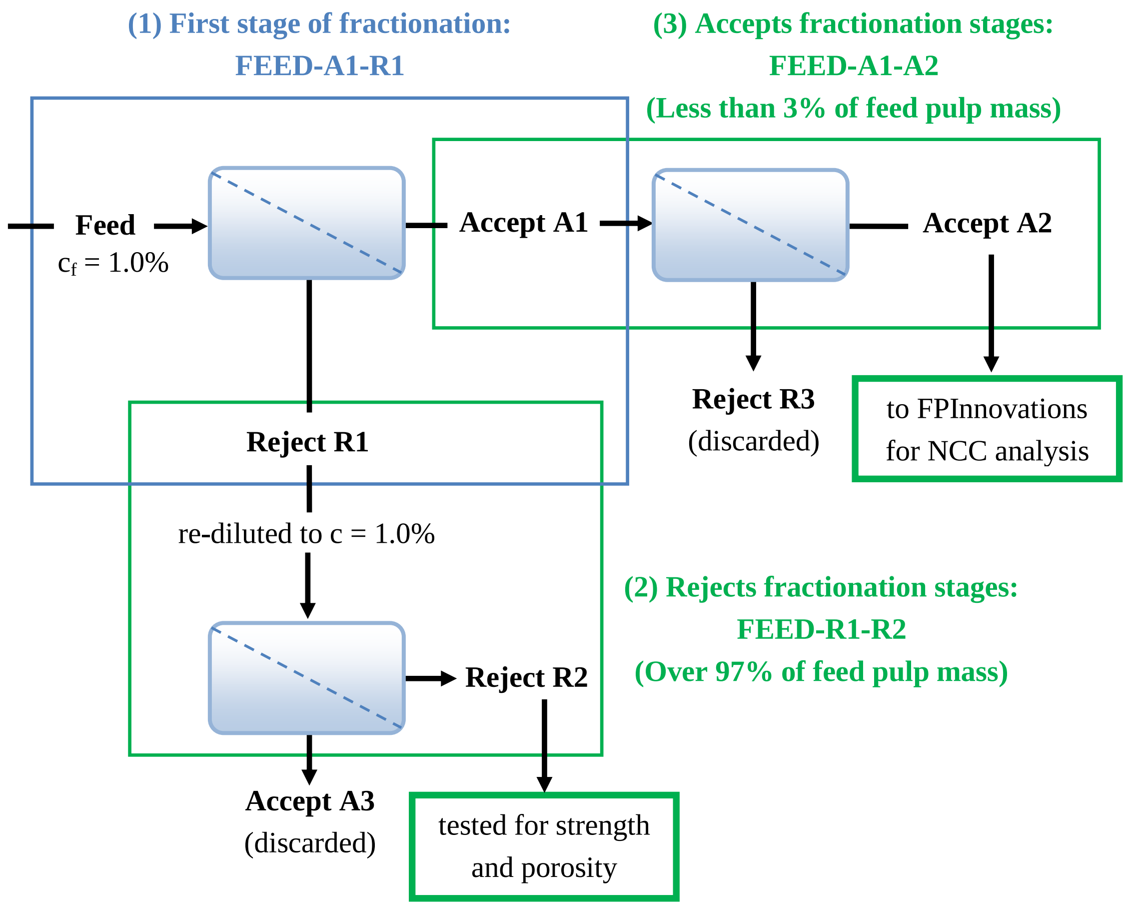

Figure 17. Schematic of the multi-stage fractionation system. Fractionation results at each stage are discussed in the next chapters.

2.4 Pulp evaluations

Samples of 2-3 litres were obtained for consistency and other various measurements from the manual sampling valves of the accept and reject lines located immediately after the screening area. Samples were taken at each volumetric reject ratio after the system reached a steady-state. The amount of samples taken was small enough not to significantly change the feed composition.

The following measurements were made:

1. **Consistency, c**. Consistency is the measure of the amount of dry fibre content in a pulp suspension and it is calculated using a simple equation as follows:

$$c = \frac{m_f}{m_w} \times 100 \qquad \textbf{2-1}$$

where m_w = total mass of a particular amount of pulp suspension
m_f = mass of dry fibrous material in that amount of pulp suspension

Consistency information is required when evaluating screening performance such as reject thickening and passage ratio. All pulp samples were evaluated for consistency.

2. **Freeness**. Freeness values were obtained by performing the Canadian Standard Freeness (CSF) test. Only feed and reject samples were evaluated for freeness because of the high fines content, the low consistency (less than 0.1%) and the difficulty to dewater the accept fraction to the required consistency of 0.3% for freeness testing.

3. **Fibre length, distribution and coarseness**. An Optest Fibre Quality Analyzer (FQA) was used to measure the length-weighted average values and distributions of the fibre samples. Each sample is diluted to a very low consistency for FQA testing. The FQA projects images of single fibres in the sample using circular polarized light and as the fibre suspension passes through an optic box, a digital camera takes pictures of the fibre projections [2].

   The average fibre length is reported here as the length-weighted average, L_w which is defined in Equation 2-2. The corresponding length-weighted distribution, p_w is given in Equation 2-3. By using the length-weighted averages, the reported values are less influenced by the presence of fines of short fibres since shorter fibres have a lower mass per fibre. In addition to fibre length, FQA also reports the coarseness, ω information when the mass of the analyzed sample is provided. Coarseness is defined as the average mass of sample per unit of length of fibres such as in Equation 2-4.

$$L_w = \frac{\sum([l_i n_i] l_i)}{\sum[l_i n_i]} \qquad \textbf{2-2}$$

$$p_w = \frac{l_i n_i}{\sum[l_i n_i]} \qquad \textbf{2-3}$$

where l_i = fibre length of class *i*
n_i = number of fibres in length class *i*

$$\omega = 1000 \times \frac{w}{L_n \times n} \tag{2-4}$$

where w = mass of the dry fibre materials [mg]

L_n = arithmetic average fibre length [mm]

n = number of fibres in the sample

4. **Fines content**. The FQA defines the dimension of fines as all detectable fibres under 0.2 mm in length. The FQA calculates the length-weighted fines percentage as the percentage of the total length of all measurable fines divided by the total length of all fibrous materials, fines included.

5. **Handsheet properties**. Handsheets with basis weight of 60 g m^{-2} were prepared from the feed pulp and the reject samples according to the procedures outlined in TAPPI Standard Methods T 205 sp-95. Handsheets formed were conditioned at 50% Relative Humidity at 23°C before testing. The properties of the handsheets produced from the samples were measured in compliance with the relevant TAPPI standards (Table 4). The handsheet strength properties were of particular interest.

Table 4. Tested handsheet properties and relevant TAPPI test methods used in this study.

Handsheet property	TAPPI Standard
Tensile breaking (tensile strength, stretch, TEA, breaking length)	T 494
Tear	T 414
Burst	T 403
Porosity	T 460

6. **Light microscope imaging**. Light microscope images of the feed pulp as well as every fraction obtained at the first- and second-stage of fractionation were taken using a digital camera attached to a Nikon Optiphot microscope.

3 Influence of pressure screen operating parameters on fractionation

The first part of this study is concerned with finding the best condition for fractionation for the later multi-stage screening. The goal of this part of the study is to obtain the best combination of pressure screen design and operating parameters that can result in (1) a reject fraction with the highest average fibre length and (2) a fines enriched accept fraction that could be used as a potential raw material for the production of Nanocrystalline Cellulose (NCC).

Pressure screen performance is strongly related to its design and operating parameters. Some of these parameters include aperture diameter, aperture velocity, V_s and volumetric reject ratio, R_v. V_s was varied while keeping R_v constant and vice versa using one screen cylinder at a time. Table 5 shows the various combination of operating parameters that were tested. The effects of varying these operating parameters on screening performance in terms of fibre passage ratio, $P(l)$ and reject thickening behaviour, T are presented in this chapter. This section also discussed the differences between accept and reject fractions in terms of average fibre length and the percentage of fines produced from various combination of operating parameters.

Table 5. Combination of operating parameters that were tested using three different screen cylinders at the first stage of fractionation.

Aperture diameter [mm]		**0.5**				**0.8**			**1.0**
Screen open area, A_o [m^2] [a]		**0.002833**				**0.007904**			**0.02139**
Rotor tip speed, V_t [ms^{-1}]		**16**							
Aperture velocity, V_s [ms^{-1}]		**0.3**	**0.5**	**0.7**	**1.0**	**0.3**	**0.5**	**0.7**	**0.3**
Accept flow rate, Q_a [GPM]		**13.47**	**22.45**	**31.44**	**44.91**	**37.58**	**62.64**	**87.70**	**101.71**
Volumetric reject ratio, R_v	**0.3**				√		√	√	√
	0.4	√	√	√	√	√	√	√	√
	0.5	√	√	√	√	√	√	√	√
	0.6	√	√	√	√	√	√	√	
	0.7	√	√	√		√			

[a] The open area is calculated by multiplying the total number of apertures to the cross sectional area of one aperture. For the screen with 0.5 mm, 0.8 mm and 1.0 mm apertures, 2.2%, 5.6% and 15.8% of the total screen cylinder area is open, respectively.

The rotational speed of the rotor was kept constant at 1500 rpm which corresponds to a rotor tip speed of 16 ms^{-1}. This rotor speed is fairly moderate and it was found to be adequate for most of the fractionation trials as screen ‘blinding’ was effectively avoided. However, for the screen cylinder with 0.8 mm apertures, the screen readily blinds at the beginning of the V_s = 1.0 ms^{-1} trial. This aperture velocity corresponds to an accept flow rate, Q_a of 125.3 GPM. At this V_s and Q_a, a higher rotor speed would be required to prevent the screen apertures from plugging. Therefore, no trials were conducted for V_s above 0.7 ms^{-1}. Also, for some trials, the R_v was not lowered to under 0.4 to reduce the risk of reject line plugging.

3.1 Fibre passage ratio and reject thickening behaviour

3.1.1 Effect of screen cylinder aperture diameter

Fibre passage ratio, P(l)

Pressure screen performance was assessed in terms of fibre passage ratio, P(l). Within the range of the operating parameters tested, as shown in Table 5, comparison of the effect of the screen aperture diameter on fibre passage was made at constant R_v = 0.5 and V_s = 0.3 ms^{-1}. Data obtained from the consistency measurement and fibre analysis from the Fibre Quality Analyzer (FQA) were used to calculate the passage ratio of each length class i, $P(l_i)$ based on Equation 1-9 over the entire range of fibre length to obtain the P(l) curves. Figure 18 shows an example of the calculated values of passage ratios as a function of fibre length for the screen cylinders with 0.5 mm, 0.8 mm and 1.0 mm apertures.

For an infinitesimally short fibre length, P(l) is the maximum at unity. As the fibre length increases, P(l) starts to decrease and begins to approach 0 which suggests difficulty in fibre passage through the screen apertures for longer fibres. At a passage ratio of zero, none of the fibres are able to pass through the apertures. The data in Figure 18 are fitted to a negative exponential function that has a form equivalent to Equation 1-10. This empirical relationship was modeled by Olson et al. for both slotted and smooth-holed screen apertures and can be characterized using a single parameter, λ [11]. This model displays good agreement with experimental data.

Reducing the screen aperture diameters changes the shape of the P(l) curves. λ was found to decrease from 1.821 to 1.075 and lastly to 0.760 for the screen cylinders with 1.0 mm, 0.8 mm and 0.5 mm apertures respectively. Consequently, the bulk passage ratio, P also decreased which to some extent implies a lower degree of fractionation. This is not unexpected given that with bigger aperture size, more long fibres are able to pass through the apertures resulting in an impure fines and short fibre fraction in the accept.

The coefficient λ is more related to the long fibre passage than to the short fibre passage. As can be seen in the example of the P(l) curves in Figure 18, generally with a decrease in λ, the passage ratio of the long fibres dropped, but that of short fibres remains fairly high. Olson et al. gave the physical interpretation of λ such that fibre with length 0.61 λ will have a passage ratio of 0.5 (50% probability of passing through the screen apertures) [10].

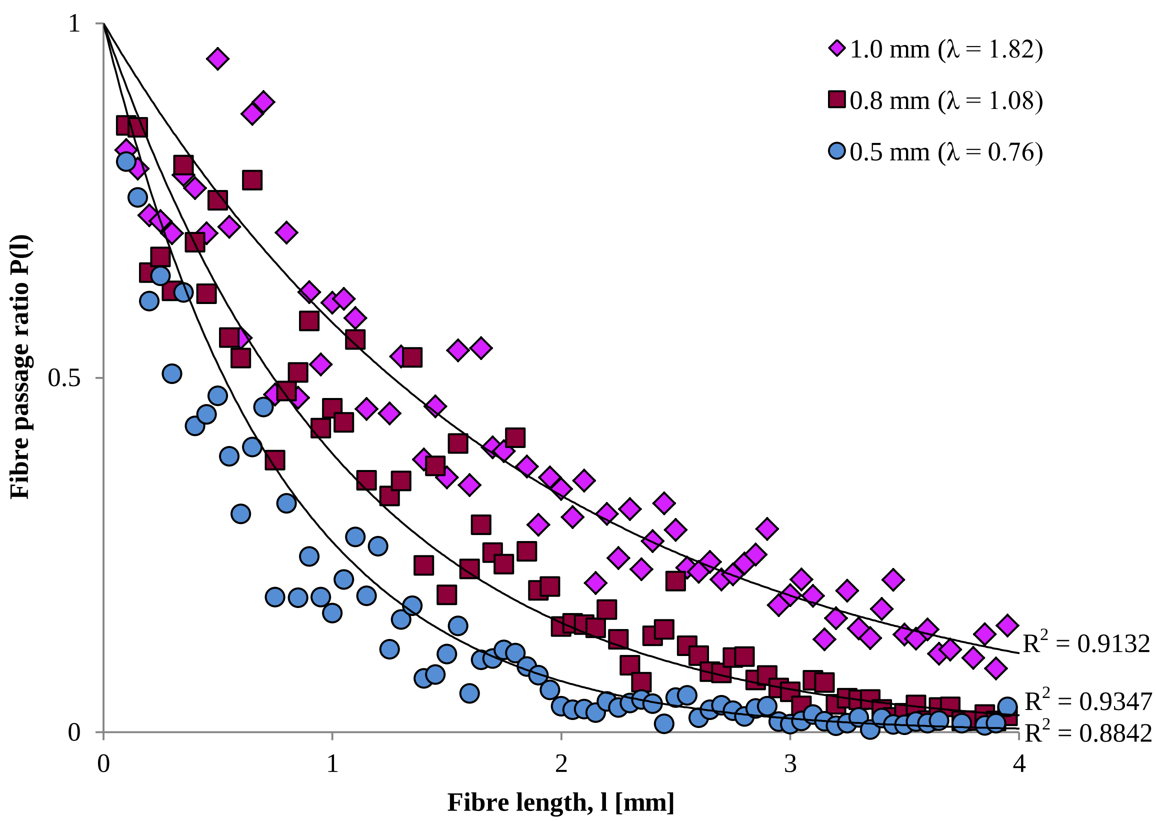

Figure 18. Fibre passage ratio plotted against fibre length for three aperture diameters at a constant R_v of 0.5 and V_s of 0.3 ms^{-1}. Solid lines represent data fitted by Equation 1-10.

The estimated coefficient λ is plotted for every V_s-R_v-aperture diameter trial combination as shown in Figure 19. The 'shape constant' β in Equation 1-10 was set to 1 when determining λ which is typical for smooth-holed screen cylinders [10]. With decreasing aperture diameter, λ decreases and thus P also decreases regardless of other operating parameters such as R_v and V_s. This means better fractionation using the screen cylinder with 0.5 mm apertures. λ was also found to exhibit a roughly exponential relationship with respect to the aperture diameter as shown in Figure 19. A linear trend was found in a study by Olson using TMP pulp for smooth-holed screen cylinders with aperture diameter ranging from 0.8 to 2.1 mm [11].

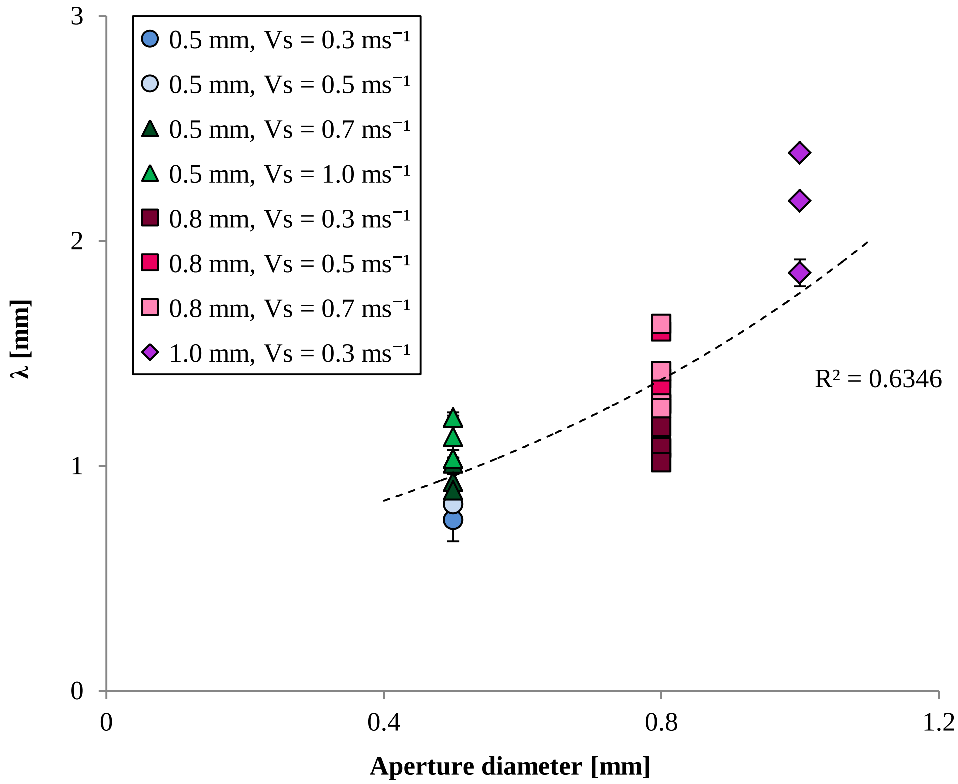

Figure 19. λ versus aperture diameter plotted for all apertures velocities, V_s and volumetric reject ratio, R_v tested. R_v ranges between 0.3 to 0.7 for each aperture diameter. Error bars represent standard deviations.

Reject thickening

Figure 20 shows the reject thickening factor, T calculated using Equation 1-2 for the three screen cylinders at constant V_s of 0.3 ms^{-1}. Predicted T was obtained using Equation 1-7. The bulk passage ratio values, P required for the reject thickening estimation were found to be equal to 0.41, 0.27 and 0.16 for the screen cylinders with 1.0, 0.8 and 0.5 mm apertures respectively. The predicted T values plotted as lines in Figure 20 demonstrate good agreement with experimental results. However, the fit of the thickening model is progressively worse for bigger aperture diameter.

Thickening increases exponentially with decreasing R_v as more water is removed from the feed to the accept side with a smaller R_v. T also increases with decreasing probability of overall fibre passage, P. Operating the pressure screen at a low R_v poses a risk of plugging the reject line due to a high reject thickening. There is a maximum value for T, after which the reject line plugging will occur. Therefore, it is desirable at times to minimize the thickening for better screen runnability.

At constant V_s and R_v, reject thickening increased with decreasing aperture diameter because less fibres are accepted with smaller apertures. In other words, rejects of the screen cylinder with 0.5 mm apertures experience a greater level of thickening due to a higher number of fibres that are not able to pass through the screen apertures as easily as during the fractionation using the screen with 1.0 mm apertures. Difficulty in fibre passage using 0.5 mm apertures or higher thickening in rejects resulted in better separation of long and short fibres, and thus better fractionation.

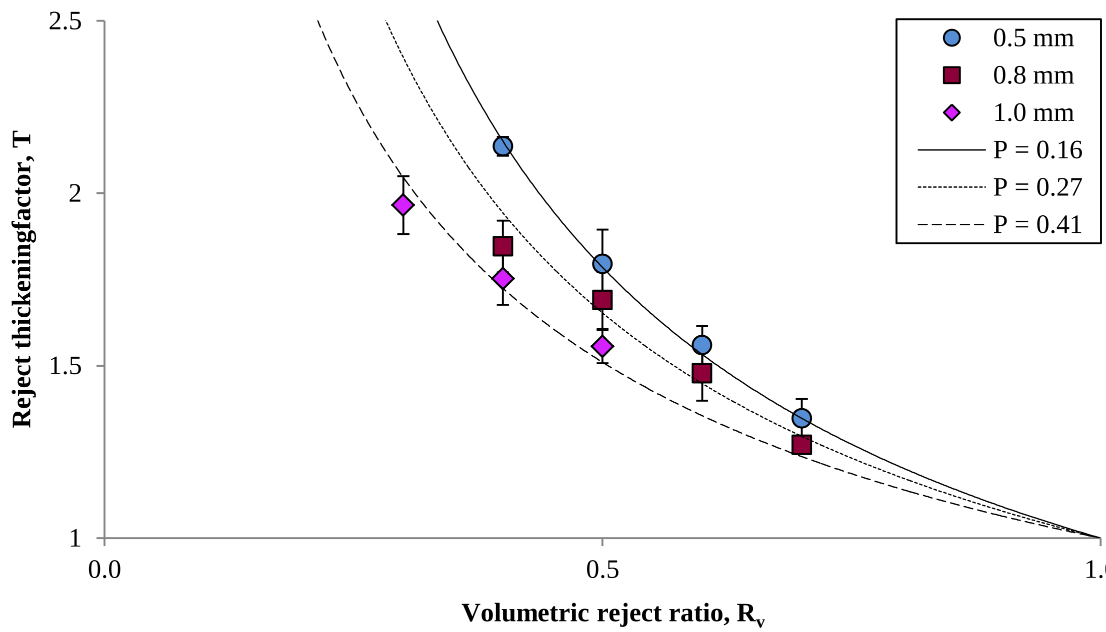

Figure 20. Calculated reject thickening factor, T as a function of volumetric reject ratio, R_v for several aperture diameters at constant V_s of 0.3 ms^{-1}. Smooth and dotted lines show predicted reject thickening calculated using Equation 1-7. Error bars represent standard deviations.

3.1.2 Effect of aperture velocity

Fibre passage ratio

Figure 21 shows λ plotted at a constant R_v of 0.5 with the aperture velocity, V_s being varied from 0.3 ms^{-1} to 1.0 ms^{-1} for the three screen cylinders. At this constant R_v, increasing V_s leads to an increase in λ. A high V_s (or accept volumetric flow rate, Q_a) assists in the pulp passage through the apertures. Also, at higher aperture velocities, the greater fluid drag forced the long fibres through the apertures more than the short fibres [22].

Previous study by Olson et al. using a TMP pulp found no dependence of fractionation efficiency on aperture velocity contrary to what is found in this study [11]. Increasing V_s increased λ linearly. An increase in λ subsequently leads to an increase in the long fibre passage through the screen apertures and therefore a decrease in the fractionation extent.

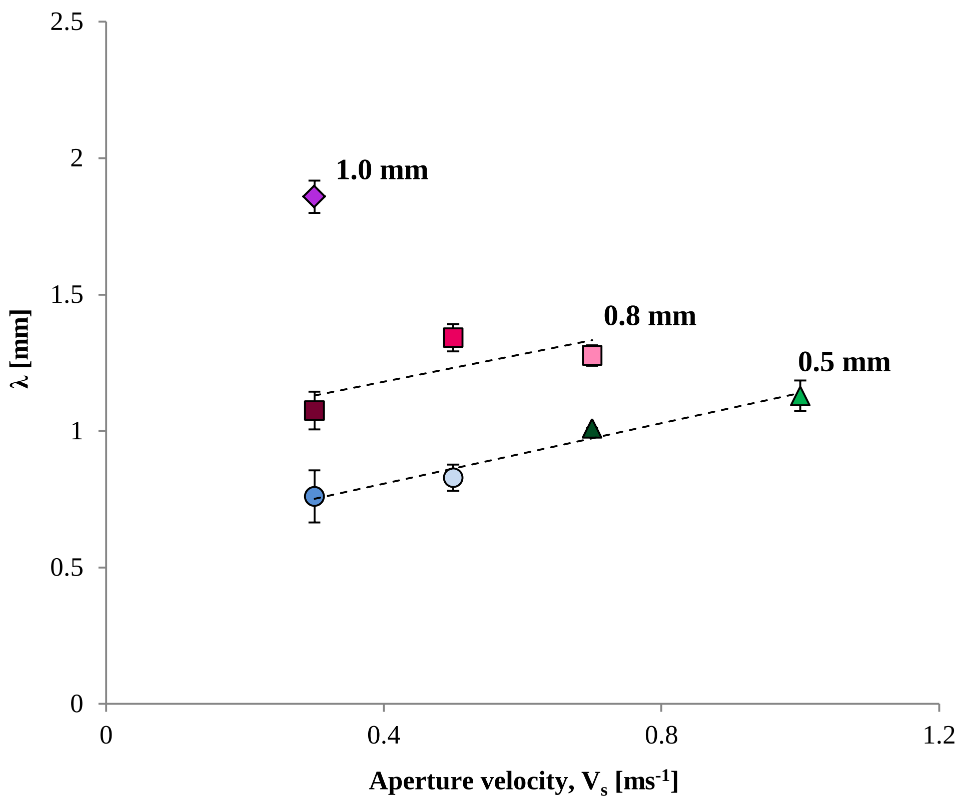

Figure 21. λ versus aperture velocity showed only for constant volumetric reject ratio of 0.5 for the three aperture diameters. Error bars represent standard deviations.

Reject thickening

Reject thickening factor, T data for various V_s is plotted in Figure 22. Changing the V_s in the range of 0.3 ms^{-1} to 1.0 ms^{-1} affected the thickening to a smaller extent than changing the aperture diameter. Increasing the V_s however reduced the level of thickening and thus indicates a lower degree of fractionation efficiency. Too high of a V_s could cause fibre crowding on the screen cylinder surface which would then lead to screen blinding.

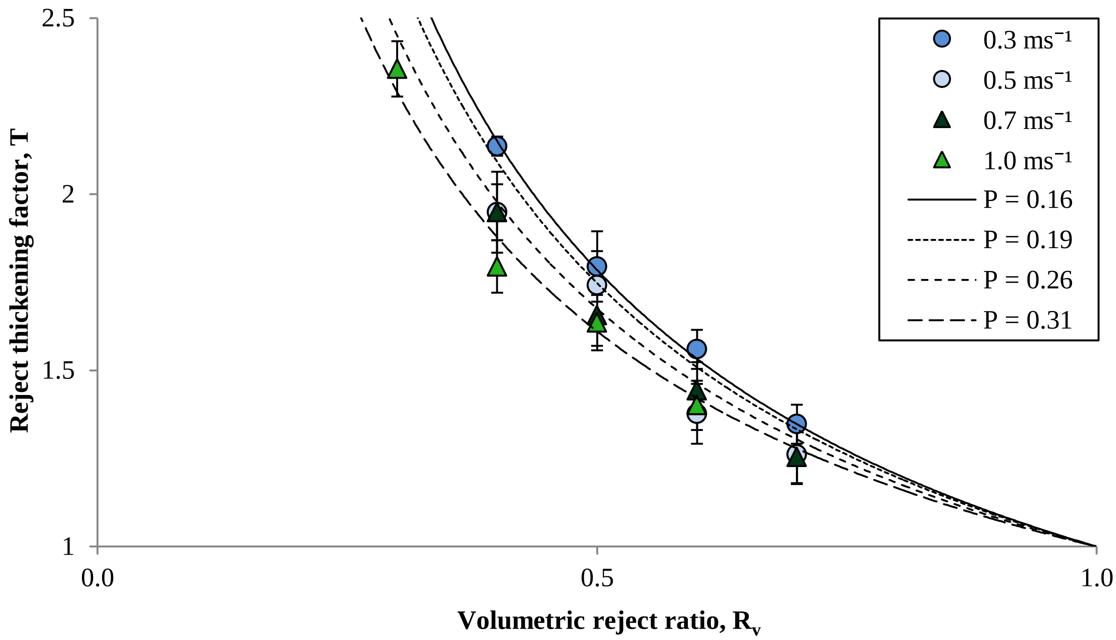

Figure 22. Reject thickening factor versus volumetric reject ratio, R_v at various aperture velocities, V_s using screen cylinder with 0.5 mm apertures. Corresponding bulk passage ratios, P are shown in the legend. Error bars represent standard deviations.

3.1.3 Effect of volumetric reject ratio

Fibre passage ratio

Comparison of the volumetric reject ratio, R_v effect on passage ratio, P for all trials conducted during the first stage is demonstrated in Figure 23. R_v and λ seem to display a negative linear relationship unlike previously shown for TMP pulp in [11] where fibre passage and fractionation efficiency are wholly dependent on aperture size. Increasing R_v has the effect of increasing the bulk fibre passage, P which is not entirely desirable in fractionation. The increase in long fibre passage through the apertures decreases fractionation efficiency. λ, and consequently P was found to have a larger dependency on R_v for the screen cylinder with 1.0 mm apertures compared to the 0.5 mm and 0.8 mm apertures.

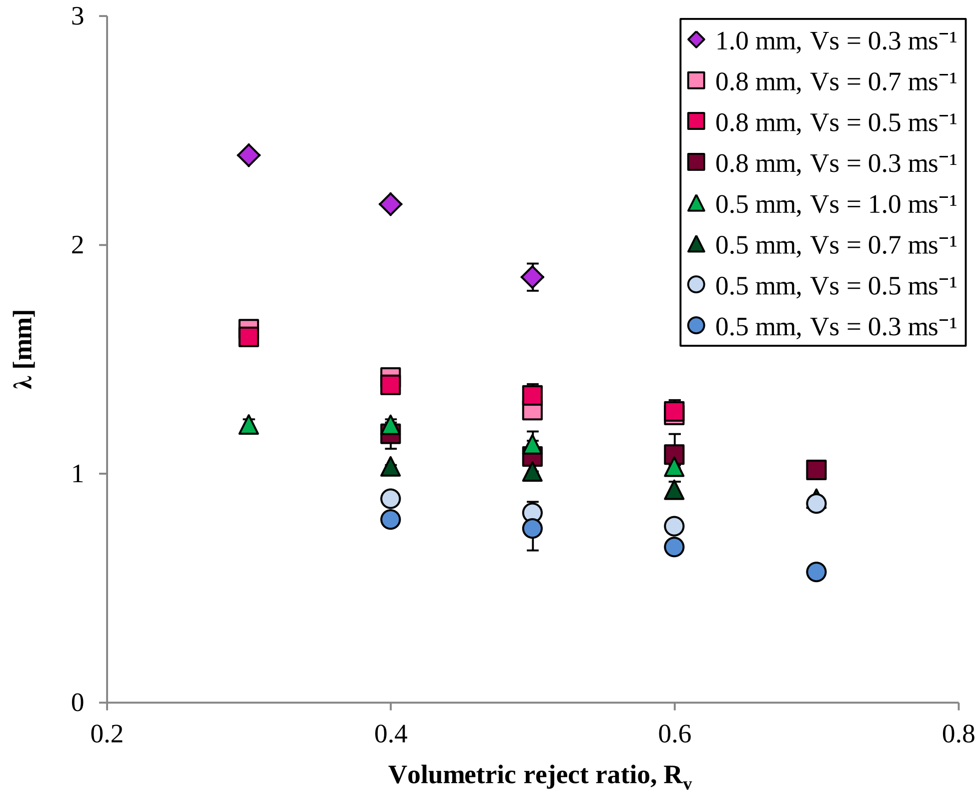

Figure 23. λ plotted against volumetric reject ratio, R_v. Increasing R_v appears to correlate negatively with λ. Error bars represent standard deviations.

In brief, reducing the aperture diameter and aperture velocity, V_s and also increasing the volumetric reject ratio, R_v evidently showed improvement in fibre separation indicated by the decreased in λ or the bulk fibre passage, P.

3.2 Accept pulp quality

Resulting accept and reject fractions were evaluated in terms of the fibre properties and the amount of the desired components in each streams in order to quantify the extent of fibre fractionation. The properties of interest are average fibre length and fines percentage which were obtained using the Fibre Quality Analyzer (FQA).

3.2.1 Length-weighted average fibre length

The length-weighted average fibre length of the accept fraction decreases marginally as the volumetric reject ratio, R_v increases as shown in Figure 24. The effect of the aperture diameters on the average fibre length of the accept fraction is more dominant than R_v. The lowest average length of about 0.92 mm was obtained using the screen cylinder with 0.5 mm apertures operating at an R_v of 0.7 and at an aperture velocity, V_s of 0.3 ms^{-1}. The low average fibre length is the result of a high proportion of fines and short fibres in the accept stream.

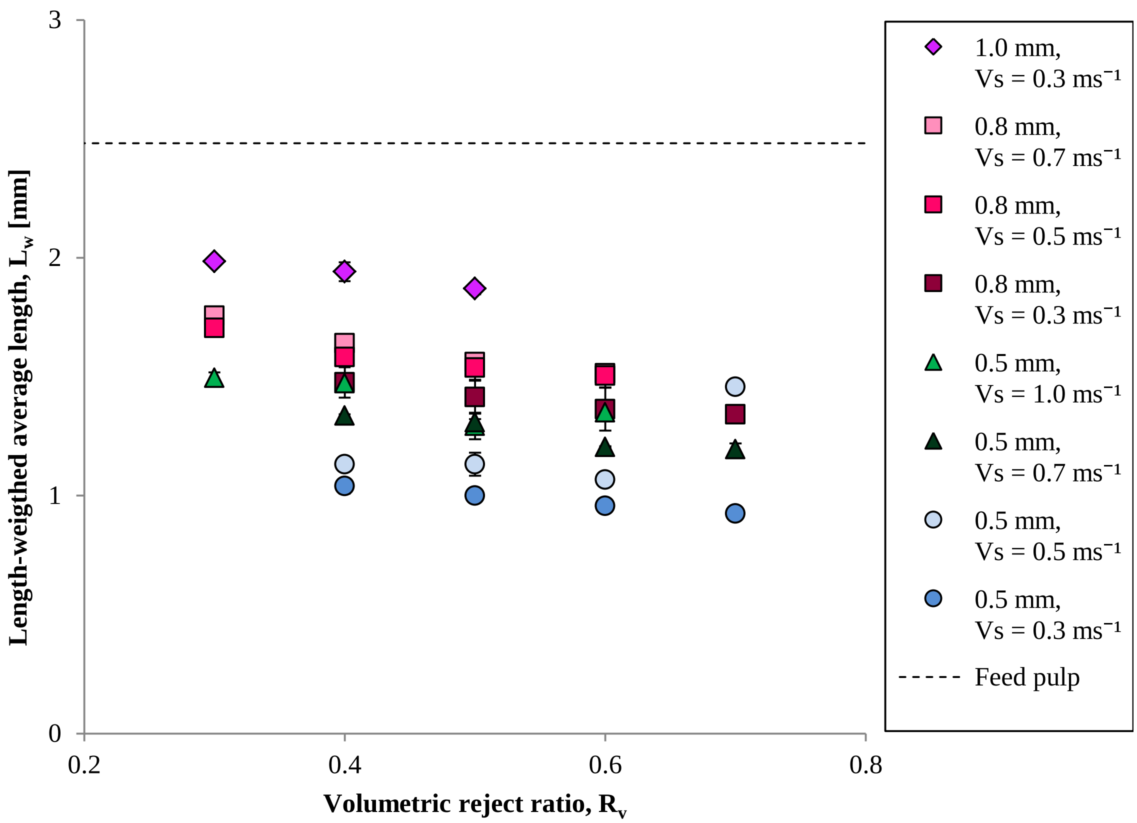

Figure 24. Accepts length-weighted average length, L_w versus volumetric reject ratio, R_v showed for all conditions that were tested. Error bars represent standard deviations.

3.2.2 Length-weighted fines percentage

The length-weighted fines percentage plotted against R_v for all trials in Figure 25 displays opposing trends as expected compared to the average length in Figure 24. FQA results of the first-stage of fractionation showed that reducing the screen aperture diameter and V_s increased the fines content in the accept stream. Using the screen with 0.5 mm apertures, less long fibres are directed into the accept stream. Also, the flow of fines seems to be dependent on R_v. Increased fines percentage in the accept was observed with an increase in the R_v.

The fines content in the feed pulp is shown as dotted line in Figure 25. The difference in the fines percentage between the accept fraction and the feed pulp was quite considerable. The highest length-weighted percentage of fines was found to be around 30% which is about 10 times higher than that of the feed pulp, produced at R_v = 0.7 using the screen cylinder with 0.5 mm apertures.

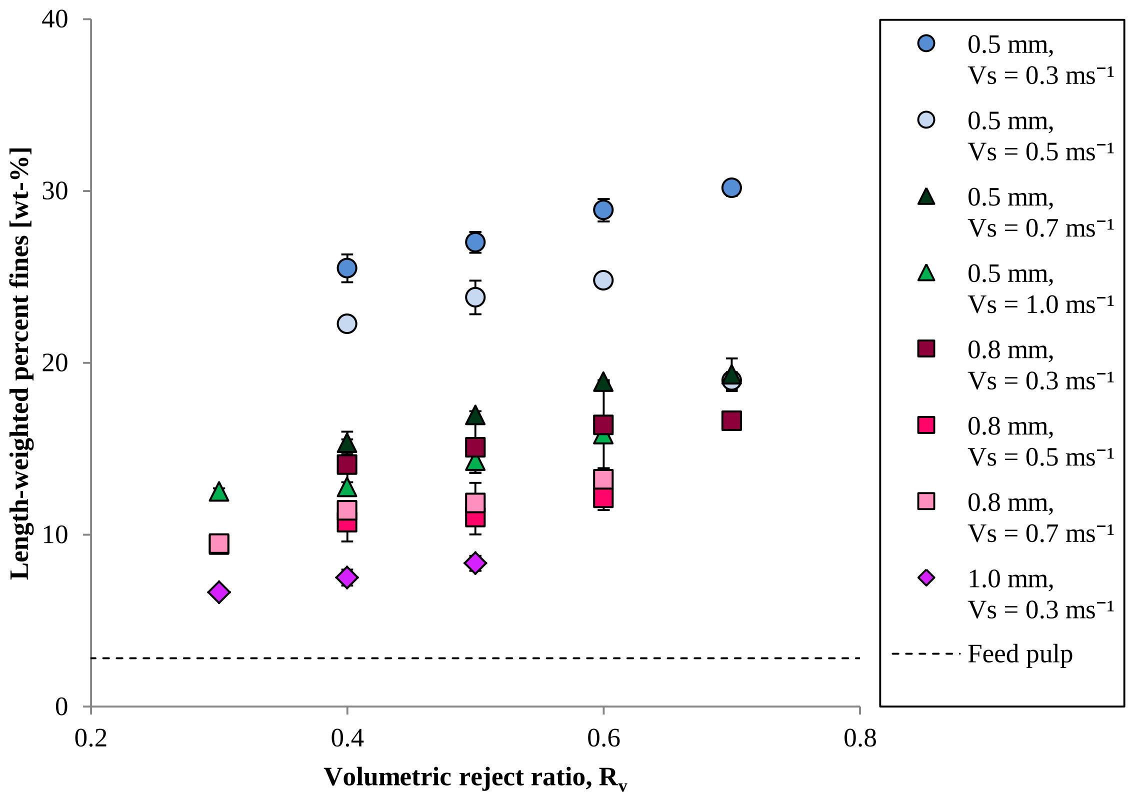

Figure 25. Accepts length-weighted percent fines versus volumetric reject ratio, R_v showed for all conditions that were tested. Error bars represent standard deviations.

Another related parameter that describes the split between the feed and reject besides R_v is the mass reject ratio, R_m expressed as Equation 3-1. The mass reject ratio is not an operating parameter and is less commonly used due to difficulties measuring the mass flows. However, an R_m value is more meaningful as it tells us how much of a dry mass of fibre is being rejected, ignoring the water.

$$R_m = \frac{m_r}{m_f} = \frac{c_r Q_r}{c_f Q_f} \qquad \textbf{3-1}$$

The percentage of fines is plotted against R_m as shown in Figure 26. The highest fines percentage in accept at 30% was obtained at $R_m = 0.97$ ($R_v = 0.7$). This means that, only 3% of the mass of the feed pulp ended up in the accept stream and it is rich with fines. With the aperture diameter of 0.5 mm, the data points from Figure 25 are shifted more towards higher values of R_m compared to the aperture diameters of 0.8 mm and 1.0 mm. With smaller aperture diameter, there is a smaller open area in this case, less fibres directed towards the accept side, less fibre mass in the accept stream and thus a higher R_m.

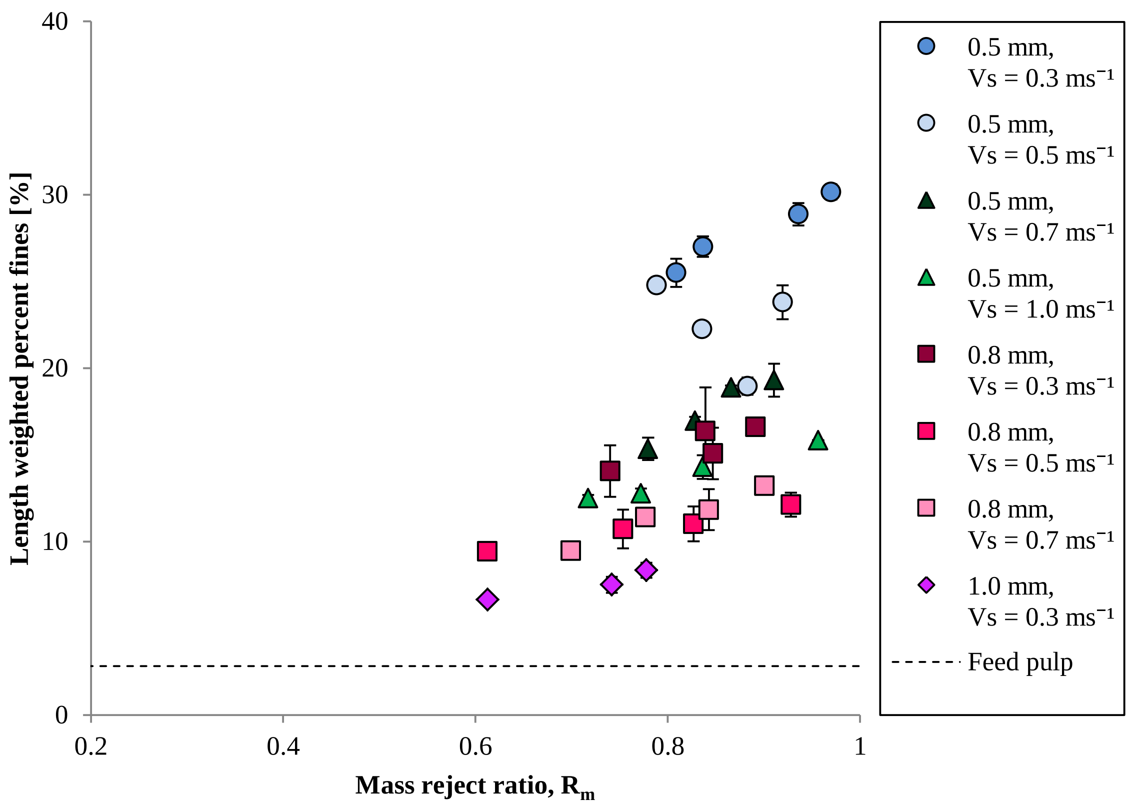

Figure 26. Length-weighted percent fines in accepts versus mass reject ratio, R_m showed for all conditions that were tested. Error bars represent standard deviations.

3.3 Reject pulp quality

3.3.1 Length-weighted average fibre length

The change in the rejects average fibre length was not significant for all operating parameters combinations that were tested. This was as predicted as little mass was removed from the feed pulp to the accept which consisted of mainly short fibres and fines, and therefore there is no significant difference in the length distribution of the feed and rejects. However, overall, the average fibre length of the rejects is higher than the average fibre length of the feed pulp that is shown as a dotted line in Figure 27.

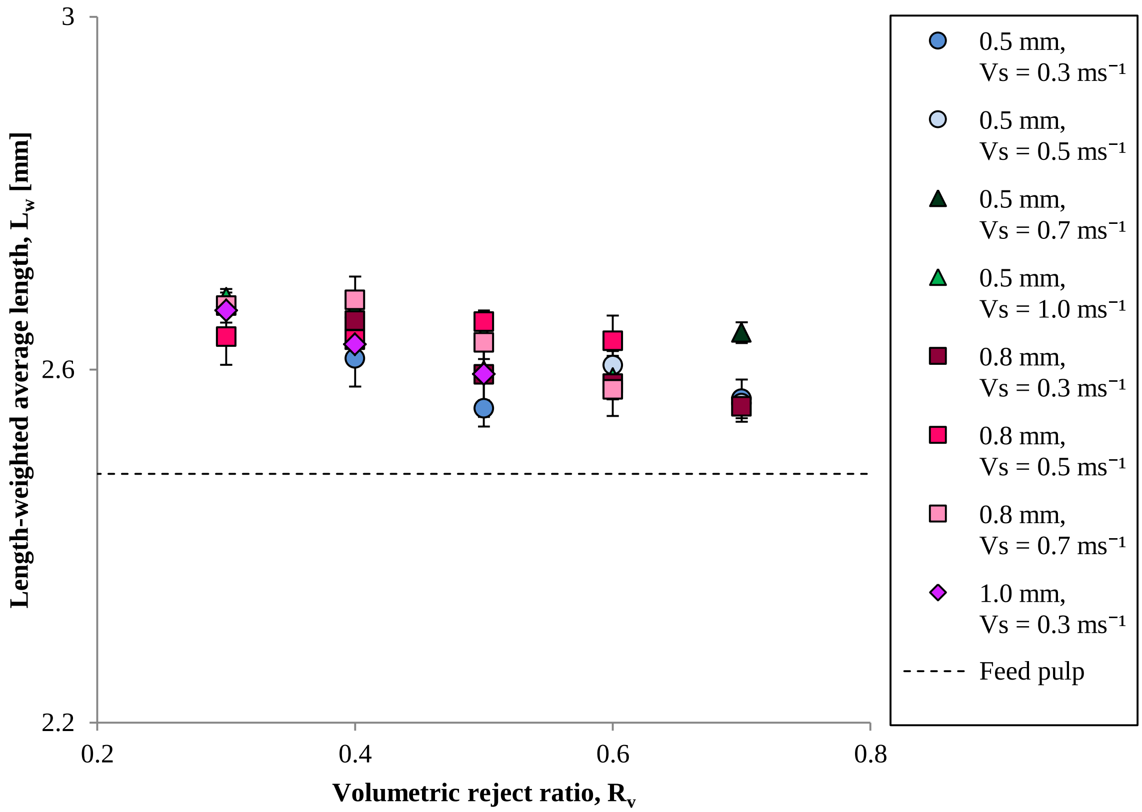

Figure 27. Length-weighted average fibre length in rejects versus volumetric reject ratio, R_v showed for all conditions that were tested. Error bars represent standard deviations.

3.3.2 Length-weighted fines percentage

NBSK pulp such as the one used in this study is low in fines percentage even prior to fractionation. Similar to the average fibre length, little change in the percentage of fines was found in the rejects with the multitude of operating parameter combination tested. However, with the increase in R_v, a small increase in the fines percentage was found and overall, the fines percentage is slightly lower than that of the feed pulp. As fines follow the flow with water, the amount of fines rejected should be proportional to R_v. The lowest fines content at 1.4% which is about half of the feed was obtained using the cylinder with 0.5 mm apertures operating at $R_v = 0.3$ and at aperture velocity, $V_s = 1.0\ ms^{-1}$.

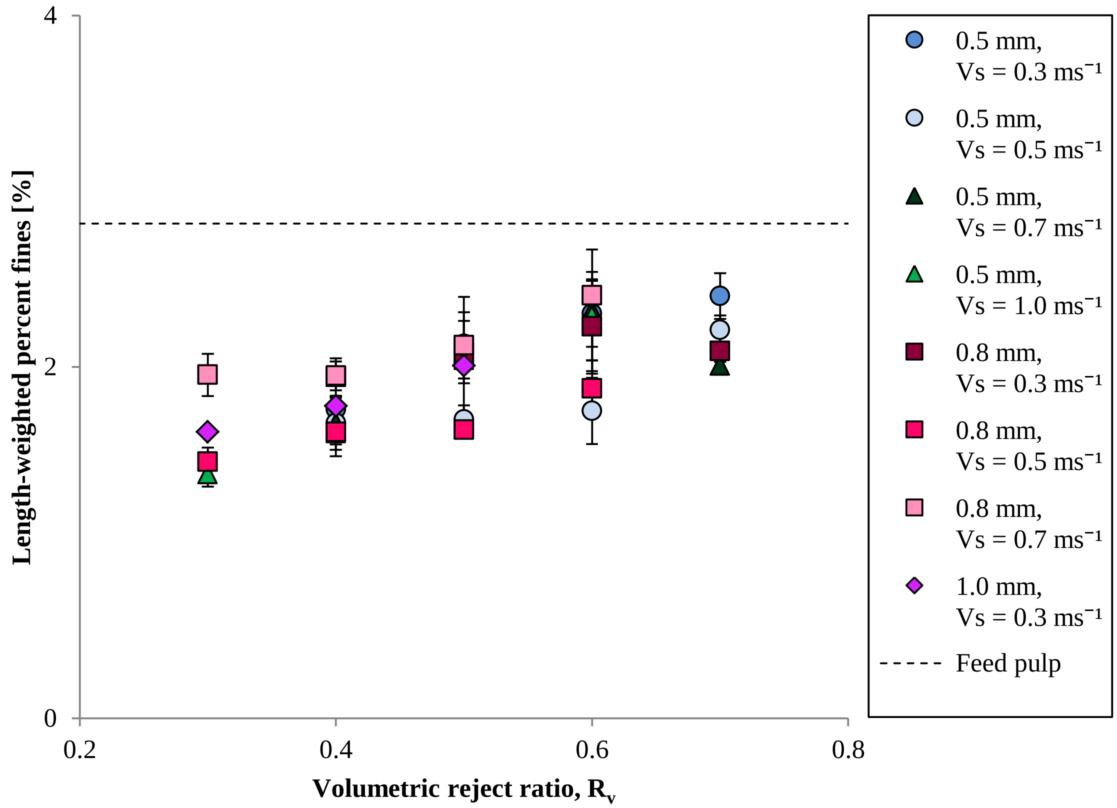

Figure 28. Rejects length-weighted percent fines versus volumetric reject ratio, R_v showed for all conditions tested. Error bars represent standard deviations.

From the results of this section, it is clear that fractionation results are strongly dependent on the combination of the pressure screen operating parameters. The best operating parameters that are suitable for the purposes of this study, which consist of using the smallest aperture diameter, lowest V_s as well as highest R_v are employed and the fractionation results are discussed in the next chapter.

4 First stage of fractionation

This section deals with the fractionation stage shown in the boxed area in Figure 29. As stated previously, the goal of the first stage of fractionation was to obtain operating parameters such that the accept fraction contains the most fines and the reject fraction has the highest average fibre length, while maximizing all the pulp mass in the rejects. The best conditions for fractionation were determined and discussed in the previous chapter and the corresponding results are presented in this chapter.

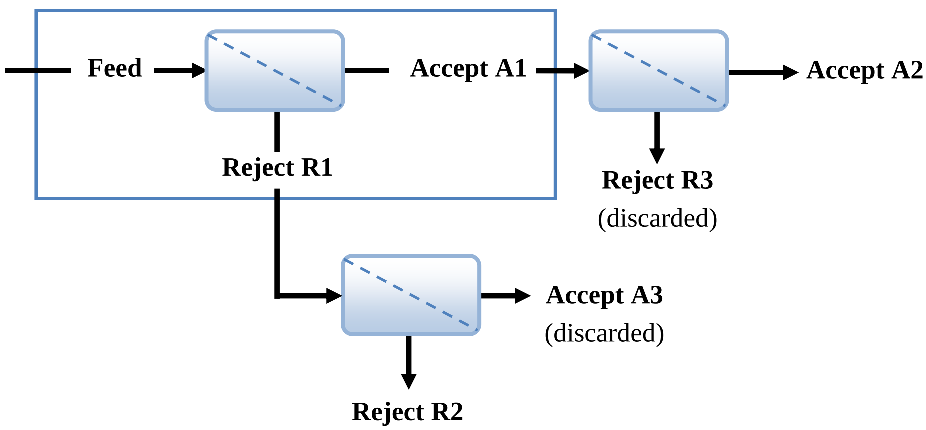

Figure 29. Multi-stage fractionation process. Boxed area shows first-stage of fractionation.

4.2 Screening conditions and their effects on fractionation

Table 6 shows the screening conditions chosen for the first stage fractionation. As anticipated, there is a clear distinction of accepts and rejects in terms of the average fibre length as the pressure screen fractionates mainly on the basis of length [9]. Under the selected conditions, the average fibre length of the accept fraction (A1) was found to be 0.92 mm while the average fibre length in the rejects (R1) is about 2.60 mm. Accept fraction also comprises of a very high proportion of fines, about 30 wt-% compared to the corresponding rejects at only 2.5 wt-% of fines as given in Table 6 and Figure 30. The differences are quite extreme and this demonstrates successful fractionation.

Accept only consisted of 3 wt-% of the mass of the feed pulp. Extracting only a slight amount of the feed pulp which contained the low extreme of the length distribution had a considerable effect on the resultant reject properties in terms of the average fibre length and fines content as can be seen in Table 6.

Table 6. Optimum screening conditions for the first stage of fractionation. Fractionation results are presented in length-weighted (LW) averages.

Screening conditions	
Aperture diameter [mm]	0.5
Aperture velocity, V_s [ms^{-1}]	0.3
Volumetric reject ratio, R_v	0.7
Rotor tip speed, V_t [ms^{-1}]	15

Fractionation results	**Feed**	**Accept (A1)**	**Reject (R1)**
Consistency [%]	1.1	0.11	2.1
Freeness [mL CSF]	660	-	700
LW average fibre length [mm]	2.48	0.92	2.58
LW percent fines [wt-%]	2.82	30.17	2.01
Volume split ratio [%]	100	30	70
Mass split ratio [%]	100	3	97

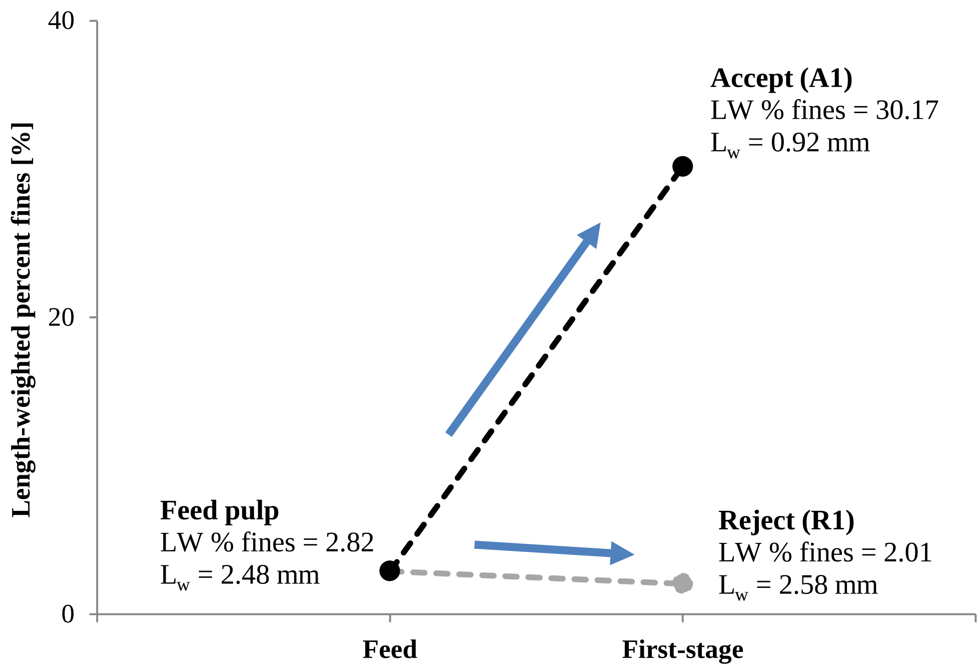

Figure 30. Changes in the length-weighted percent fines (LW % fines) and length-weighted average fibre length, L_w after the first stage of fractionation.

4.1.1 Freeness change

The freeness level of the feed and reject fractions were measured using a Canadian Standard Freeness (CSF) test. A freeness value has a direct relation to the fines content in a pulp suspension [4]. Reducing the fines content in a pulp suspension can also provide a more open network in a pulp and therefore, water is able to drain through the suspension more readily. Freeness values are virtually inversely proportional to the amount of fines in a pulp suspension.

The freeness value of the reject fraction is found to be higher than the feed; it increased from 660 mL CSF to 700 mL CSF. Fines removal from the feed improved the drainage and freeness of the R1 fraction. At the selected screening conditions, a high proportion of fines and short fibres ended up in the accept stream and this supports the freeness results.

The accept fraction was not tested for freeness. Accepts are assumed to have a very low freeness value based on the extended duration required to dewater the accept samples during filtration for consistency evaluation. The dewatering tendency of a pulp suspension is related to the freeness values. A drop in freeness is known to cause poor dewatering [4].

A high freeness value is desirable for pulp or paper machine productivity as it provides higher runnability in fast paper machines. Also, a rise in freeness (and thus a drop in fines content) allows pulp to be refined to a higher strength. Refining process develops the tensile strength of a pulp though fibrillation of the cell wall and at the same time it generates more fines fraction in that pulp. By fractionating out fines from the reject fraction before the refining process, pulp can be refined to a higher strength [5].

4.2 Fibre length distribution changes

Fractionation modifies the fibre length distribution of the resulting fractions. Knowledge of the fibre length distribution is important as two heterogeneous pulps can sometimes have the same average values but different proportion of short and long fibres. Figure 31 shows the fibre length distribution of the feed and the fractions produced during the first stage of fractionation. The reject fraction length distribution is similar to that of the feed pulp. On the other hand, a difference in the feed and accept length distributions was clearly observed. Accept fraction can be seen to contain a much higher quantity of short fibres and fines compared to feed and rejects.

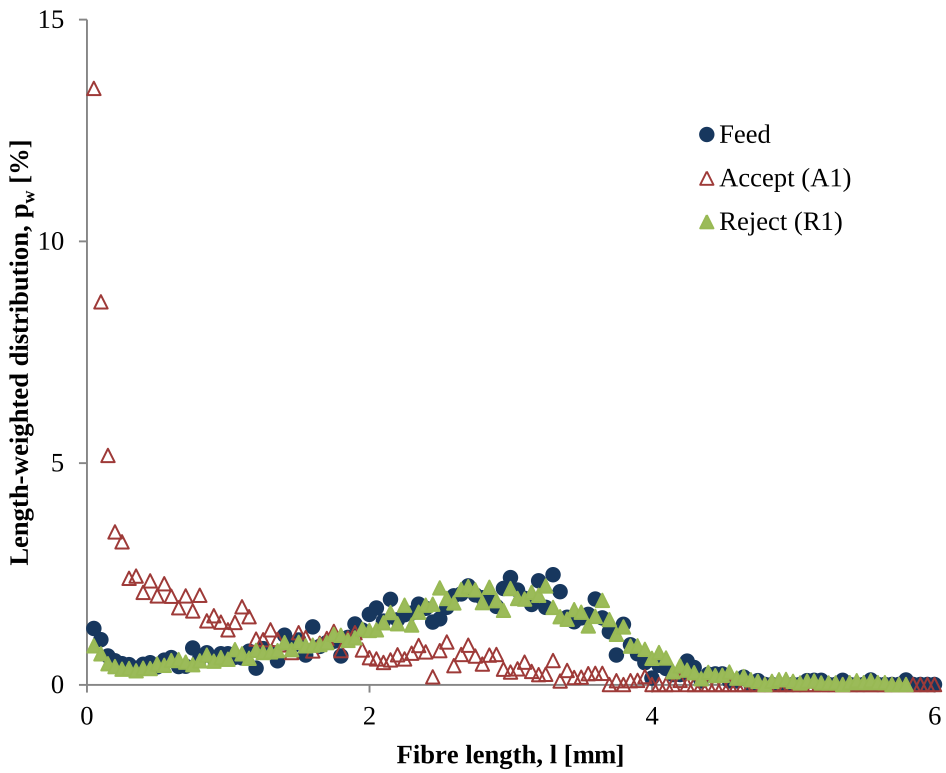

Figure 31. Comparison of fibre length distribution of the feed, accept and reject fractions after the first stage of fractionation.

4.3 Qualitative differences of resulting fractions

Light microscope images of the feed, accept and reject fractions of the first stage of fractionation were taken using a digital camera attached to a light microscope in a dark field mode to determine the physical characteristics of the resulting accept and reject fractions. Each image was photographed using a constant picture ratio and the transformation ratio from pixel to μm was determined. The images obtained are shown in Figure 32. The microscope image of the feed pulp is shown earlier in Chapter 1 as Figure 4. There is a much larger portion of fibre fragments or fines in the accept compared to feed and rejects.

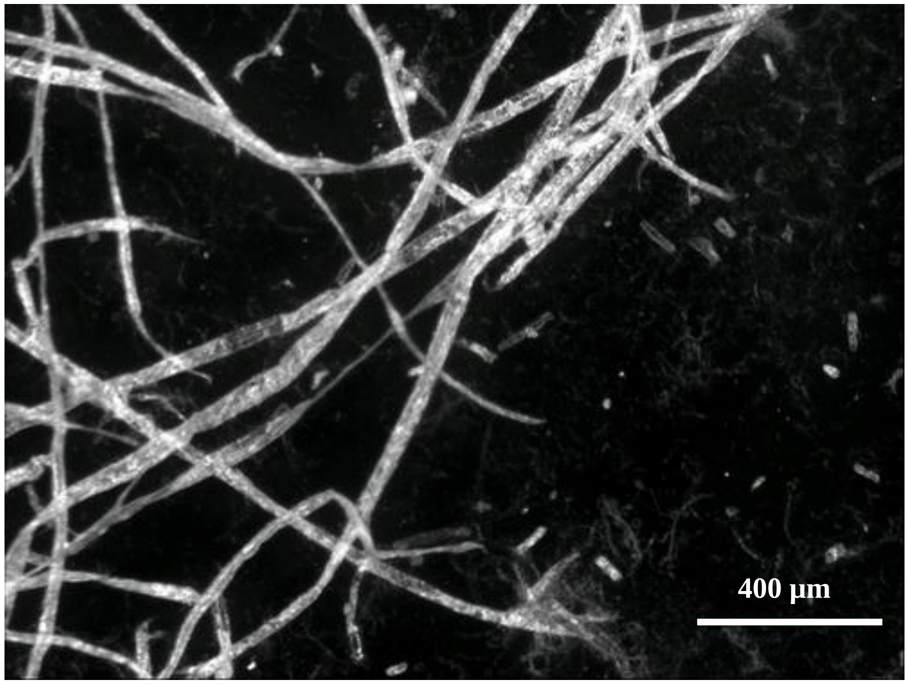

(a)

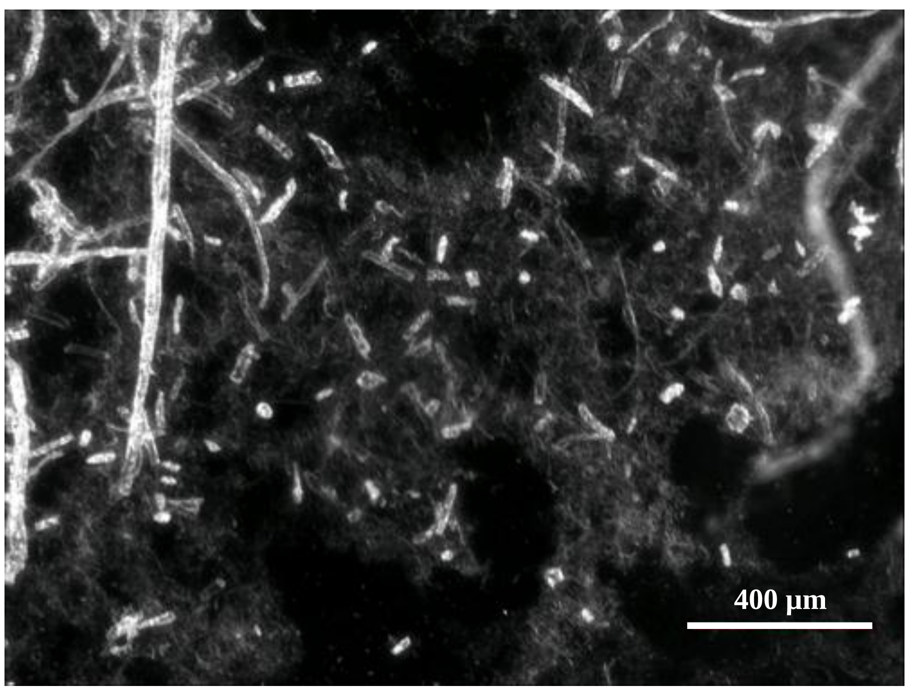

(b)

Figure 32. Images of the reject fraction R1 (a) and accept fraction A1 (b) obtained after the first stage of fractionation. Rejects contain a higher amount of long fibres. Scale bar 400 µm.

5 Rejects fractionation stages

This chapter describes the subsequent fractionation step of the reject fraction, R1 produced from the first-stage as shown in Figure 33. Multi-stage screening was anticipated to enhance the fibre fractionation by further eliminating the fines and short fibres in the reject, which would then result in a reject pulp with a higher average fibre length and a lower percentage of fines.

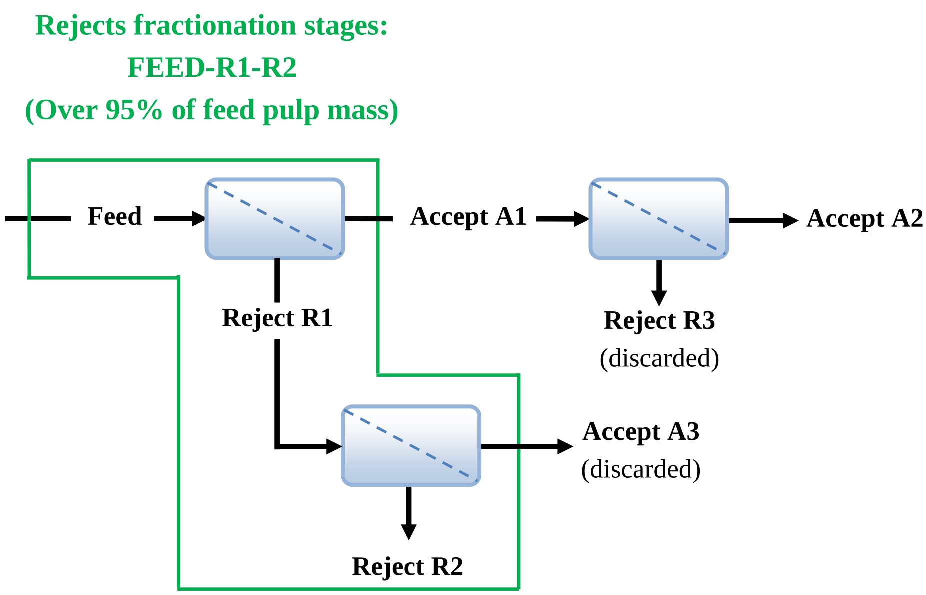

Figure 33. Multi-stage fractionation process. Boxed area shows rejects fractionation featuring two stages in cascade.

Only the screen cylinder with 0.5 mm apertures is used during the second stage. Pressure screen operating parameters used at this stage and its results are presented. Fibre passage ratios at both stages were compared. Furthermore, the results from the testing of the handsheets made using the reject fractions are discussed. Fractionation efficiency at each fractionation stage in terms of long fibre enrichment in the rejects is presented at the end of the chapter.

5.1 Effect of changing operating parameters at second-stage

5.1.1 Effect of volumetric reject ratio and aperture velocity

Significant amount of the feed pulp was rejected during the first stage (more than 97 wt-%), and minor changes in the average fibre length and fines content were observed in the reject fraction when varying the volumetric reject ratio, R_v and aperture velocity, V_s.

At the second stage, R_v and V_s were varied and their effects on average fibre length and fines content in the rejects R2 are shown in Figure 34 and Figure 35. By varying R_v at a constant V_s of 0.3 ms^{-1}, it was possible to obtain a reject fraction R2 with an average fibre length of up to 2.70 mm (Figure 34a) that contains the lowest amount of fines of about 1.55 wt-% (Figure 34b) at $R_v = 0.6$. Figure 35 shows that the percentage of fines is higher in the rejects for a higher R_v. As fines follow the flow of water, this was expected.

V_s was adjusted between 0.3 ms^{-1} and 1.3 ms^{-1} at a constant $R_v = 0.6$. Decreasing V_s decreased the average fibre length and increased the fines content as shown in Figure 35. However after the V_s reached 0.7 ms^{-1}, the effect of decreasing the V_s started to level off. Final reject R2 with average length of 2.72 mm and fines content of 1.29% was obtained when operating the screen at $R_v = 0.6$ and $V_s = 0.3$ ms^{-1}.

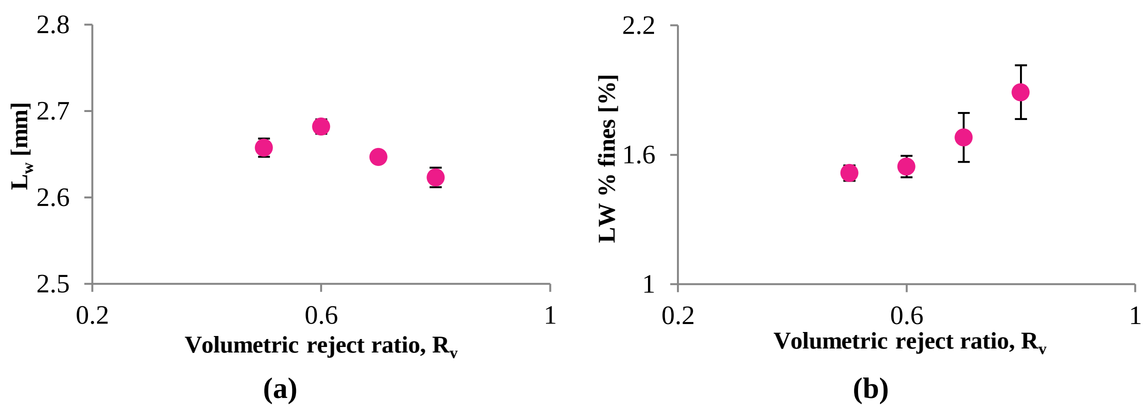

Figure 34. Changes in (a) average fibre length and (b) fines content of reject R2 after varying volumetric reject ratio, R_v. R_v was varied at a constant V_s of 0.3 ms^{-1}. Error bars represent standard deviations.

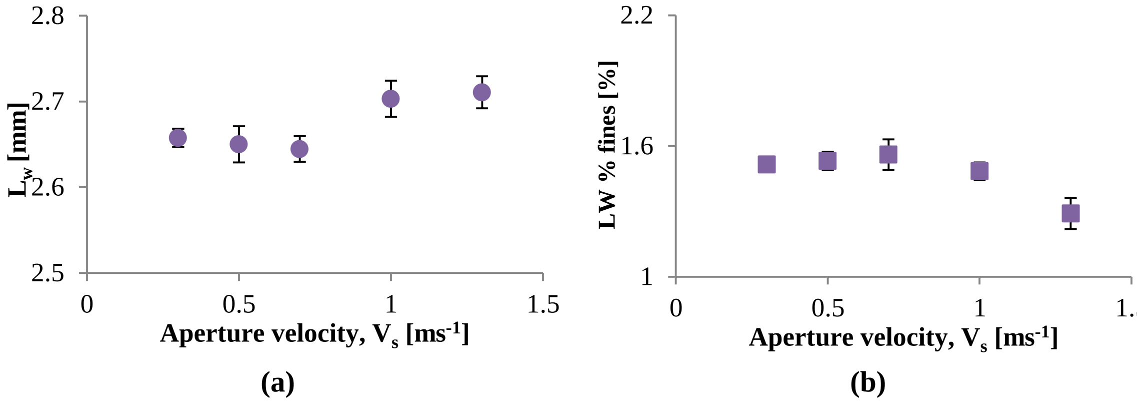

Figure 35. Changes in (a) average fibre length and (b) and fines content of reject R2 after varying aperture velocity, V_s. V_s was varied at a constant R_v of 0.6. Error bars represent standard deviations.

5.1.2 Effect of rotor tip speed

As mentioned previously, the rotor tip speed, V_t was kept constant at 16 ms^{-1} during all trials in the first stage. To ensure that there was no adverse effect of using this particular V_t on fibre fractionation, a trial that consisted of varying V_t at a constant R_v and V_s was carried out and the results are presented in Figure 36. There is a minimal dependency of fractionation on V_t over the range tested.

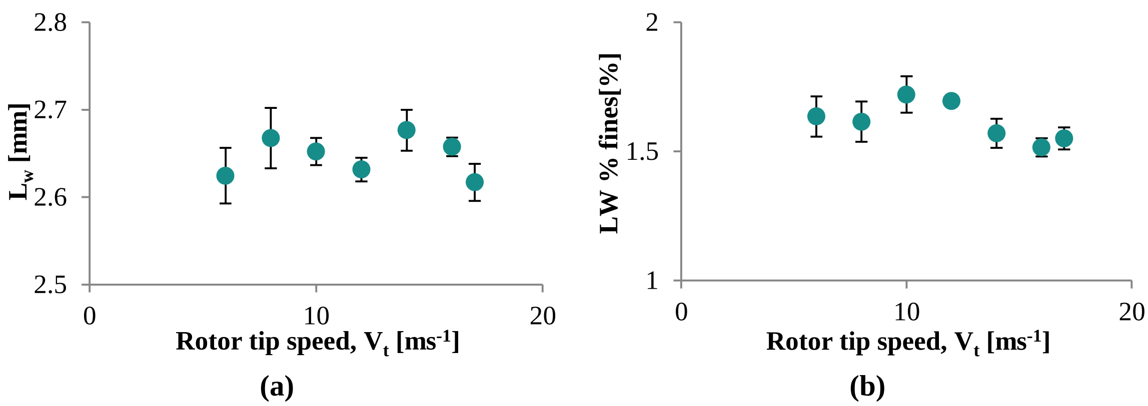

Figure 36. Changes in the average fibre length (a) and fines percentage (b) of reject R2 after varying the rotor tip speed, V_t. V_t was varied at a constant R_v of 0.6 and V_s of 0.3 ms^{-1}. Error bars represent standard deviations.

5.2 Screening conditions and their effects on fractionation

The operating parameters that were chosen for the second stage are presented below in Table 7. After the final reject fractionation stage, the pulp produced had an average length almost 10% higher than the original pulp. Fines content was reduced from 2.90% to 1.30%. These changes are illustrated in Figure 37. Fractionation had a clear effect on the fines content of the reject fractions. The freeness of the R2 pulp increased slightly from 697 mL CSF to 701 mL CSF as a result of the removal of the fines. However, the increase is within the error margin.

Fibre curl and kink were also measured using the FQA. The curl index and kink index which are indicative of fibre deformations showed insignificant changes after fractionation. The curl index was reduced from 0.156 to 0.140 and kink index from 1.59 to 1.55. The mass reject rate, R_m at the first stage was 0.97 and 0.975 at the second stage, resulting in the overall mass reject rate, R_m of 0.95.

Table 7. Screening conditions for the reject fractionation series and the fractionation results at each stage.

Screening conditions	First-stage	Second-stage
Aperture diameter [mm]	0.5	0.5
Aperture velocity, V_s [ms^{-1}]	0.3	1.3
Volumetric reject ratio, R_v	0.6	0.6
Rotor tip speed, V_t [ms^{-1}]	16	16

Fractionation results	Feed	Reject (R1)	Reject (R2)
Consistency, c [%]	1	2.1	2.5
Thickening factor, T	-	2.1	2.5
Freeness [mL CSF]	667	697	701
Average fibre length, L_w [mm]	2.48	2.58	2.72
LW percent fines [wt-%]	2.90	2.06	1.30
Curl index	0.156	0.147	0.14
Kink index [mm^{-1}]	1.585	1.556	1.553

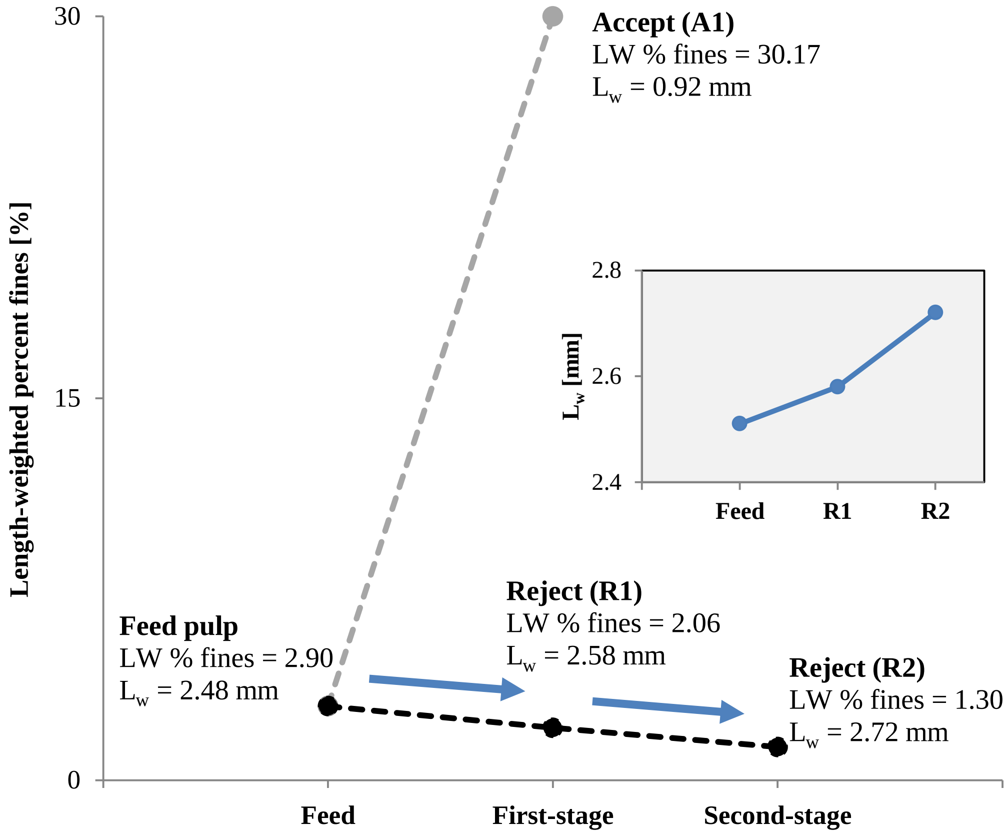

Figure 37. Changes in fines percentage of reject R1 and R2 after the first- and second-stage of reject fractionation. Inset plot shows the change in the average fibre length, L_w.

5.3 Fibre length distribution changes

When comparing the fibre length distributions of the feed and reject fractions R1 and R2, little differences were observed. The distributions of the reject fractions as shown in Figure 38 almost resemble that of the feed. The amount of fibres extracted from the feed is too low to significantly influence the fibre length distribution. However, the average length and fines content are quite different as presented previously. The difference in the fines distribution ($L < 0.2$ mm) is not captured well by the FQA as the bin size is reported by FQA in a 0.05 mm increment.

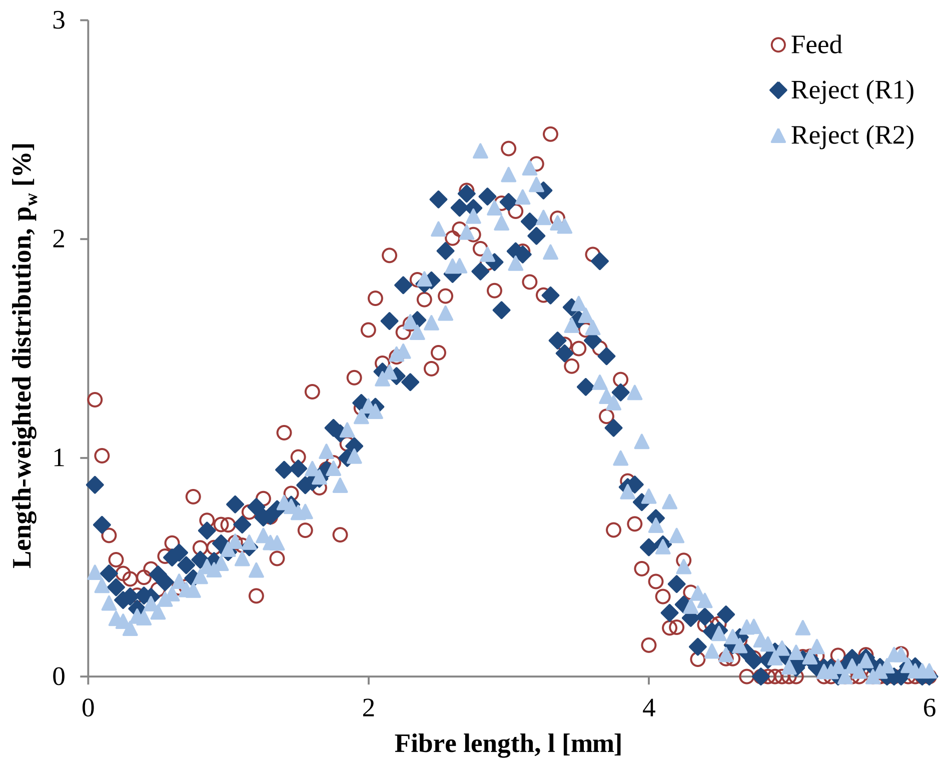

Figure 38. Comparison of fibre length distribution of the feed and reject fractions, R1 and R2. All operating parameters were kept constant at both stages except V_s. V_s = 0.3 ms^{-1} at the first stage and 1.3 ms^{-1} at the second stage.

5.4 Qualitative differences of rejects R1 and R2

5.4.1 Microscope images

The reject fractions were analyzed using a light microscope. Microscope images of the R1 and R2 fractions are shown in Figure 39. The following observations were made; for R1, there is some amount of fibre fragments and fines in the sample. Some fine fibrils were also observed in the image of the R1 sample. On the other hand, R2 sample comprises mostly fibres and no other small particles. Most fines have been successfully removed from R2.

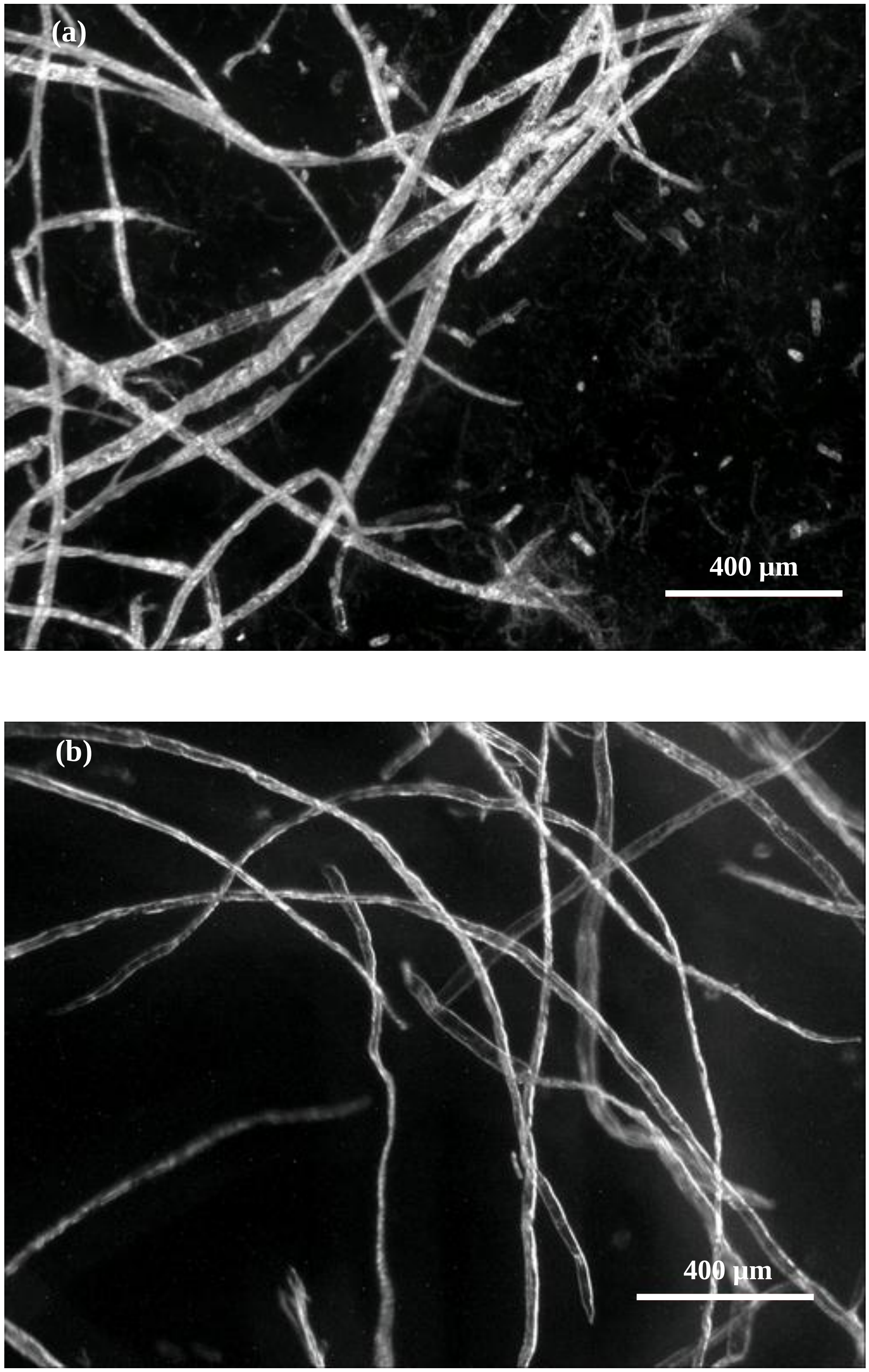

Figure 39. Microscope images of the reject fraction (a) R1 obtained after the first-stage of fractionation and (b) R2 obtained after the second-stage of reject fractionation, both at similar operating conditions except the aperture velocity, V_s. Scale bar 400 µm.

5.4.2 Handsheet analyses

Handsheets were prepared from the feed and rejects fractions with a target grammage of 60 gm^{-2} in accordance to the TAPPI standard procedures. Handsheets produced were then conditioned at 50% relative humidity at 23^{o}C and tested for various properties as summarized in Table 8. Despite minimal changes in the fibre length distributions as illustrated in Figure 38, considerable improvements in all strength properties of the handsheets made from the reject fractions R1 and R2 were observed when compared to the handsheets made from the feed pulp. R1 and R2 handsheets are also less bulky than the feed handsheets.

Table 8. Handsheet properties of feed, reject R1 and R2 fractions. Percent changes of the final R2 properties with respect to the properties of handsheets made from the original pulp are shown.

Handsheet property	Feed pulp	R1	R2	Percent change
TEA index [Jkg^{-1}]	363.33	520.37	560.90	+54%
Tensile index [Nmg^{-1}]	31.55	39.04	44.15	+40%
Breaking length [km]	3.07	3.73	4.00	+30%
Burst index [$kPam^2g^{-1}$]	1.99	2.29	2.76	+39%
Tear index [mNm^2g^{-1}]	19.24	24.72	26.45	+37%
Stretch [%]	1.63	1.75	2.06	+26%
Gurley air resistance [s 100 mL^{-1}]	4.25	2.78	2.28	-46%
Bulk [cm^3g^{-1}]	1.90	1.71	1.68	-12%

The tensile energy absorption (TEA) indicates the ability of paper to absorb energy. The TEA index of the final reject pulp is over 50% greater than that of handsheets made from the feed pulp. Tensile index is mostly dependent on the fibre length as shown many times in the literature, for example in [12], [16] and [28]. An increased average fibre length is expected to give a higher tensile index. The highest tensile index was achieved with sheets made from the final reject R2 fraction which has the highest average fibre length. A decrease in the fines content in the final reject fraction also probably contributed to the increase in the tensile index.

Breaking length is the maximum length of a strip of paper with a uniform width before rupture if it were to be suspended on one end. The breaking length of the final reject R2 was found to be 30% higher than that of the feed handsheets. Tearing resistance has also benefited from the fractionation process. The tearing resistance of the R2 handsheets is 37% higher than the feed handsheets. Bursting strength tells how much pressure a paper can tolerate before rupture. Higher bursting strength means higher resistance to external and also internal mechanical stresses. Burst index of the R2 handsheets are much higher than then feed. The final reject fraction possessed a somewhat higher stretch than the original pulp. However, the increase is within the margin of error.

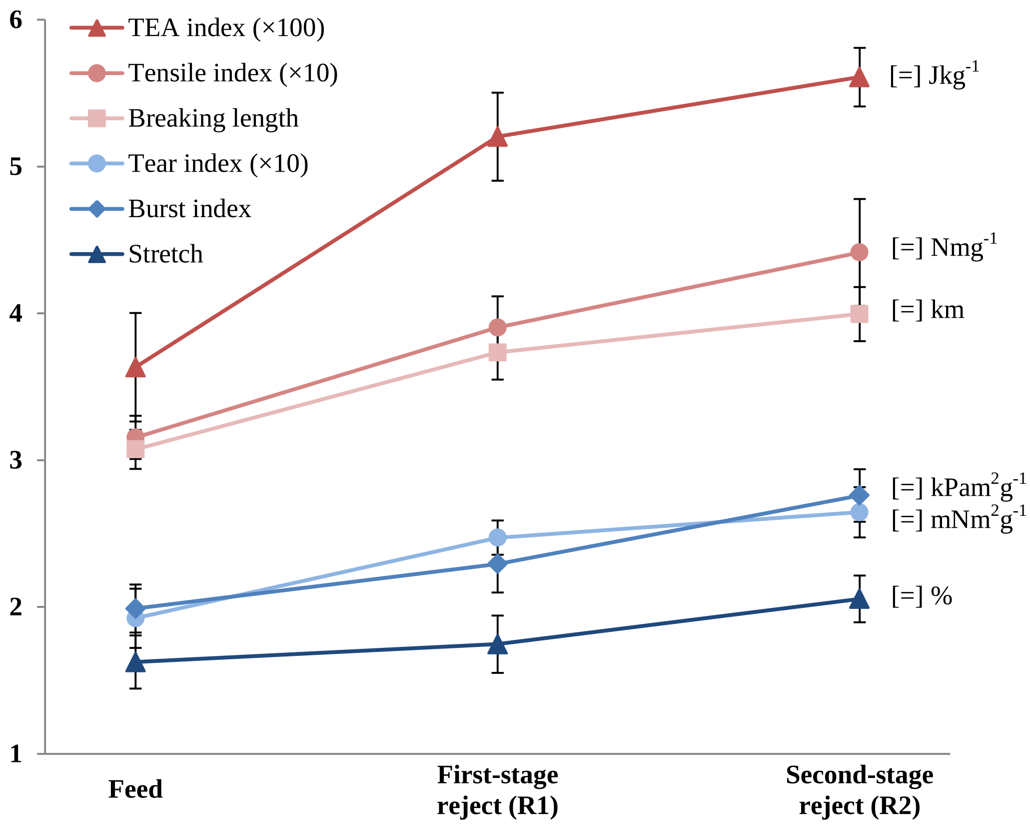

Figure 40. Handsheet strength properties plotted for the resulting fractions. Error bars represent standard deviations.

Porosity was measured using a Gurley densometer. The porosity test consisted of measuring the amount of time required for a given volume of air to flow through a specific area of the handsheets. A low Gurley air resistance value means a high porosity. NBSK pulp is porous to begin with but the removal of fines further increase the air permeability or porosity of the handsheets. Feed pulp is the least porous handsheet; this is most likely due to a higher amount of fines filling the voids between the fibre networks compared to that in the rejects. Porosity was decreased as much 46% compared to the feed handsheets. Removal of fines by means of fibre fractionation has also been found to increase the porosity in another study [5].

Sheet volume (bulk) is the inverse of the sheet density. At the same sheet grammage, the bulk of the R2 handsheets decreased slightly when compared to the unfractionated pulp.

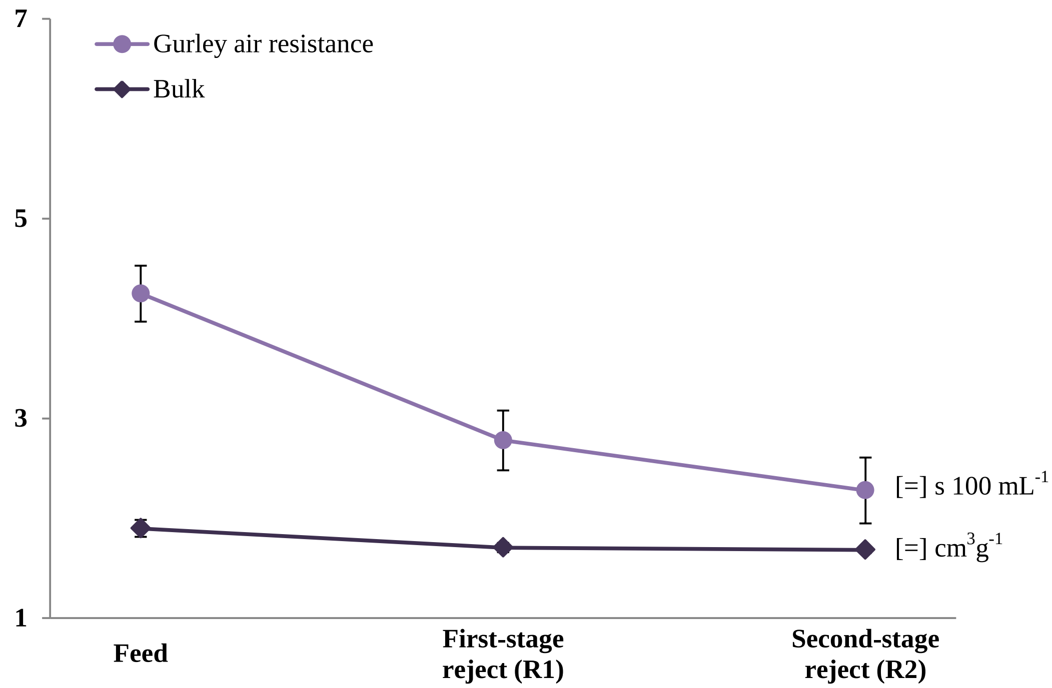

Figure 41. Bulk and porosity of handsheets plotted for the resulting fractions. Error bars represent standard deviations.

5.3 Fibre passage ratio at second stage

Fibre passage ratio, P(l) describes the changes in the number concentration of fibres in each length class. Fibre length analysis was performed using the FQA. The FQA measures the total number of fibres contained in each 0.05 mm length class with a total of 200 classes for fibres between 0 to 10 mm in length and reports the length-weighted distribution such as shown in Equation 2-2.

To reduce noise in the data, these length classes were regrouped into 28 classes of 0.15 mm length each for fibre length between 0-4 mm. Equation 1-9 was used to calculate the fibre passage ratio of length fraction *i*, $P(l_i)$ where *i* indexes the 0.15 mm length class, l_i is the average length in the length class *i* and n = 28. The average number concentration per unit volume, C_n in Equation 1-9 was expressed as the pulp consistency, c. Calculated P(l) is shown in Figure 42.

The average passage ratio, P at the second stage is slightly higher than the first-stage. However, the overall shape of the curves is similar. Passage ratio of pulp, P under constant screening conditions depends on the passage ratios of each fibre length class, P(l). Thus, at the second stage of fractionation, P increased as the pulp is fractionated. In addition, at the second stage, an increase in P is potentially a result from the increase in the aperture velocity, V_s.

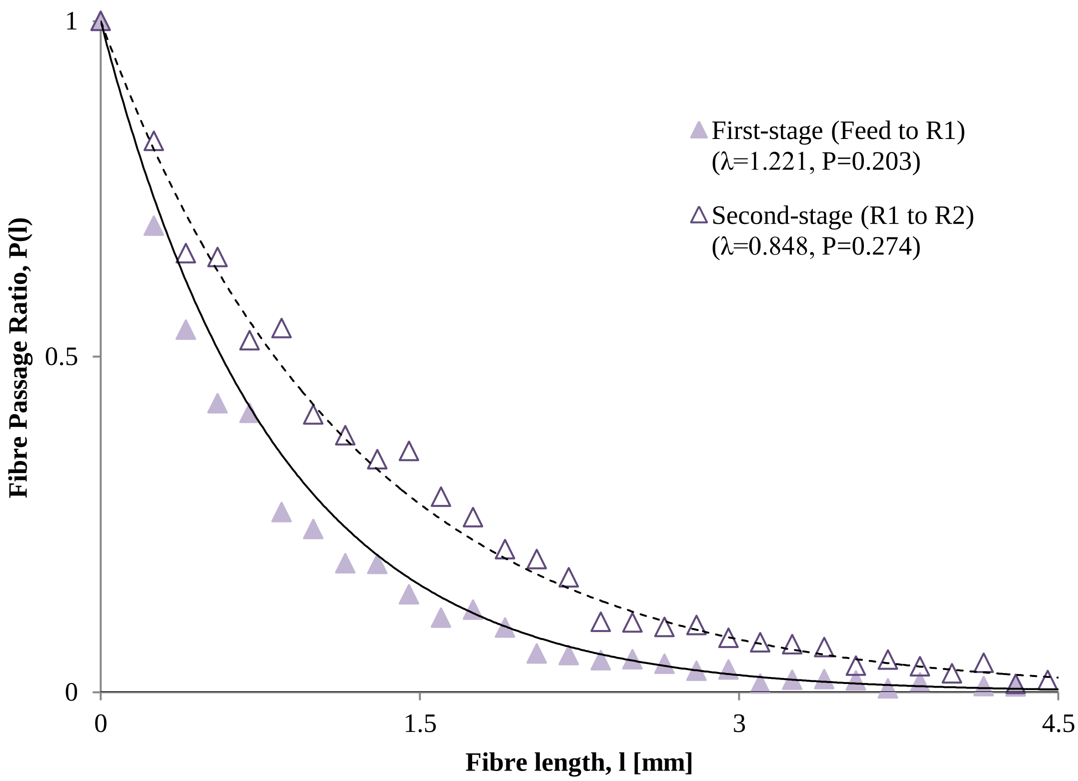

Figure 42. Fibre passage ratio at the first- and second-stage of rejects fractionation. λ was determined for both stages, λ = 1.22 at the first-stage and 0.85 at the second-stage.

5.4 Fractionation efficiency

In this study, fractionation efficiency is assessed in terms of the enrichment of long fibres in the reject streams. Estimation of the long fibre mass in the rejects and the feed pulp was done based on a coarseness versus length relationship, ω(l) as well as an overall mass balance.

5.4.2 Mass balance around a pressure screen

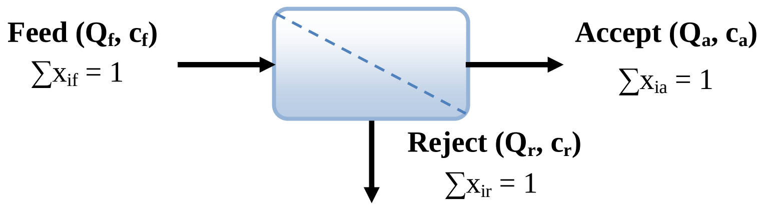

Figure 43. Flow streams around a pressure screen.

From the conservation of mass, a mass balance around the overall screen is as follows, where ṁ is the mass flow in kg min^{-1}:

$$\dot{m}_f = \dot{m}_a + \dot{m}_r \quad \textbf{5-1}$$

The mass balance can also be written in terms of more practical measurements since the mass flow information is usually not readily available. At low consistencies, the mass flow rate, m can be replaced with the volumetric flow rate, Q (in L min^{-1}) multiplied by the consistency:

$$c_f Q_f = c_a Q_a + c_r Q_r \quad \textbf{5-2}$$

In fibre length fractionation, the objective usually is to separate a length fraction of interest from the rest of the feed pulp. For a length class *i* the mass balance can be written as follows:

$$x_{if} c_f Q_f = x_{ia} c_a Q_a + x_{ir} c_r Q_r \quad \textbf{5-3}$$

where x_i = mass proportion of fibres in length class *i* to the total mass

The length-weighted distribution, p_w is normally used to represent the mass fraction x_i. This is incorrect as pulp fibres are distributed in width and wall thickenesses. The length-weighted distribution would only equal to the mass fraction if all the fibres have the same cross-sectional dimensions. The average coarseness of a sample over the entire fibre length can be measured easily. However, there is no technique available to provide the distribution of fibre coarseness in a sample. Madani et al. recently presented a novel method to estimate the average coarseness as a function of fibre length [27].

5.4.3 Coarseness versus length relationship, ω(l)

A coarseness versus length relationship, ω(l) was derived according to a recent work by Madani et al. (See Appendix B) [27]. Four coarseness values for the following length classes were obtained; 0-1.5 mm, 1.5-3.0 mm, 3.0-4.5 mm and 4.5-6.0 mm. The data were fitted with a second-order polynomial to estimate the intermediate points on the curve as shown in Figure 44. The results suggest that coarseness increase with increasing fibre length.

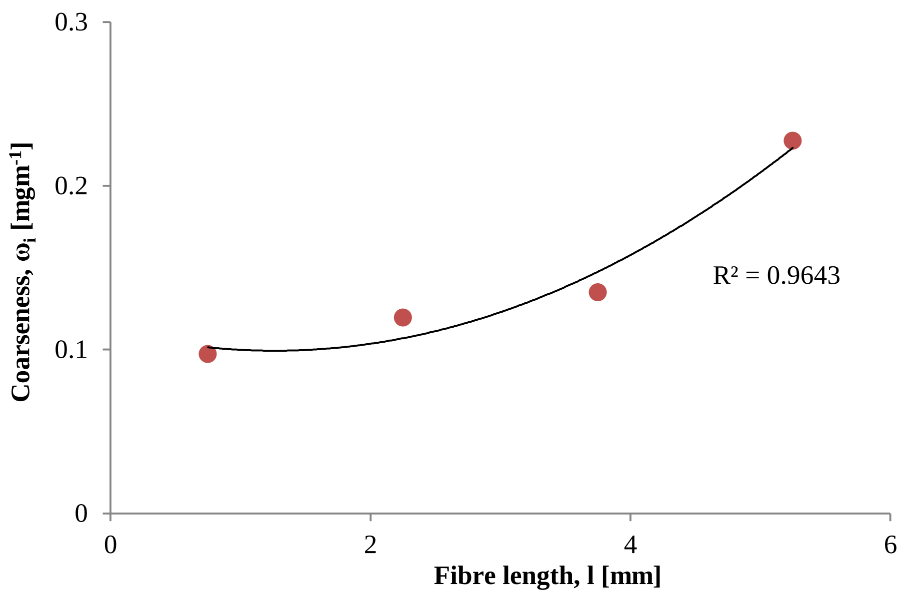

Figure 44. Coarseness values estimated from Madani et al. regression method. Solid line shows the best fitting curve.

The mass of fibres in length class *i*, m_i was calculated based on the estimated value of coarseness from Figure 44 using Equation 5-4. The mass fraction or mass percentage, x_i is then calculated by dividing m_i by the total mass of the fibres. Figure 45 shows the generated mass fractions.

$$m_i = n_i \times \omega_i l_i \qquad \textbf{5-4}$$

where n_i = number of fibres in length class *i*

ω_i = coarseness of length class *i* (mgm^{-1})

l_i = average fibre length of length class *i* (mm)

At both stages, accepts A1 and A3 contained significantly more fines and short fibre fractions (0-1.5 mm). The feed and reject fractions R1 and R2 have mostly a high amount of fibres in the length class 3.0 to 4.5 mm and a low amount of fibres in bin 0-1.5mm as well as 4.5-6.0 mm.

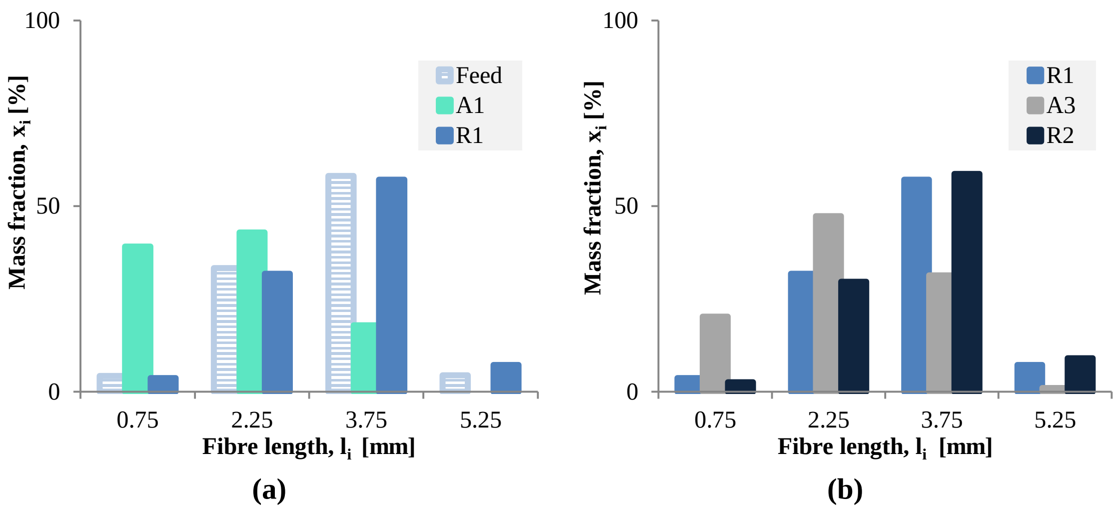

Figure 45. Mass percent of four fibre length classes estimated from mass balance (Range: 0-1.5 mm, 1.5-3.0 mm, 3.0-4.5 mm and 4.5-6.0 mm) of the feed, accept and reject fractions obtained after (a) first- and (b) second-stage of rejects fractionation

5.4.4 Enrichment of long fibres in the reject streams

In this study, the effectiveness of fibre length separation is represented as the enrichment of the long fibred pulp and the removal of fines and short fibred pulp in the reject streams. The fibre length is arbitrarily divided into three classes; long fibres for fibres within the length range of 3 to 6 mm, medium fibres for fibres between 1-3 mm in length and short fibres as the rest of the fibres under 1 mm in length. Table 9 shows the mass fraction results summarized in terms of the three length classes in feed and reject streams.

Table 9. Mass percent of fibres in feed and reject streams calculated using estimated ω_i.

Fibre length classes	Mass fraction, x_i [%]			Relative change in x_i
	Feed	R1	R2	
0-1.0 mm (Fines and short fibres)	1.81	1.44	1.00	-0.81%
1.0-3.0 mm (Middle fraction)	33.11	32.32	30.40	-2.71%
3.0-6.0 mm (Long fibres)	65.06	65.59	68.17	+3.11%

The difference in the mass proportion of the long fibres in comparison to the feed is plotted below in Figure 46. The reject fraction R2 contains over 3% higher mass of long fibres compared to the feed.

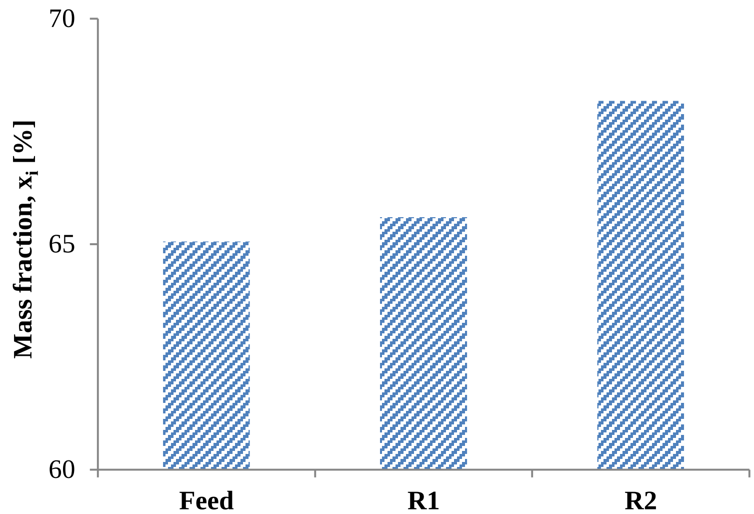

Figure 46. Enrichment of long fibres in rejects in terms on mass fraction.

6 Accepts fractionation stages

The goal of this part of the study is to concentrate the undesirable fines materials through multiple consecutive accept fractionation steps. The schematic of the fractionation stages is shown in Figure 47. The fines sample from the final fractionation stage is to be evaluated by FPInnovations as a potential raw material for NCC production.

Based on the results from the previous section, operating conditions were chosen for the second stage of accept fractionation. The effects of some operating parameters such as the volumetric reject ratio, R_v and the rotor tip speed, V_t are reexamined to obtain the best possible combination of operating parameters. This chapter also reports the fibre length distribution changes of the feed and accepts after fractionation as well as the fibre passage ratio at both stages. Microscope images of the resulting accept fractions were taken and compared. The enrichment of fines in the accept streams were estimated from a mass balance. The results from NCC analysis by FPInnovations are discussed briefly at the end of the chapter.

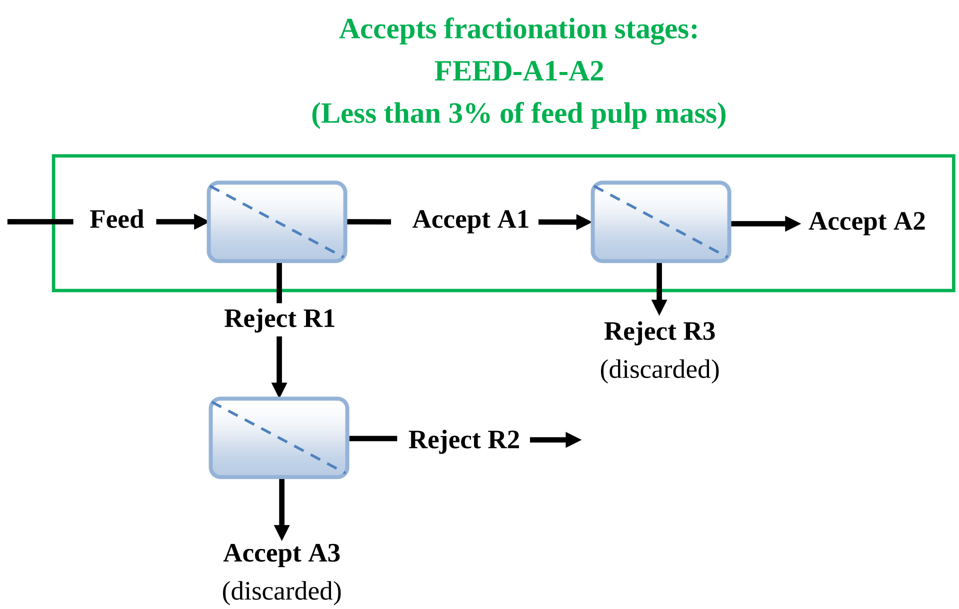

Figure 47. Multi-stage fractionation process. Boxed area shows accepts fractionation featuring two stages in series.

6.1 Effect of operating parameters at second-stage

6.1.1 Effect of volumetric reject ratio

The feed and reject flow rates; Q_f and Q_r were varied during the second-stage of accept fractionation in order to study the effect of changing the volumetric reject ratio, R_v on the fines percentage in the accept stream A2. Results shown in Figure 48 are consistent with findings in Chapter 3. Increasing R_v increases the fines content in the accept. However, the fines percentage in the accept A2 was more or less unchanged with increase in the R_v above 0.6.

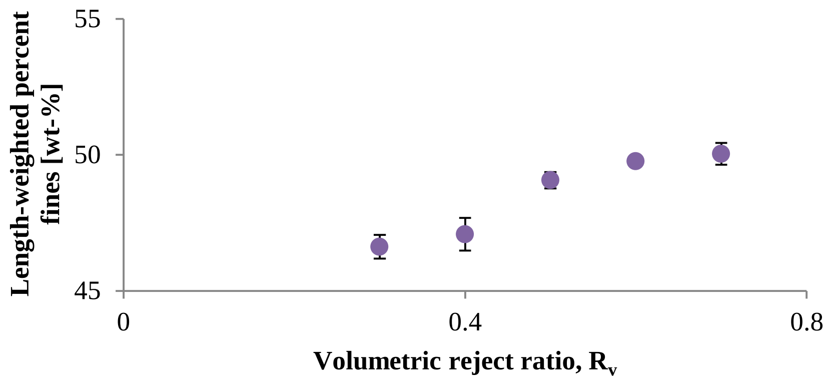

Figure 48. Effect of varying volumetric reject ratio, R_v on fines percentage of accept A2 at a constant aperture velocity, $V_s = 0.3$ ms^{-1}. Error bars represent standard deviations.

6.1.2 Effect of rotor tip speed

At the second stage, the rotor tip speed, V_t was varied to study the effect of changing V_t on the fines percentage. As the accept A1 consistency is extremely low, operating the rotor at 16 ms^{-1} such as during the first stage would have been unnecessarily high.

From Figure 49, changing the rotor tip speed had a clear effect on the fines percentage in accepts. A less vigorous rotor action seemed to improve the separation of fines. A decrease in V_t from 16 ms^{-1} to 4 ms^{-1} caused an up to 20% increase in the fines percentage of the accept pulp. As the rotor tip speed decreases the fines percentage in the accept stream increases as less long fibres are forced to go through the screen apertures. At higher V_t, it is presumed that the turbulence increased and thus more fibres are directed towards the accept and thus decreasing the percentage of fines.

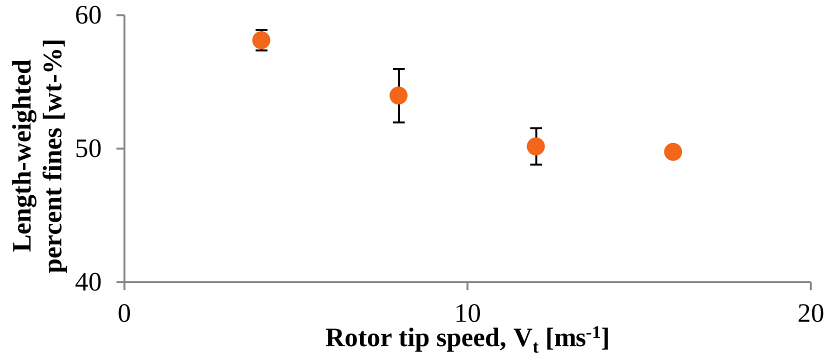

Figure 49. Effect of varying rotor tip speed, V_t on the fines percentage of accept A2. V_t was varied at a constant $R_v = 0.6$ and $V_s = 0.3$ ms^{-1}. Error bars represent standard deviations.

6.2 Screening conditions and their effects on fractionation

The operating parameters used at both stages of accept fractionation are given in Table 10. Under these conditions, the fractionation process successfully generated a final accept fraction A2 that contains 20 times more fines compared to the feed pulp.

Table 10. Screening conditions for the accept fractionation series.

Screening conditions	First-stage	Second-stage
Aperture diameter [mm]	0.5	0.5
Aperture velocity, V_s [ms^{-1}]	0.3	0.3
Rotor tip speed, V_t [ms^{-1}]	16	4
Volumetric reject ratio, R_v	0.6	0.6

Fractionation results	Feed	Accept (A1)	Accept (A2)
Consistency [%]	1.1	0.11	0.052
LW average fibre length [mm]	2.48	0.92	0.30
LW fines content [wt-%]	2.90	30.17	58.13

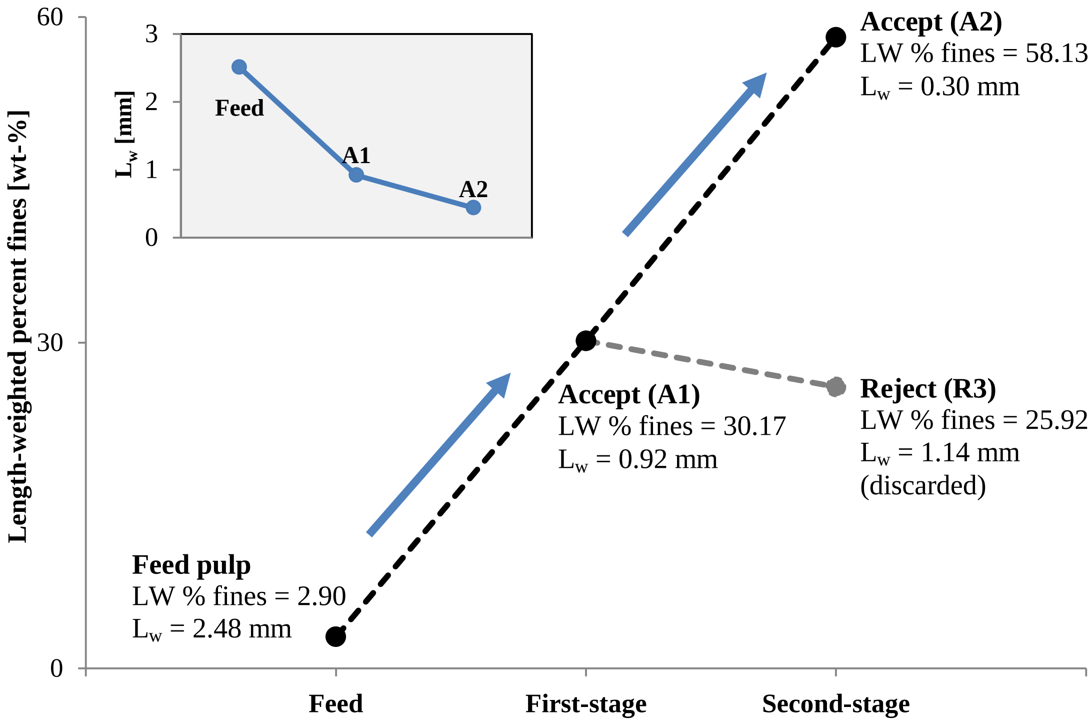

Figure 50. Changes in fines percentage and average fibre length of accept stream after the first- and second-stage of accept fractionation. Inset graph shows the changes in the average fibre length, L_w. Fines percentage was increased significantly after the multiple fractionation stages.

6.3 Fibre length distribution changes

The fibre length distribution of the feed pulp as well as the accept fractions A1 and A2 can be seen in Figure 51. There is a notable difference in the feed and the accept distributions, mainly in the shorter fibre region. It can be seen that the fines and short fibre content in the accept fractions are significantly higher than that of the feed. The A2 accept also has a very narrow length distribution and there is essentially no fibres above 2 mm in A2. The multi-stage fractionation process has effectively changed the fibre length distribution at each stage.

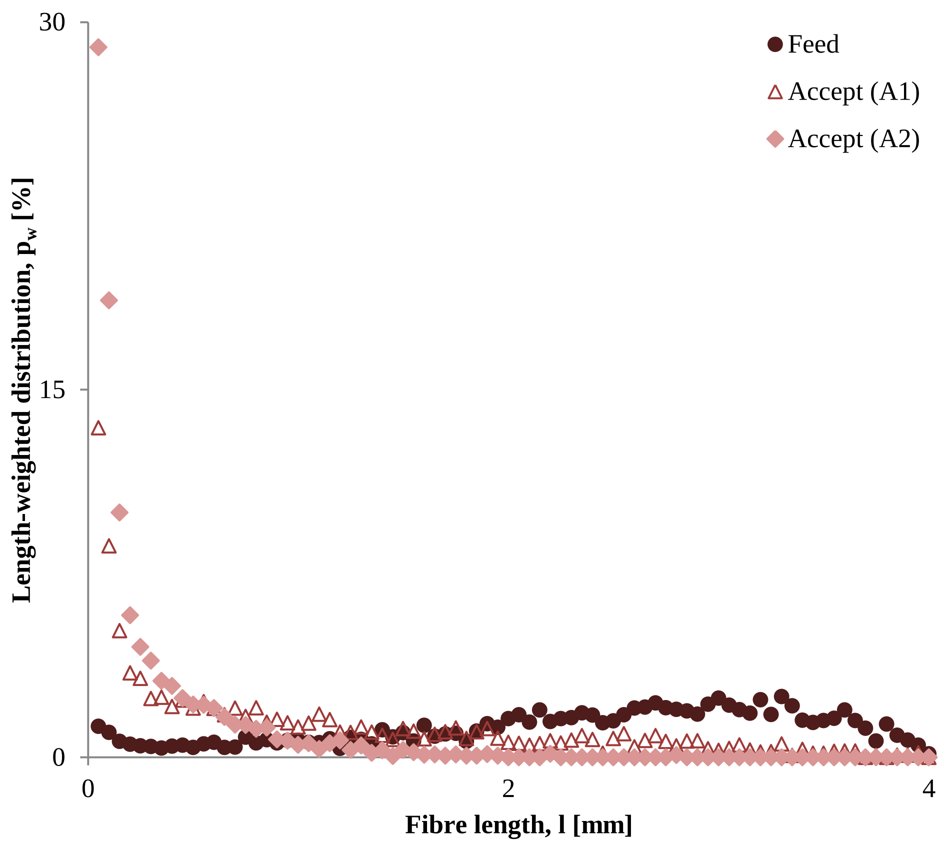

Figure 51. Comparison of fibre length distribution of the feed and accept fractions, A1 and A2. All operating parameters were kept constant at both stages except V_t. V_t = 16 ms^{-1} at the first stage and 4 ms^{-1} at the second stage.

6.4 Qualitative differences of accepts A1 and A2

The A1 and A2 accept fractions were studied under a light microscope to assess the physical differences between each fraction. The micrographs taken, shown in Figure 52, reveal that the A1 fraction still contains some long fibres while the A2 fraction contains only very short fibres and fines. Chunky fines materials and clusters of cellulose fibrils (threadlike structures) are visible in both samples. Compared to the rejects (See Figure 39), accepts contain a higher amount of fibrils.

It is clear that the accepts fraction contains a broad variety of different type of small particles. For chemical pulp, the fines materials could be of primary fines (coarser ray-cell rich fines) or secondary fines (finer fibril rich fines generated during further refining stages) [3]. To characterize these different types of fines and fibrils in the accepts, microscope technique such as SEM/TEM would be necessary.

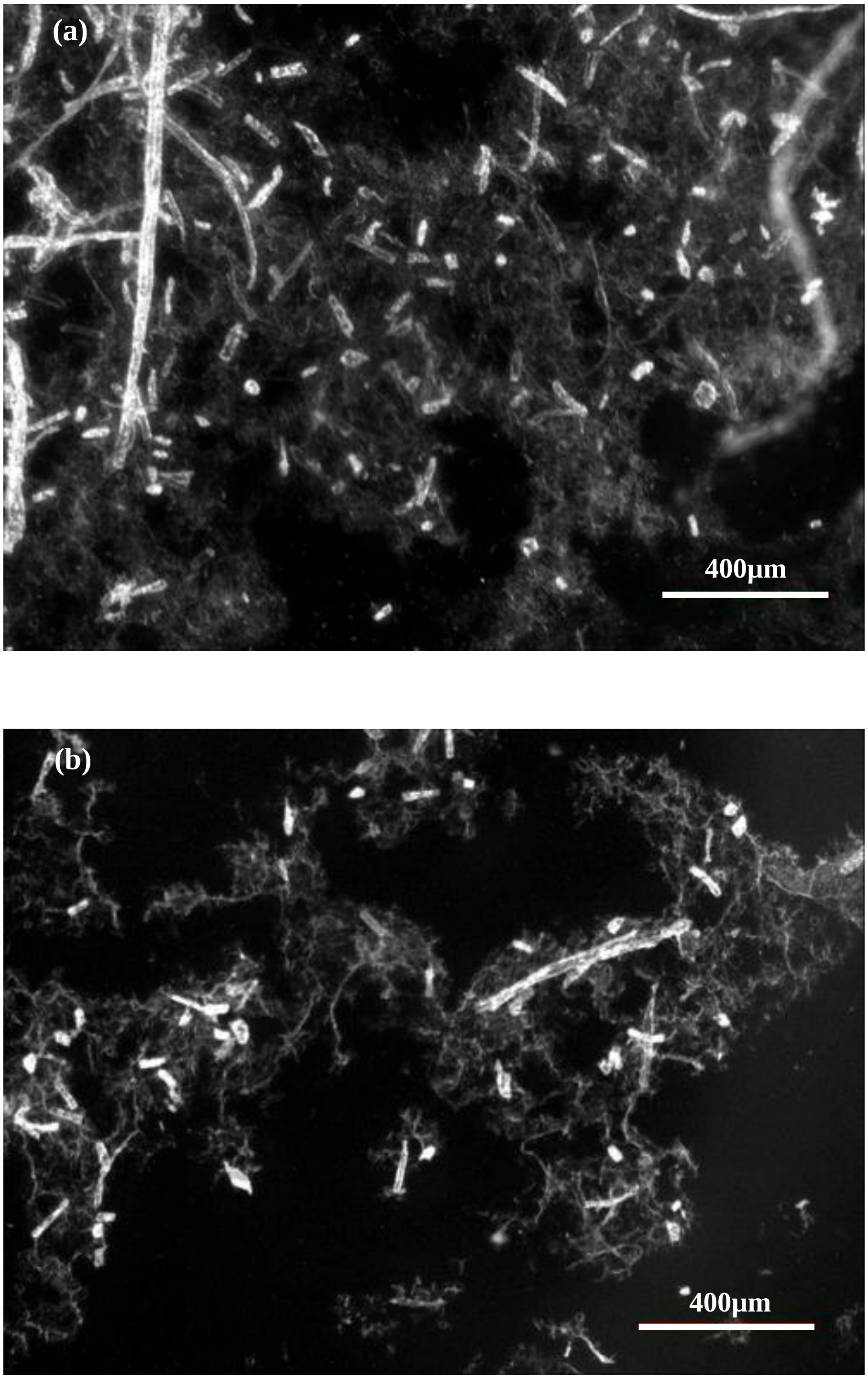

Figure 52. Microscope images of the accept fraction (a) A1 obtained after the first-stage of fractionation and (b) A2 obtained after the second-stage of accept fractionation, both at similar operating conditions except the rotor tip speed, V_t. Scale bar 400 µm.

6.5 Fibre passage ratio at second stage

Fibre passage ratio was calculated at both stages and is presented below in Figure 53. A curve was fitted to the data using Equation 1-10. Interestingly, similar fibre passage behavior was found at both stages. The second-stage of fractionation did not seem to depend on the second feed (A1) pulp properties.

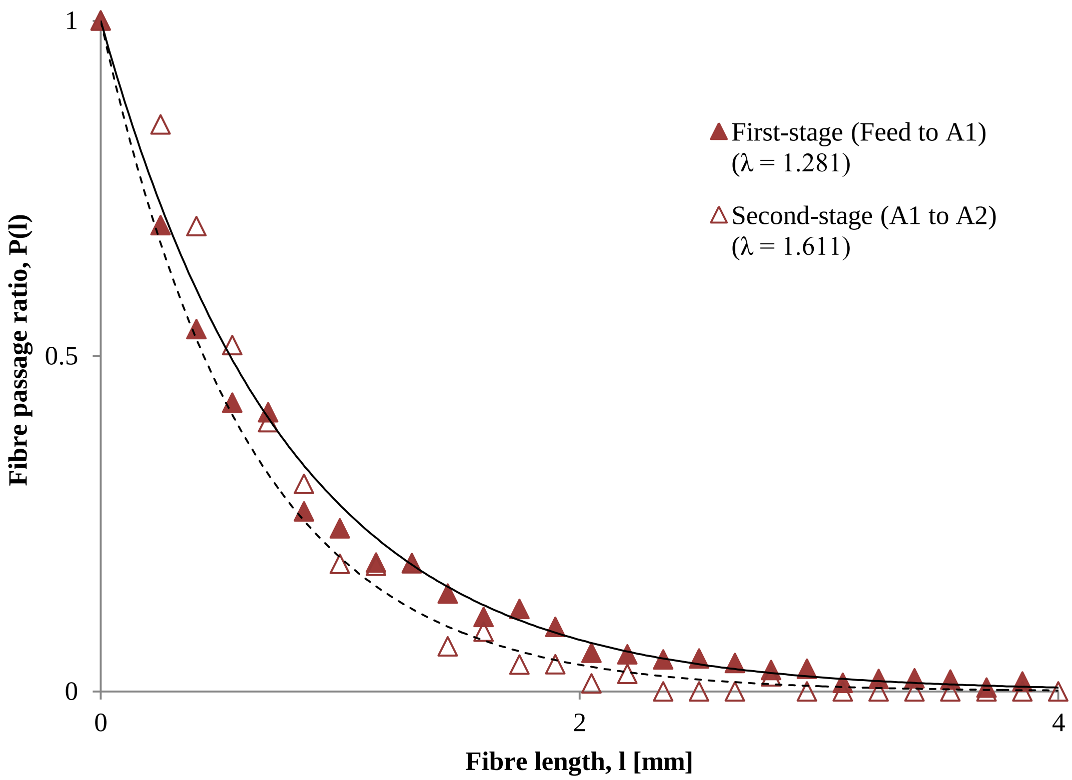

Figure 53. Fibre passage ratio at the first- and second-stage of accepts fractionation. λ was determined for both stages, λ = 1.22 at the first-stage and 1.61 at the second.

6.6 Enrichment of fines in the accept streams

The mass percentage of fines and fibres in the unfractionated stream as well as the resulting accepts A1 and A2 were calculated by solving the overall mass balance and applying the coarseness versus length relationship. Figure 54 shows the calculated mass percentage for the entire length range divided into four length classes. Accept A2 contains mostly fibres between 0 to 1.5 mm and no fibre above 3 mm in length.

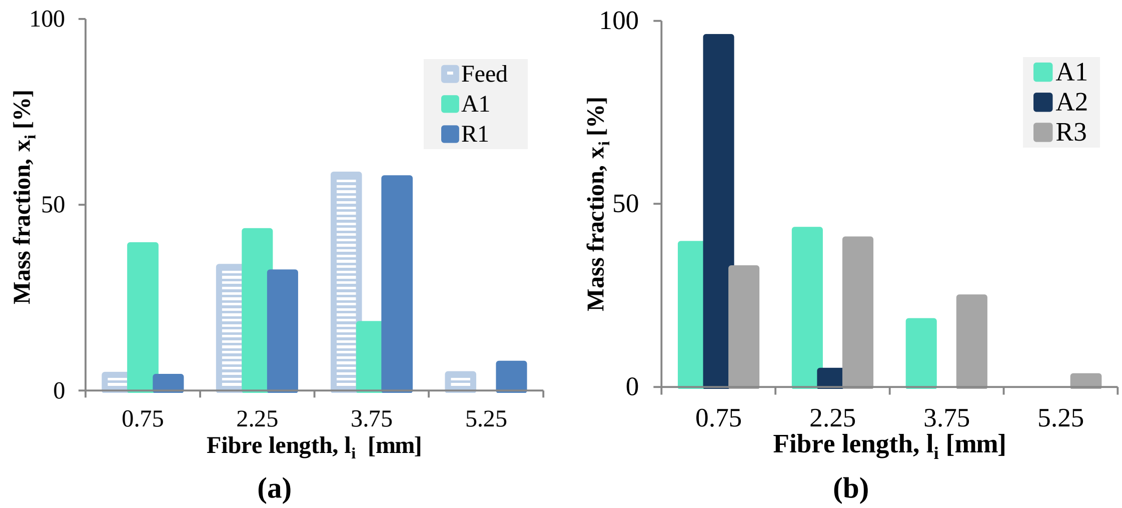

Figure 54. Mass percent of four fibre length classes estimated from mass balance (Range: 0-1.5 mm, 1.5-3.0 mm, 3.0-4.5 mm and 4.5-6.0 mm) of the feed, accept and reject fractions obtained after (a) first stage of fractionation and (b) second-stage of accept fractionation .

Figure 55 shows the mass percent of fines (L < 0.2 mm) in the feed, accept A1 and accept A2. There is a pronounced enrichment of fines at the second stage. The fines percentage was increased from less than 0.15 wt-% in the feed to 10 wt-% in the accept A2 stream. It should be pointed out that the values calculated from the mass balance are much lower than the length-weighted percentage of fines calculated by the FQA (See Figure 48 and Figure 49). The results from the analyzer are meaningless due to the assumption made during the fines percentage calculation; that is, all particles, fines and fibres have the same coarseness - i.e., mass per unit length.

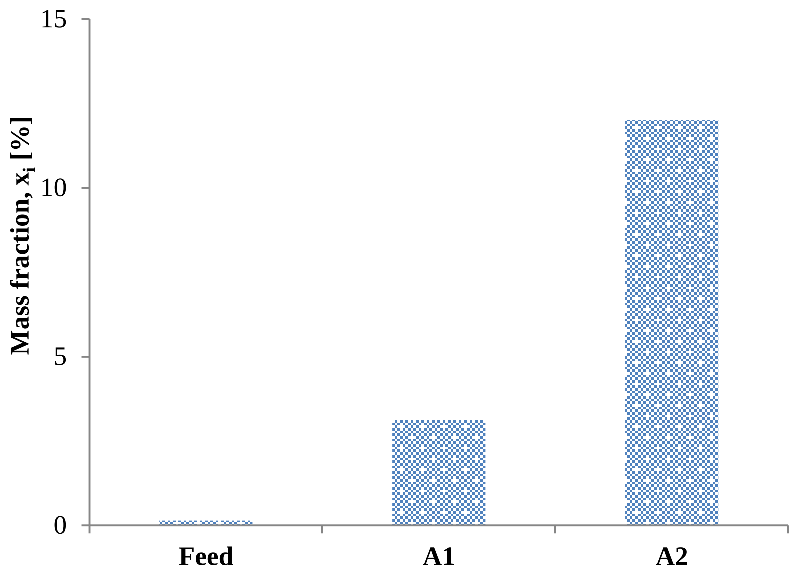

Figure 55. Enrichment of fines (L<0.2mm) in the accept streams.

6.7 Fines fraction for NCC production

The fines enriched accept fraction was evaluated by FPInnovations (FPI) in Montreal, QC for its potential suitability as a raw material for a novel fibre-based product, Nanocrystalline Cellulose (NCC) production. The source of NCC comes from the cellulose fibril isolated from fibres, and therefore it might not be affected by the fibre morphology itself. Possible savings was anticipated through replacing a high quality pulp for NCC production with the fines enriched fraction produced from the multistage fractionation.

The acid hydrolysis of the fines sample and the filtration process of the NCC materials were carried out independently by FPI and therefore a detailed procedure is not included in this thesis. The results of the fines analysis showed that it was possible to produce NCC using kraft pulp fines. However, the yield is extremely low (less than 10%). Also, the optical properties of the produced NCC are inferior compared to the NCC produced using a high quality pulp. This is most likely due to lignin-related impurities affecting the acid hydrolysis efficiency. From the literature, it is known that fines contain an excessively high content of lignin as well as extractives [3]. To obtain a better yield, a kappa number of the accept fraction which measures the residual lignin content should be determined and should somehow be lowered before the hydrolysis process.

7 Conclusion

The best conditions to carry out fractionation were determined by conducting experiments to investigate the effect of varying volumetric reject ratio, R_v aperture velocity, V_s aperture diameter and rotor tip speed, V_t on reject thickening and passage ratio using several smooth-holed screen cylinders. In general, increasing fines content in the accept and increasing fibre length in the rejects – i.e. decreasing fibre passage ratio or λ were found by using the smallest aperture diameter, in this case 0.5 mm, the highest R_v of 0.6 and the smallest V_s of 0.3 ms^{-1}.

Multi-stage fractionation successfully created a final reject fraction, R2 that is up to 10% longer than the original feed pulp, from 2.48 mm to 2.70 mm in average length. Significant difference in the fines content was also obtained, from 2.90 wt-% to 1.30 wt-%. Pulp with fines materials removed evidently lead to a pulp with enhanced strength. All of the final reject R2 strength properties were improved and the Gurley air resistance was 46% reduced compared to the handsheets made from the feed. The R2 tensile strength was increased up to 40% higher, the TEA index 54% higher, breaking length 30% higher, burst index 39% higher and finally the tear index 37% higher. An increase in freeness was also observed from 667 mL CSF to 701 mL CSF.

Most of the fines in the original feed pulp was successfully isolated into the accept A2 fraction after the multistage fraction.

7.1 Recommendations for future work

The effect of the pressure screen operating and design parameters as well as fibre furnish on fractionation is only partially studied in this thesis. This study can be extended to study other parameters such as the effect of feed consistency, feed pulp type, screen aperture type, rotor design.

With a high average fibre length, superior strength properties and a high freeness, the final reject pulp R2 has the potential to be developed as reinforcement for mechanical pulp. Also, at such high freeness, even higher strength is possible with further refining of the reject pulp. In addition, another suitable application of the reject R2 pulp includes sack kraft paper. Superior TEA and porosity are of particular importance for sack paper. Strength properties, especially tensile strength and TEA are essential for sack paper as high durability is required during filling while high porosity enables a quick filling process, such as discussed in [5].

The yield of NCC from using fines was unfortunately low likely due to the lignin content in the fines poisoning the acid hydrolysis process. To possibly obtain a better yield of NCC, a kappa number of the fines enriched accept fraction which measures the residual lignin content should be determined and should somehow be lowered before the acid hydrolysis process. Also, similar experiments such as in this study could be conducted for hardwoods to isolate vessel elements in the accept stream which could then be used for NCC production. The remaining vessel element free hardwood pulp would be more competitive in the market.

References

[1] G. A. Smook, Handbook For Pulp & Paper Technologists, Vancouver: Angus Wilde Publications Inc. , 2002.

[2] J. Meyers and H. Nanko, "Effect of fines on the fibre length and coarseness values measured by the Fibre Quality Analyzer (FQA)," in *The World of Market Pulp*, Appleton, WI, WOMP, LLC, 2005, pp. 127-133.

[3] H. Sixta, Handbook of Pulp, Weinheim: Wiley-VCH , 2006.

[4] R. S. Seth, "The measurement and significance of fines," *Pulp & Paper Canada,* vol. 104, no. 2, pp. 47-50, 2003.

[5] J. Olson, B. Allison, T. Friesen and C. Peters, "Fibre Fractionation For High Porosity Sack Kraft Paper," *TAPPI Journal Peer Reviewed Paper,* vol. 84, no. 6, 2001.

[6] B. L. Peng, N. Dhar, H. L. Liu and K. C. Tam, "Chemistry and applications of Nanocrystalline Cellulose and its derivatives: A nanotechnology perspective," *The Canadian Journal of Chemical Engineering,* vol. 9999, pp. 1-16, 2011.

[7] A. Kumar, R. W. Gooding and R. J. Kerekes, "Factors controlling the passage of fibers through slots," *TAPPI Journal,* vol. 81, no. 5, pp. 247-254, 1998.

[8] F. Julien Saint Amand and B. Perrin, "Fundamentals of Screening: Effect of Screen Plate Design," in *TAPPI Pulping Conference*, Boston, 2000.

[9] J. Olson, N. Roberts, B. Allison and R. Gooding, "Fibre Length Fractionation Caused by Pulp Screening," *Journal of Pulp and Paper Science,* vol. 24, no. 12, pp. 393-397, 1998.

[10] J. Olson, "Fibre Length Fractionation Caused by Pulp Screening: Slotted Screen Plates," *Journal of Pulp and Paper Science,* vol. 27, no. 8, pp. 255-261, 2001.

[11] J. Olson, B. Allison and N. Roberts, "Fibre Length Fractionation Caused By Pulp Screening: Smooth-Hole Screen Plates," *Journal of Pulp and Paper Science,* vol. 26, no. 1, pp. 12-16, 2000.

[12] S. Abubakr, G. Scott and J. Klungness, "Fibre fractionation as a method of improving handsheet properties after repeated recycling," *TAPPI Journal,* vol. 78, no. 5, pp. 123-126, 1995.

[13] E. Afra, H. Resalati, J. A. Olson and Pourtahmasi, "Assessment of OCC pulp fractionation using fibre passage ratio model," *Appita Journal,* vol. 62, no. 5, pp. 350-354, 2009.

[14] C. M. Sloane, "Kraft pulp processing - pressure screen fractionation," *Appita Journal,* vol. 53, no. 3, pp. 220-226, 2000.

[15] H. Vomhoff and K.-J. Grundström, "Fractionation and separate refining of a bleached softwood pulp," *STFI Report PUB6,* 2002.

[16] K. El-Sharkawy, K. Koskenhely and H. Paulapuro, "Tailoring softwood kraft pulp properties by fractionation and refining," *TAPPI Journal,* vol. 7, no. 11, pp. 15-22, 2008.

[17] M. Sloane, P. Kibblewhite, M. Riddell and S. Williams, "The pressure screen - a tool for the modern fibre alchemist," in *60th Appita Annual Conference and Exhibition*, Melbourne, 2006.

[18] R. W. Gooding and D. F. Craig, "The effect of slot spacing on pulp screen capacity," *TAPPI Journal,* vol. 75, no. 2, pp. 71-75, 1992.

[19] R. Gooding, J. Olson and N. Roberts, "Parameters for assessing fiber fractionation and their application to screen rotor effects," *TAPPI Journal* , vol. 3, no. 3, 2004.

[20] R. W. Gooding and R. J. Kerekes, "Consistency changes caused by pulp screening," *TAPPI Journal,* vol. 75, no. 11, p. 109, 1992.

[21] M. Walmsley and Z. Weeds, "Plug flow versus mixed flow modelling of a pressure screen," in *55th Appita Annual Conference*, Hobart, Australia, 2001.

[22] K. R. Braaten and R. F. Wakelin, "Fiber length fractionation of TMP using pressure screens," *TAPPI Journal,* vol. 82, no. 6, pp. 129-135, 1999.

[23] Z. Weeds and M. Walmsley, "Flow characteristics of Eucalypt and Radiata Pine suspensions in a pressure screen with smooth 1 mm holes and 150 micron contoured slot apertures," in *TAPPI Pulping Conference*, Montreal, 1998.

[24] J. Olson and G. Wherrett, "A Model of Fibre Fractionation by Slotted Screen Apertures," *Journal of Pulp and Paper Science,* vol. 24, no. 12, pp. 398-403, 1998.

[25] A. J. Ämmälä, "Dual effect of foil tip speed on reject thickening in pressure screening," *Appita Journal,* vol. 57, no. 2, pp. 28-31, 2004.

[26] J. A. Olson and B. J. Allison, "Optimization of Multiple Screening Stages for Fibre Length Fractionation: Two-Stage Case," *Journal of Pulp and Paper Science,* vol. 26, no. 3, pp. 113-119, 2000.

[27] A. Madani, J. A. Olson, D. M. Martinez and A. Fung, "Novel methods to characterize and fractionate papermaking fibres," *Nordic Pulp & Paper Research Journal,* vol. 25, no. 40, pp. 448-456, 2010.

[28] A. J. Ämmälä, *Fractionation of thermomechanical pulp in pressure screening,* 2001.

[29] R. W. Gooding and J. A. Olson, "Fractionation in a Bauer-McNett Classifier," *Journal of Pulp and Paper Science* , vol. 27, no. 12, pp. 423-428, 2001.

[30] *TAPPI Test Method T 233: Fiber Length of pulp by classification*, 1995.

[31] J. Sirviö and I. Nurminen, "Systematic changes in paper properties caused by fines," *Pulp & Paper Canada,* vol. 105, no. 8, pp. 39-42, 2004.

[32] I. Pulkkinen, K. Ala-Kaila and J. Aittamaa, "Characterization of wood fibers using fiber property distributions," *Chemical Engineering and Processing,* vol. 45, pp. 546-554, 2006.

[33] R. W. Gooding and R. J. Kerekes, "Derivation of performance equations for solid-solid screens," *The Canadian Journal of Chemical Engineering,* vol. 67, pp. 801-805, 1989.

[34] R. F. Wakelin, "Prediction of fractionation efficiency for pressure screens," *Appita Journal,* vol. 50, no. 4, pp. 295-300, 1997.

[35] J. Niinimäki, "Phenomena affecting the efficiency of a pressure screen," in *TAPPI Pulping Conference*, Orlando, 1999.

[36] M. M. Nazhad and S. Sodtivarakul, "OCC pulp fractionation-a comparative study of fractionated and unfractionated stock," *TAPPI Journal,* vol. 3, no. 1, 2004.

[37] R. F. Wakelin and S. R. Corson, "Reject thickening behavior of TMP screening," *Pulp & Paper Canada,* vol. 99, no. 1, pp. 27-30, 1998.

[38] B. J. Allison and J. A. Olson, "Optimization of multiple screening stages for fibre length fractionation: two-stage case," *Journal of Pulp and Paper Science,* vol. 26, no. 3, pp. 113-119, 2000.

[39] H. Jokinen, M. Karjalainen, J. Niinimäki and A. Ämmälä, "Effect of furnish quality on pressure screen performance," *Appita Journal*, vol. 60, no. 1, pp. 35-40, 2007.

[40] J. Sirviö and I. Nurminen, "Systematic changes in paper properties caused by fines," *Pulp & Paper Canada,* vol. 105, no. 8, pp. 39-42, 2004.

Appendices

Appendix A: Multi-stage fractionation system layout

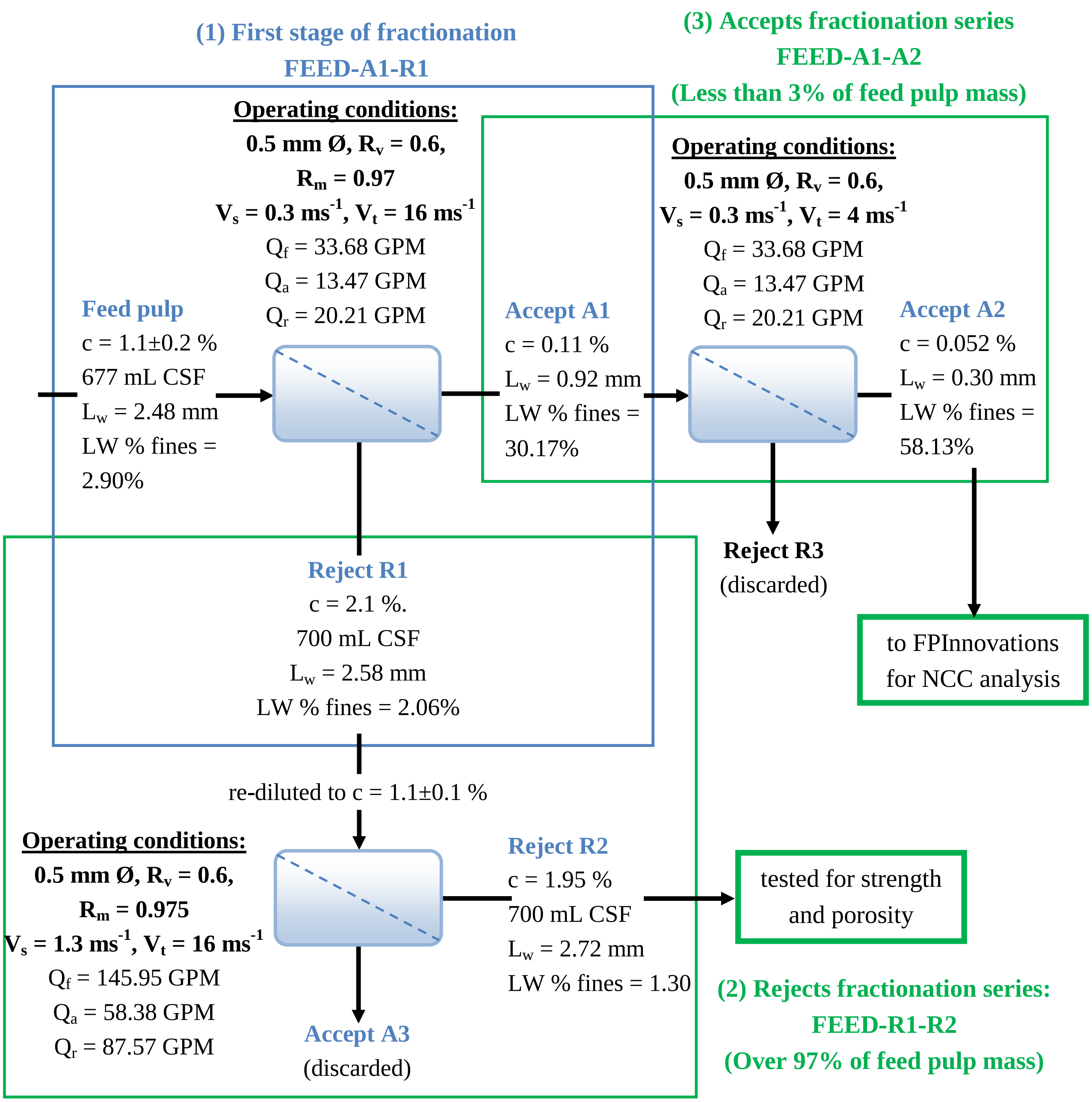

Figure 56. Schematic of two-stage fractionation systems of (1) accept and (2) reject fractions. Fractionation results at each stage are shown.

Appendix B: Fibre length fractionation in a Bauer-McNett classifier

Bauer-McNett classifier is a laboratory device that consists of a series of chambers with five screens of decreasing aperture sizes that is used to fractionate fibres on a laboratory scale, usually about 10 g of dry pulp per operation. Fibre length fractionation in a pressure screen and Bauer-McNett classifier are analogous [29]. The schematic of a Bauer-McNett classifier and the aperture size of each screen are shown in Figure 57. Materials that can pass through the R200 mesh are the fines portion of the sample and it is sometime named the -200 fraction. A more detailed mechanism of fibre length fractionation in a Bauer-McNett classifier including its operating procedures are described elsewhere [29] [30].

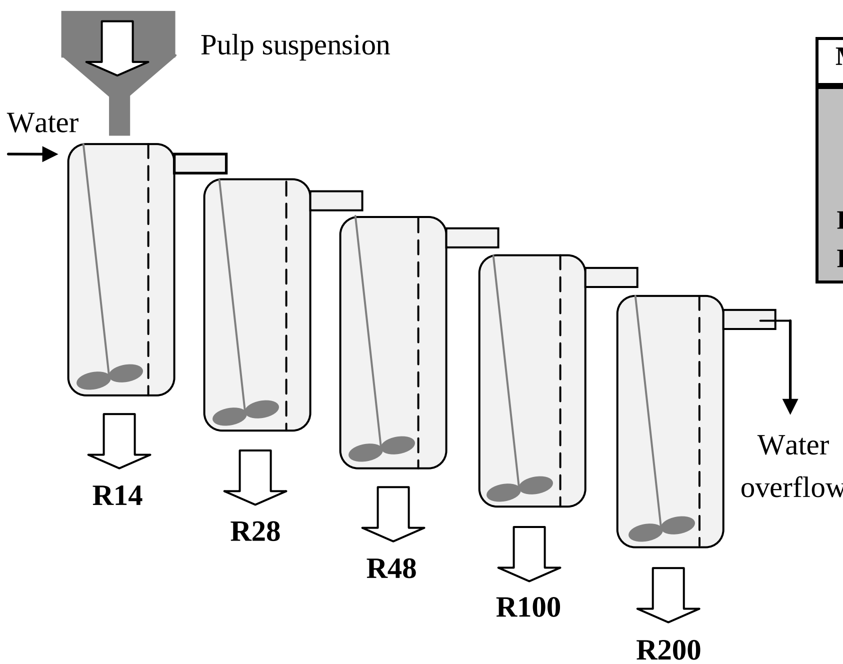

Mesh	Aperture size
R14	1.2 × 1.2 mm
R28	0.6 × 0.6 mm
R48	0.3 × 0.3 mm
R100	0.15 × 0.15 mm
R200	0.074 × 0.074 mm

Figure 57. Schematic of a Bauer-McNett classifier.

The fibre length distribution of a pulp sample as well as coarseness were determined using the Fibre Quality Analyzer (FQA) after consecutive screening steps using the classifier. An example of the fibre length distributions of the Bauer-McNett fractionated samples is shown in Figure 58, together with the average fibre length of each fraction. Figure 59 shows the width distribution of each fraction.

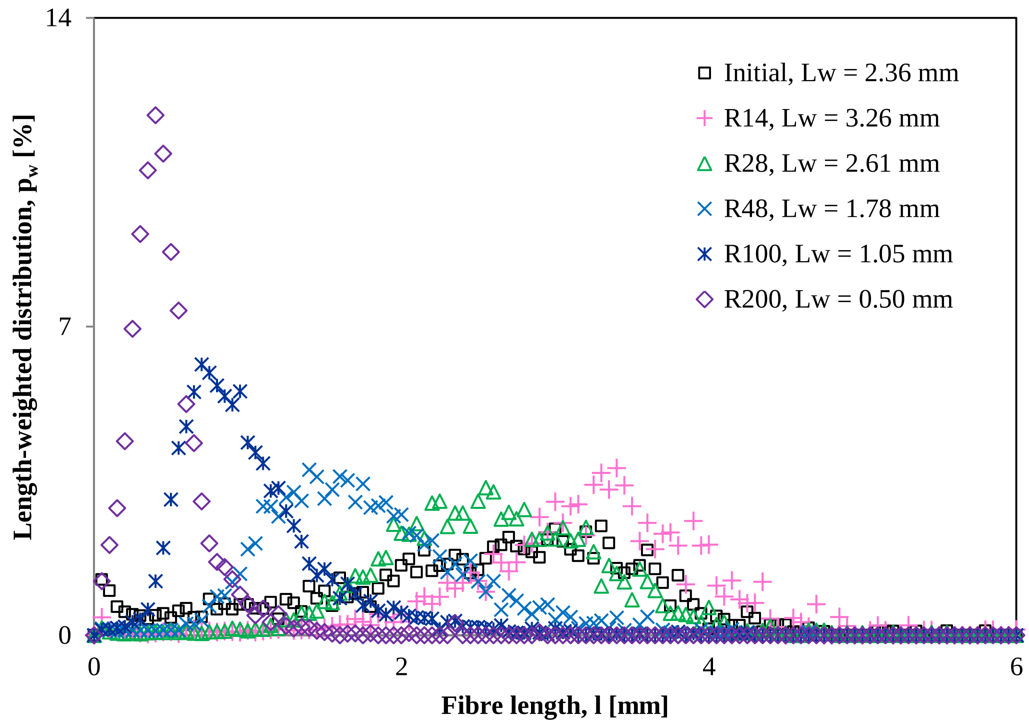

Figure 58. Fibre length distributions of the Bauer-McNett fractionated samples.

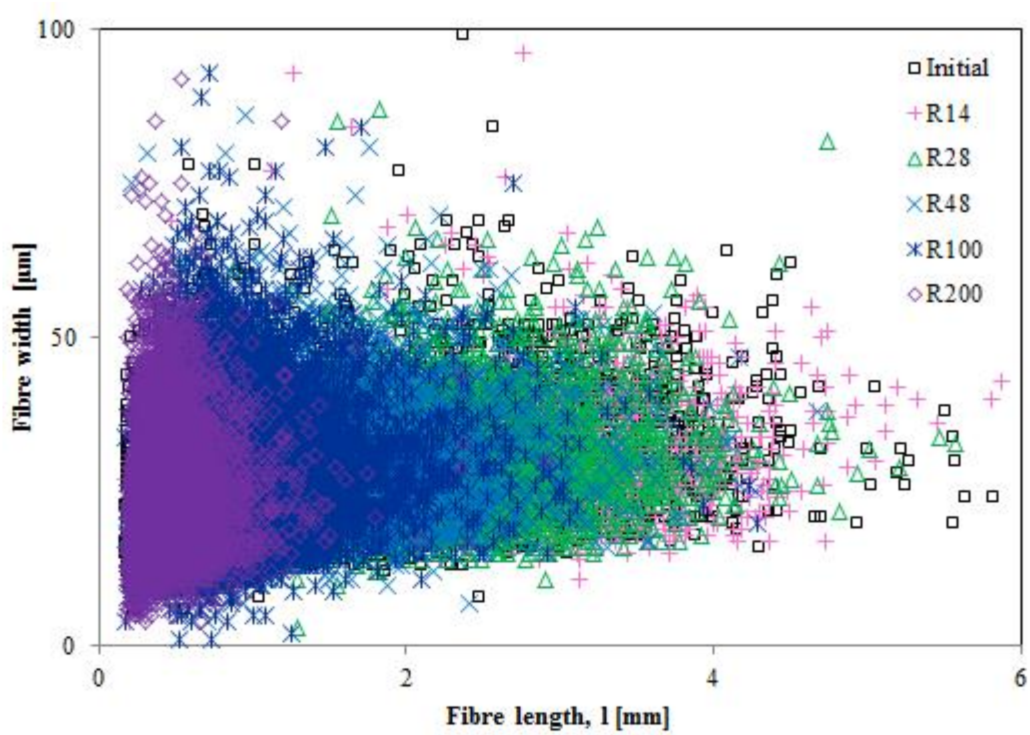

Figure 59. Raw data from FQA of fibre width versus fibre length.

Appendix C: Coarseness versus length relationship, ω(*l*)

The average coarseness of a sample over an entire fibre length, ω can be measured easily using a Fibre Quality Analyzer (FQA). However, the distribution of fibre coarseness in a sample is not as readily avalilable. A recent paper by Madani et al. [27] introduced a new technique to estimate the average coarseness of fibres over smaller length fractions, shown as $\bar{\omega}_i$ in Figure 60.

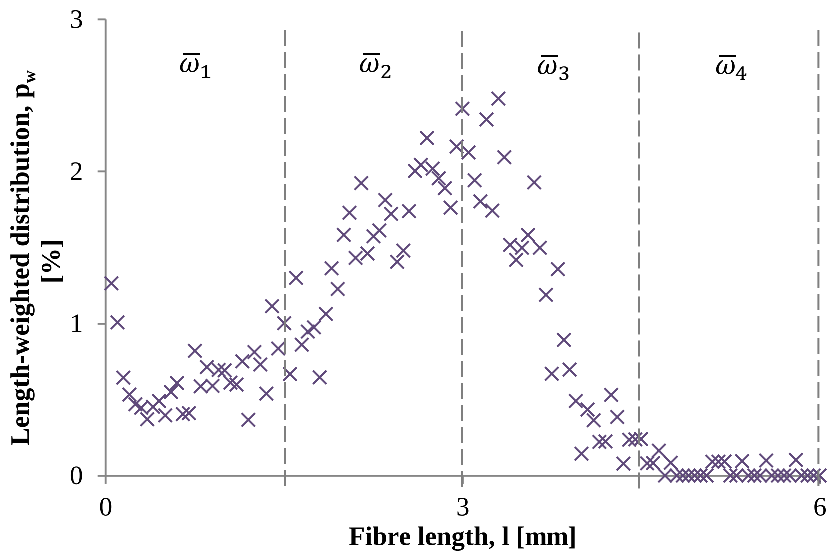

Figure 60. Average coarseness of each length class.

Over 18 statistically different samples were collected for coarseness measurements through multiple operations of the Bauer-McNett Classifier (BMC) (See Appendix B) using samples from the feed, accept and reject of the pressure screen fractionation as the feeds to the BMC. The regression method introduced by Madani et al. [27] was applied to the data to estimate the average coarseness as a function of fibre length. This method is described in detail in the aforementioned work. The results are shown in Figure 61. Also plotted in Figure 61 are the data points obtained from Bauer-McNett fractionation. The results suggest that coarseness increases as fibre length increases.

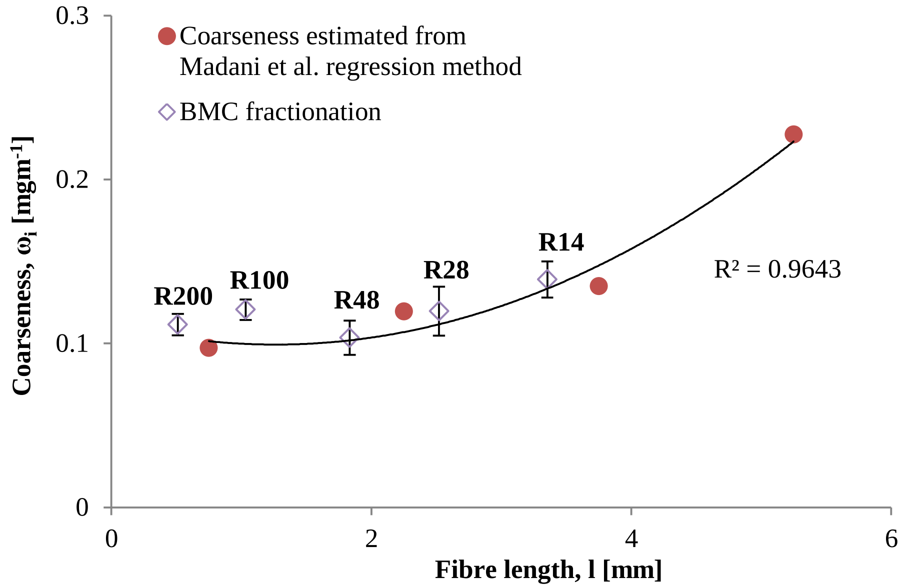

Figure 61. Coarseness values (filled red circles) obtained from Madani et al. regression method. Solid line shows the best fitting curve. Data points obtained from Bauer-Mcnett fractionation are shown with error bars representing the standard deviation.